INVESTIGATING THE INFLUENCE OF SURFACE MELTWATER ON THE ICE DYNAMICS OF THE GREENLAND ICE SHEET

by

William T. Colgan

B.Sc., Queen's University, Canada, 2004

M.Sc., University of Alberta, Canada, 2007

A thesis submitted to the

Faculty of the Graduate School of the

University of Colorado in partial fulfillment

of the requirement for the degree of

Doctor of Philosophy

Department of Geography

2011

This thesis entitled:

Investigating the influence of surface meltwater on the

ice dynamics of the Greenland Ice Sheet, written by William T. Colgan,

has been approved for the Department of Geography by

_____

Dr. Konrad Steffen (Geography)

_____

Dr. Waleed Abdalati (Geography)

_____

Dr. Mark Serreze (Geography)

_____

Dr. Harihar Rajaram (Civil, Environmental, and Architectural Engineering)

_____

Dr. Robert Anderson (Geology)

_____

Dr. H. Jay Zwally (Goddard Space Flight Center)

Date _____

The final copy of this thesis has been examined by the signatories, and we find that both the content and the form meet acceptable presentation standards of scholarly work in the above mentioned discipline.

Colgan, William T. (Ph.D., Geography)

Investigating the influence of surface meltwater on the ice dynamics of the Greenland Ice Sheet

Thesis directed by Professor Konrad Steffen

Abstract

This thesis explains the annual ice velocity cycle of the Sermeq (Glacier) Avannarleq flowline, in West Greenland, using a longitudinally coupled 2D (vertical cross-section) ice flow model coupled to a 1D (depth-integrated) hydrology model via a novel basal sliding rule. Within a reasonable parameter space, the coupled model produces mean annual solutions of both the ice geometry and velocity that are validated by both *in situ* and remotely sensed observations. The modeled annual velocity cycle reproduces the broad features of the annual basal sliding cycle observed along this flowline, namely a summer speedup event followed by a fall slowdown. The summer speedup event corresponds to conditions of increasing hydraulic head during inefficient subglacial drainage, while the fall slowdown event corresponds to conditions of decreasing hydraulic head during efficient subglacial drainage. Calculated coupling stresses diminish to less than 10 % of total driving stress within 6 km upstream of the Sermeq Avannarleq terminus. This suggests that the annual ice velocity cycle observed at CU/ETH ("Swiss") Camp (46 km upstream) is unlikely to be the result of velocity perturbations being propagated upstream via longitudinal coupling, but instead reflects local surface meltwater induced ice acceleration.

This thesis also compares high-resolution 1985 and 2009 imagery of the Sermeq Avannarleq ablation zone to assess changes in crevasse extent and supraglacial hydrology. The area occupied by crevasses > 2 m wide significantly increased (13 ± 4 %) over the 24-year period. This increase consists of an expansion of existing crevasse fields, and is accompanied by

widespread changes in crevasse orientation (up to 45°). The increase in crevasse extent is likely due to a combination of ice sheet thinning and changes in flow direction, both stemming from the recent acceleration of nearby Jakobshavn Isbrae. A first-order demonstration that moulin-type drainage is more efficient than crevasse-type drainage in transferring meltwater fluctuations to the subglacial system suggests that this transition may dampen the basal sliding sensitivity of portions of the ice sheet that are not presently crevassed. An increase in crevasse extent may also enhance mass loss through increased surface ablation and increased deformational ice velocities due to facilitated cryo-hydrologic warming.

Acknowledgements

I thank the Natural Science and Engineering Research Council (NSERC) of Canada for support through a Post-Graduate Scholarship and the Cooperative Institute for Research in Environmental Sciences (CIRES) for support through a Graduate Research Fellowship. This work was supported by National Science Foundation (NSF) Doctoral Dissertation Research Improvement Award 0926911 and National Aeronautics and Space Administration (NASA) Cryospheric Science Program grants NNX08AT85G and NNX07AF15G to Dr. Konrad Steffen.

This thesis reflects the ideas (and labors!) of a team of researchers -- to each of whom I am greatly indebted. Firstly, I am very grateful for all the guidance and encouragement that my advisory committee has given me over the past 3.99 years. They have fostered my development in everything from Coleman cooking to Picard Iteration. Secondly, I would be remiss not to mention the important contributions of Roman Motyka, W. Scott McLamb, Ian Joughin, Thomas Phillips and Henry Brecher -- their generosity with data and ideas greatly improved the insights of this thesis. Thirdly, "Reviewer 1" -- I appreciate your toils.

I have been very grateful for the pleasure and comfort of a far-flung network of friends and family throughout the voyage of self-discovery known as graduate school. It's been quite a journey, but I will have to agree with Mark Twain's assessment of such rites of passage: "I'm glad I did it, partly because it was worth it, but mostly because I shall never have to do it again." Finally, I would like to express a deep thanks to my wife, Christine Bennett, for agreeing to, and providing unwavering support for, this extended road trip to Colorado. Pursuing your aspirations is always easier with someone by your side.

Table of Contents

List of Tables

List of Figures

Chapter 1

ARCTIC CLIMATE AND GREENLAND MASS BALANCE OVERVIEW

1.1 Arctic climate

The Arctic Ocean is the central feature of the Arctic climate. Annual freshwater input to the Arctic Ocean is comprised of river discharge (~ 38 %), inflow through the Bering Strait (~ 30 %) and net precipitation (~ 24 %). Annual freshwater export from the Arctic Ocean is dominated by transport through Fram Strait (~ 51 %) and the Canadian Archipelago (~ 35 %), with liquid and ice export occurring in approximately equal parts (*Serreze and others*, 2006). Freshwater in the Arctic Ocean has a mean residence time of about a decade. Sea ice forms in the freshwater cap of the Arctic Ocean. Arctic sea ice extent usually varies between ~ 7 Mkm^2 in September and ~ 16 Mkm^2 in March. Sea ice strongly regulates Arctic climate and poleward atmospheric energy transport (*Serreze and others*, 2006). During January, oceanic sensible heat loss and sea ice formation result in an upward surface flux of ~ 55 W/m^2 (in comparison, the energy flux due to atmospheric transport convergence is ~ 85 W/m^2). During July however, the net surface flux of the Arctic Ocean is ~ -100 W/m^2, due to sea ice melt and sensible heat gain that slightly exceeds the energy flux due to atmospheric transport convergence (~ 90 W/m^2). The Arctic Ocean therefore acts as heat sink during the summer and a heat source during winter (*Serreze and others*, 2007a).

There is a pronounced temperature inversion over the Greenland Ice Sheet that is created by strong cooling of the atmosphere at the ice sheet surface. As a result, cold air sinks from the summit of the ice sheet toward its periphery. As a consequence of the Coriolis effect, the katabatic winds created by this sinking air are deflected to the right, resulting in clockwise circulation along the coast of Greenland (*Steffen and Box*, 2001). During the fall and winter, the east coast of Greenland generally experiences meridional atmospheric flow from the north, while

the west coast experiences meridional flow from the south. Zonal circulation is dominant over Greenland in the summer (*Steffen and Box*, 2001). The strong thermal gradient between the Greenland Ice Sheet and adjacent open water induces baroclinic instabilities that contribute to cyclogenesis in the atmospheric low pressure cells above Baffin Bay and Iceland (*Steffen and Box*, 2001; *Tsukernik and others*, 2007).

Prior to 1920, the Arctic likely experienced a slight warming due to reduced volcanic aerosol forcing and increasing solar insolation. Since 1920, however, the influence of the positive radiative forcing associated with increasing greenhouse gas concentrations has overtaken these natural factors (*Serreze and others*, 2000). In the warming Arctic, surface air temperature anomalies reach a maximum in autumn over the Arctic Ocean, with a minimum in summer. The relatively small change in summer surface air temperatures suggests that melting ice and increased heat uptake by open water compensates for increased radiative warming (*Serreze and others*, 2009). The increase in autumnal Arctic Ocean surface air temperatures is most clearly linked to an increase in surface longwave radiation emission, rather than changes in the turbulent sensible and latent heat fluxes (*Serreze and others*, 2007b; *Serreze and others*, 2009). Also important in the observed warming of the Arctic are shifts in atmospheric circulation, specifically extended positive and negative phases of the North Atlantic Oscillation (NAO) and the El Niño Southern Oscillation (ENSO), respectively (*Serreze and others*, 2000). A clear record of the NAO signal over the past 700 years in the stable isotopes of southern Greenland ice cores suggests that the surface mass balance of the Greenland Ice Sheet is sensitive to these oscillation conditions, which enhance the transport of warm and moist air into the Arctic (*Vinther and others*, 2003).

Arctic sea ice extent has exhibited a dramatic decrease over the observational record (1979 to 2010), ~ 12 % per decade during the month of September (*Stroeve and others*, 2011). From limited upward-looking submarine sonar data, it appears that mean sea ice thickness has

decreased from ~ 3.1 m during the 1950 to 1980 period to ~ 1.8 m in the 1990s. This translates into an ~ 40 % volume reduction in sea ice (*Johannessen and others*, 2004). This decline in sea ice is due to both thermodynamic and dynamic processes. During the 1980s and 1990s, sea ice motion and export through Fram Strait was correlated strongly with the NAO. Presently however, only a third of the variability in sea ice extent is explained by changes in circulation induced by the NAO. This suggests that a thermodynamic albedo feedback mechanism has likely surpassed natural dynamic variability in determining sea ice extent (*Johannessen and others*, 2004; *Serreze and others*, 2007b). Currently, however, no models predict a fall season sea ice decline that is as strong as the one being observed. This suggests that models may be either lacking a key physical process or natural variability that is enhancing the decline in fall sea ice extent (*Serreze and others*, 2009).

The Arctic has also experienced substantial terrestrial changes over the last century. In the Western Arctic, model output indicates an accelerated warming signal over land in comparison to the warming signal over the ocean. This modeled warming signal penetrates up to 1500 km inland and exists throughout the year, reaching a peak in autumn (*Lawrence and others*, 2008). It has been suggested that this amplified land response is due to the decreasing trend in sea ice cover, which is allowing more heat to escape from the relatively warm Arctic Ocean throughout the year. When relatively warm oceanic air masses pass over land (or the Greenland Ice Sheet) they enhance downward longwave radiation due to their relatively high moisture content (*Lawrence and others*, 2008). In Alaska, permafrost boreholes exhibit a warming of up to 4 °C over the last ~ 50 years. Observed changes in air temperature alone cannot explain the warming of these boreholes, which suggests that borehole temperatures are likely also responding to changes in snow cover or vegetation type. Changes in vegetation may be due to changes in soil moisture, as a result of changes in precipitation and evaporation, rather than direct effects of increasing temperature on plant respiration (*Serreze and others*, 2000).

Northern Hemisphere snow cover extent has also decreased over the observational record. Snow cover anomalies were generally positive prior to 1985/1990, but have become increasingly negative since that time in both North America and Eurasia (*Serreze and others*, 2000; *McCabe and others*, 2010). This decrease in Northern Hemisphere snow cover extent has been accompanied by a decrease in winter and spring snow depth. This loss of snow cover is not due to a change in precipitation. In North America, north of 55 °N, there have been significant increases in annual precipitation over the past 40 years, up to 20 % at some stations, but these increases have been offset by increases in evaporation (*Serreze and others,* 2000). Increasingly negative snow cover extent anomalies are due warming winter air temperatures (*McCabe and others*, 2010).

Similar to the Alaskan boreholes, firn temperatures from the Greenland Ice Sheet also indicate strong climate warming. Firn temperatures at 10 m depth at dry snow zone sites (taken to be representative of decadal mean temperature) have been found to be colder than mean annual air temperatures. This suggests an increasing trend in mean annual air temperatures at these sites (*Steffen and Box*, 2001). Below the dry snow zone firn temperatures can be artificially raised by the release of latent heat during the refreezing of meltwater (*Steffen and Box,* 2001).

Until recently, the Arctic warming anomaly of 1.7 °C between 1930 and 1940 was a touchstone for climate change skeptics. The scientific community, however, has now provided clear evidence that natural variability was responsible for this anomalously warm period, while anthropogenic radiative forcing is responsible for the current Arctic warming (*Bengtsson and others*, 2004; *Johannessen and others*, 2004). The early twentieth century warming was likely due to a positive feedback of circulation changes that maintained favorable conditions for the Barents Sea to act as a heat source, due to enhanced atmospheric and oceanic heat transport from the comparatively warm North Atlantic (*Bengtsson and others*, 2004). This positive feedback may have been initiated by an extended NAO positive phase during the 1920s, which led to the

import of warm water via stronger than normal westerly circulation over the North Atlantic (*Bengtsson and others*, 2004). Other variations in natural forcing during the 1930 to 1940 period included a quiescent phase of volcanic activity and anomalously high solar irradiation (*Overpeck and others*, 1997; *Serreze and others*, 2000; *Bengtsson and others*, 2004). Additionally, the early twentieth century warming was spatially limited to the Arctic, while the current warming encompasses the whole planet. Models have not been able to recreate this discrepancy without the inclusion of greenhouse gases (*Bengtsson and others*, 2004; *Johannessen and others*, 2004).

1.2 Projected Arctic climate change

Arctic mean air temperatures have increased at almost twice the average global rate in the past 100 years. Over the next century, surface warming is expected to be greater in the Arctic than anywhere else on Earth. Winter warming in the Arctic could be ~ 40 % greater than the global mean while mean annual warming may be equivalent to 3 or 4 °C by 2100 (*Johannessen and others*, 2004). Increased greenhouse gas concentrations will lengthen the open water season of the Arctic Ocean, leading to the production of thinner spring sea ice. Models suggest a near-complete, or complete, loss of September sea ice between 2040 and 2100 (*Johannessen and others*, 2004; *Serreze and others*, 2007b). As sea ice extent decreases, due to processes such as decreased ocean albedo and increased sensible heat flux, the extent of open water in the Arctic Ocean increases both spatially and temporally. Linear trends show that sea ice extent is presently declining in every month, with the strongest trend of ~ 12 % per decade during the month of September (*Stroeve and others*, 2011).

A decreasing sea ice extent in the Arctic will enhance upward heat fluxes from the ocean to the atmosphere, especially during the fall season (*Serreze and others*, 2009). This will result in strong warming of the near-surface troposphere, enhanced by low-level stability that inhibits vertical mixing. Essentially there will be less insulation between the relatively cool atmosphere

and the relatively warm ocean during the fall season (*Lawrence and others*, 2008; *Serreze and others*, 2009). As air over the Arctic Ocean warms, its moisture content will increase, resulting in greater downwelling longwave radiation. The spatial anti-correlation between maximum temperature anomalies and minimum sea ice anomalies, combined with the vertical structure of the warming, provides convincing evidence that the ongoing Arctic warming is due to an anomalous surface heat source (*Serreze and others*, 2009).

As increasingly moist and warm air, produced by decreasing sea ice extent, is advected over land and the Greenland Ice Sheet, terrestrial downwelling longwave radiation can be expected to increase (*Lawrence and others*, 2008). Thus, the decreasing trend in insulating sea ice extent results in an increasing trend in net longwave surface radiation throughout the Arctic. Amplified warming of the land surface via atmospheric forcing has the potential to lead to the rapid degradation of permafrost, and the release of greenhouse gases that are currently sequestered in the Arctic soil (*Lawrence and others*, 2008). Considerable interests surrounds the potential for widespread releases of methane hydrates that are currently sequestered through a combination of low temperature and high pressure in the tundra and shallow continental shelves of the Arctic.

Model simulations suggest an acceleration of the Arctic hydrologic cycle over the next century, with net precipitation increasing over both ocean and land areas and more freshwater remaining stored in the Arctic Ocean. An increase in freshwater transport out of Fram Strait is also projected (*Holland and others* 2007). Changes in the flux of Arctic freshwater to the North Atlantic, via Fram Strait, may have important implications for the global thermohaline circulation. A freshening of the North Atlantic can theoretically cause either a cessation of North Atlantic downwelling (i.e. Younger Dryas initiation mechanism) or a southward shift in the downwelling location (*Holland and others* 2007).

Arctic warming will also influence future cyclone frequency and precipitation

distribution. Total daily precipitation from cyclones is expected to increase during the 21st century, primarily due to increased available atmospheric moisture (due to increased atmospheric temperature; *Finnis and others*, 2007). During the May to September season, there may also be an increase in cyclone frequency in the high latitudes, while there is a decrease in cyclone frequency in the midlatitudes (*Finnis and others*, 2007). The increase in high latitude cyclone frequency will be accompanied by an increase in cyclone intensity, due to greater heat and moisture exchange between the ocean and atmosphere (*Finnis and others*, 2007). As cyclones work to reduce the Equator-to-Pole temperature gradient, by promoting meridional mixing and condensing atmospheric moisture through their rising motion, cyclones perform a poleward latent heat transfer (*Finnis and others*, 2007). The projected increase in cyclone intensity will therefore increase the efficiency of poleward heat transport by storms, which may modify the magnitude and/or frequency of regional atmospheric eddies (*Finnis and others*, 2007).

Finally, a warmer Arctic will also store less water as terrestrial ice. During the last interglacial warm period (~ 125 KaBP) global temperatures were ~ 4 °C warmer than present due to variations in Earth's orbit. At that time, sea level was ~ 5 m higher than present day (*Overpeck and others*, 2006). This increase in sea level was largely due to a loss of terrestrial Arctic ice (as opposed to terrestrial Antarctic ice), as a result of negative mass balance conditions. The mass balance of the Greenland Ice Sheet and its potential sea level rise contribution are discussed in detail in Section 1.4. In summary, projected Arctic climate changes will result in: (i) a loss of sea ice with a consequent increase in downwelling radiation, (ii) a degradation of permafrost and possible release of sequestered greenhouse gases, (iii) an accelerated hydrologic cycle, (iv) an increase in cyclone frequency and intensity, and (v) a reduction in terrestrial ice storage. Statistical analysis of ice core records from Greenland suggests that rapid and abrupt climate shifts, on the time-scale of decades, are possible in the Arctic (*Ditlevsen and others*, 1996). Thus, these consequences should not be expected to occur in a gradual or linear fashion.

1.3 Glacier surface energy balance

The energy balance at a glacier surface is normally taken as positive when there is an energy gain and negative when there is an energy loss. The net radiation balance at a glacier surface may be expressed as:

$$Q_N = (I + D_s + D_t)(1-\alpha) + L\downarrow + L\uparrow \qquad \text{Eq. 1.1}$$

where I is direct solar radiation, D_s is diffuse sky radiation, D_t is reflected radiation from the surrounding terrain (therefore $I + D_s + D_t$ is the global radiation), α is albedo, $L\downarrow$ is incoming longwave radiation and $L\uparrow$ is outgoing longwave radiation (*Hock*, 2005). The net radiation balance is comprised of both shortwave (0.15 to 4 μm) and longwave (4 to 120 μm) radiation. Albedo is the portion of shortwave (solar) radiation that is reflected by a glacier surface. Albedo decreases with increasing grain size, and increases with cloudiness / atmospheric water content and decreasing incidence angle (*Hock*, 2005). Although the albedo of snow (0.7 to 0.9) is higher than that of ice (0.3 to 0.5), in the infrared part of the electromagnetic spectrum both snow and ice behave as almost perfect black-body emitters (i.e. an emissivity > 0.97; *Hock*, 2005).

Net radiation is just one term of the surface energy balance of a glacier, which may be expressed as:

$$0 = Q_N + Q_H + Q_L + Q_G + Q_R + Q_M \qquad \text{Eq. 1.2}$$

where Q_H is the sensible heat flux, Q_L is the latent heat flux (together Q_H and Q_L are referred to as turbulent heat fluxes), Q_G is the ground / geothermal heat flux, Q_R is the sensible heat flux supplied by rain and Q_M is the energy consumed by melt (*Hock*, 2005). In addition to melt, outgoing longwave radiation (contained within the Q_N term) may be regarded as an energy sink

(*Ohmura*, 2001). The turbulent heat fluxes are driven by temperature and moisture gradients between the air and glacier surface, as well as by vertical air exchange due to turbulence in the lower atmosphere (*Hock*, 2005). As the surface temperature of a melting glacier does not exceed 0°C, strong temperature gradients (~ 5 °C/m) can develop in the air immediately above the surface. This creates a stable stratification of the boundary layer during the melt season which suppresses turbulence and induces gravity flows or katabatic winds (*Hock*, 2005). Over large glaciers, this boundary layer is capable of filtering out large-scale climatic signals (*Oerlemans*, 2000). The melting ice surface favors vapor pressure gradients towards the surface, leading to condensation, which is an important energy source for melt (*Oerlemans*, 2000; *Hock*, 2005). Most models calculate the turbulent heat fluxes using a bulk aerodynamic approach. The bulk aerodynamic approach, however, is highly dependent on specified roughness lengths. Changes in roughness length by an order of magnitude can change the turbulent heat fluxes by a factor of two (*Hock*, 2005). In addition to melt, sublimation can also remove mass from a glacier. Maximum sublimation from the ice surface to the atmosphere occurs when temperature and wind speeds are greatest in the summer. Reduced albedo due to surface melt allows extra solar absorption and increased sublimation during this time (*Box and Steffen*, 2001). As relatively windy and warmer years have been observed to result in greater sublimation, sublimation from the Greenland Ice Sheet is expected to increase under projected warming (*Box and Steffen*, 2001).

Albedo is a parameter of particular interest when assessing ice sheet surface energy balance. Albedo values theoretically range from 0 to 1 and are defined as the spectrally integrated reflectively over the shortwave radiation spectrum (0.35 to 2.8 μm; *Jonsell and others*, 2003). Snow typically has albedo values that range between 0.7 and 0.9, while ice has lower albedo values between 0.3 and 0.5 (*Hock*, 2005). Over a glacier ice surface, albedo values typically experience a diurnal cycle of ~ 0.3, with values being highest during low angles of solar

incidence as a result of Mie scattering (*Jonsell and others*, 2003; *Hock*, 2005). Even over snow-covered surfaces albedo values are spatially heterogeneous, with variations of ~ 0.1 between closely spaced sampling points (*Konzelmann and Braithwaite*, 1995; *Jonsell and others*, 2003). This spatial variation in albedo makes it difficult to parameterize snow albedo for inclusion into surface energy balance models of the Greenland Ice Sheet (*Hanna and others*, 2005).

Albedo feedbacks are very important for both snow-covered and blue-ice glaciers. The albedo of snow increases with increasing cloudiness. As clouds preferentially absorb near infrared radiation, the proportion of visible light is enhanced, which results in an albedo increase as the visible spectrum has a much higher reflectivity than the near infrared spectrum (*Jonsell and others*, 2003; *Hock*, 2005). Albedo also decreases with increasing snow water content. Therefore, as a snowpack begins to experience melt, and snow water content increases, its albedo decreases. This causes the snowpack to absorb even more shortwave radiation and experience even more melt, further increasing its snow water content and decreasing its albedo (*Hock*, 2005). Snow melt can act as a vapour source for cloud formation. Although clouds can act to increase atmospheric albedo, it is possible for this effect to be dominated by increased downwelling longwave radiation from the clouds themselves, further enhancing surface melt (*Abdalati and Steffen*, 1997). The melting of a snowpack, both seasonally and other longer time-scales, is generally regarded as including a positive snow-albedo feedback mechanism.

The amount of energy available for melt at a glacier surface can be deduced by solving all other terms of the energy balance (Equation 1.2). It can be difficult, however, to obtain values for all terms in the energy balance. Therefore, temperature-index methods (or "positive degree day" models), which rely only on surface air temperature, are often used to parameterize glacier melt, as it is easier to obtain and interpolate temperature data than energy balance fluxes (*Ohmura*, 2001). Although a gross simplification, these methods are justified because there is a

high correlation between temperature and longwave incoming radiation, which is by far the most important heat source for melt (*Oerlemans*, 2000; *Ohmura*, 2001; *Hock*, 2005). Net radiation, which is also a major energy source, is more poorly correlated with melt in comparison to temperature, as net radiation is comprised of four different irradiances with four different origins (*Ohmura*, 2001). Under cloudless-sky conditions, 34 % of the entire longwave irradiance received at a glacier's surface originates within the first 10 m of the atmosphere; 67 % in the first 100 m and 89 % from the first 1 km. This increases with cloudy conditions and atmospheric moisture concentration (*Ohmura*, 2001). The relation between temperature and melt is quantified by degree-day factors, which vary considerably in space and time because they implicitly account for all terms of the energy budget. Degree-day factors generally range between 2.5 and 11.5 mm/d/°C for snow and between 6.5 and 20.0 mm/d/°C for ice (*Hock*, 2005).

1.4 Greenland Ice Sheet mass balance

The rate of change of ice mass (or "mass balance") of an ice sheet is the difference between the rate of mass gain through accumulation, and the rate of mass loss through meltwater runoff and iceberg calving (*Murphy and others*, 2002; *Hooke*, 2005). Surface mass balance is described as the difference between accumulation and runoff. In marginal zones of the Greenland Ice Sheet ~ 40 % of annual surface mass balance variation may be due to an albedo-meltwater feedback, rather than temperature variations (*Greuell*, 2000). Increased surface meltwater production across the Greenland Ice Sheet, due to a lengthening and intensifying of the melt season, has caused albedo values to decrease across the ice sheet. The wet snow (or melt) area of the Greenland Ice Sheet has been increasing at ~ 40,000 km^2/a over the past 14 years (*Tedesco*, 2007), an acceleration over the pre-2000 trend (*Abdalati and Steffen*, 1997). The ablation area of the Greenland Ice Sheet has grown over the observational period by an amount sufficient to decrease the accumulation-ablation ratio of the Greenland Ice Sheet by 3 % (*Box and others*,

2006). In blue-ice zones near the margin of the Greenland Ice Sheet, sublimation is an especially important mechanism of mass loss, and decreasing surface albedo values are providing increasing solar radiation absorption to drive sublimation (*Box and Steffen*, 2001). Under future global warming scenarios, the increased surface melt can be expected to decrease albedo at CU/ETH ("Swiss") Camp, Greenland by ~ 0.1. This translates into an ~ 30 W/m^2 of absorbed energy by the snow surface, which is expected to result in an additional sublimation of ~ 4.2 % of the annual accumulation (*Steffen*, 1995).

In terms of overall mass balance, the Greenland Ice Sheet may have been in near balance in the colder climate of the 1970s and 1980s. More recently, however, the ice sheet has responded rapidly to post-1990 warming (*Rignot and others*, 2008). Since the 1990s, there has been a significant increase in runoff from the Greenland Ice Sheet. This has been partly offset by increased precipitation, but calculated net surface mass balance has declined from 22 km^3/a during the 1961 to 1990 period to -36 km^3/a during the 1998 to 2003 period (by definition this surface mass balance estimate ignores any changes in ice dynamics or iceberg calving over this interval; *Hanna and others*, 2005). Since 1961, the five highest Greenland Ice Sheet runoff years have all occurred within the last decade, while the three lowest runoff years all follow major volcanic events (1963, 1982 and 1992; *Hanna and others*, 2005). Runoff accounts for ~ 50 % of mass loss, while ice dynamics account for the remaining ~ 50 % of annual mass loss (*Hanna and others*, 2005; *van den Broeke and others*, 2009). Modeling suggests that a 1 °C increase in surface air temperature will increase Greenland Ice Sheet surface melt by between 20 and 50 %. A 2 °C increase in air temperature would approximately double the melt extent of the ice sheet, and therefore almost double total melt (*Hanna and others*, 2005). However, considerable uncertainty still exists regarding how much melt leaves the ice sheet as runoff, versus the fraction that remains and refreezes in the snowpack (*Pfeffer and Humphrey*, 1996; *Pfeffer and Humphrey*, 1998; *Parry and others*, 2007).

Repeat laser altimetry surveys suggest that the Greenland Ice Sheet lost 80 ± 12 km^3/a of ice between 1997 and 2003. This is an increase over the mass loss rate previously estimated by laser altimetry (~ 60 km^3/a) between 1993/4 and 1998/9 (*Krabill and others*, 2004). Laser altimetry has some disadvantages, including a narrow laser footprint, which requires interpolation, and a strong influence of clouds on laser returns. Additionally, satellite laser systems appear to have a relatively short lifetime (*Alley and others*, 2007). Interferometric synthetic aperture radar (InSAR) can be used to establish ice surface flow velocities. Observed accelerations in ice discharge have been used to suggest that Greenland's mass imbalance doubled between 1996 and 2006, from ~ 90 to 220 km^3/a (*Rignot and Kanagaratnam*, 2006). Radar can also be used as an altimetry instrument. Radar altimetry, however, has trouble with sloping ice surfaces, as well as changes in surface roughness and snow stratigraphy that influence the waveform returned to the satellite. Also, as volume backscatter does not automatically scale with melt intensity, it is difficult to compensate for the effects of seasonal melt (*Parry and others*, 2007; *Alley and others*, 2007). Both altimetry methods are also sensitive to changes in the rate of firn densification, which can be influenced by changes in annual accumulation rate, snowpack temperature, air expulsion and snowpack stratigraphy (*Alley and others*, 2007). Short-term variations in elevation may be especially misleading in the percolation zone, where temperature-driven variations of melting/refreezing rates have a strong impact on near surface density (*Parry and others*, 2007; *Reeh*, 2008). In the lower percolation zone, temperature-induced density changes, rather than fluctuations of accumulation, are the dominant cause of short term elevation changes. In the upper percolation zone, elevation changes are driven by accumulation (*Reeh*, 2008).

Gravimetry is cited as an improvement over altimetry because it does not require firn density estimations. The spherical harmonic solutions (Stokes coefficients) of Gravity Recovery and Climate Experiment (GRACE) data can resolve monthly mass changes over Greenland to

accuracies of ~ 10 mm water-equivalent thickness averaged over discs of radius 600 to 700 km (*Velicogna and Wahr*, 2005). GRACE data suggests that the Greenland Ice Sheet lost mass at a rate of ~ 137 Gt/a during 2002/03 and ~ 286 Gt/a over the 2007/09 period. This suggests a possible acceleration in mass loss of ~ 30 ± 11 Gt/a^2 over the 2002/09 period (*Velicogna*, 2009). It is highly unlikely that this scale of mass loss is possible from surface mass balance alone. Therefore, the increased rate of mass loss suggests an accelerated dynamical loss of ice into the ocean (*Velicogna and Wahr*, 2006; *Velicogna*, 2009). A large uncertainty surrounds GRACE estimates due to the uncertainties in possible changes in: (i) continental water storage, (ii) water storage in the surrounding ocean, (iii) atmospheric mass, and (iv) post-glacial rebound in the solid earth (*Velicogna and Wahr*, 2006). Uncertainty in GRACE measurements is dominated by uncertainty in the post-glacial rebound correction (*Velicogna and Wahr*, 2005). Changes in bedrock elevation, due to isostatic response, are important in gravimetry. Mantle rocks have a much higher density than ice (3300 kg/m^3 versus 910 kg/m^3), so a given elevation change will affect the gravitational field ~ 3.6 times more if caused by isostasy than if caused by changes in ice thickness (*Alley and others*, 2007).

By the year 2100 Arctic temperatures may have reached warm levels not seen since marine isotope stage (MIS) 5e (127 to 130 KaBP). This warm period was likely caused by orbital changes that led to excess solar insolation reaching the Northern Hemisphere. During that time, sea level was ~ 5 m above contemporary levels (*Overpeck and others*, 2006). Paleoreconstructions suggest that the mean rate of sea level rise during the MIS 6 to 5e deglaciation (127 KaBP) was ~ 20 mm/a, while the mean rate of sea level rise during the last deglaciation (MIS 2 to 1; 14 KaBP) was ~ 11 mm/a (*Overpeck and others*, 2006). This suggests that the Earth is capable of delivering higher rates of sea level rise than are currently being observed (3.3 ± 0.4 mm/a; *Cazenave and Llovel*, 2010). Over the 2003/07 period, the Greenland Ice Sheet contributed to global sea level rise at a rate of between 0.4 and 0.5 mm/a (*Velicogna*

and Wahr, 2006; *Cazenave and Llovel*, 2010). Preliminary ice flow modeling of the Greenland Ice Sheet response to a warming climate suggests that over the next century the margin of the Greenland Ice Sheet may retreat, decreasing the size of the ablation zone, with an accompanying mass gain in the accumulation zone (*Parizek and Alley*, 2004). This would result in a steeper ablation zone with an increased mean ice thickness, and should theoretically increase driving stresses and hence ice velocities (*Parizek and Alley*, 2004). Elevated ice flux into the ablation zone would likely be maintained for several centuries (*Parizek and Alley*, 2004). An increase in mass loss due to iceberg calving, resulting from the widespread acceleration of Greenland outlet glaciers (described in detail in Section 1.6), will also increase the future ice dynamic contribution of the Greenland Ice Sheet to sea level rise. Significant uncertainty remains in forecasting the ice dynamic contribution of the Greenland Ice Sheet to sea level rise (*IPCC*, 2007).

1.5 Contrasting the Greenland and Antarctic Ice Sheets

Unlike the Greenland Ice Sheet, ablation and runoff are not significant mechanisms of mass loss in the East and West Antarctic Ice Sheets. As a consequence of the minimal surface melt that the Antarctic Ice Sheets experience each year, their mass loss is dominated by iceberg calving. Partly as a result of this difference in dominant mass loss mechanism, the contemporary mass balance regimes of the Greenland and Antarctic ice sheets differ. While several recent studies demonstrate that the Greenland Ice Sheet is losing mass (*Zwally and others*, 2005; *Velicogna and Wahr*, 2006; *Alley and others*, 2007), the mass balances of the Antarctic Ice Sheets are more uncertain than the Greenland Ice Sheet at present. The marine-based West Antarctic Ice Sheet appears to be losing mass, while the land-based and higher elevation East Antarctic Ice Sheet is gaining mass. Together, these processes suggest a total Antarctic mass loss rate of ~ 100 Gt/a, equivalent to a sea level rise contribution of ~ 0.3 mm/a (*Alley and others*, 2007; *Cazenave and Llovel*, 2010).

The Arctic and Antarctic climates have very different mean annual temperatures. If climate change persists at the current rate for the next century, there will be significant implications for the surface mass balance of the Greenland Ice Sheet. In contrast, the surface ablation rate of the Antarctic Ice Sheet will not change significantly. In 100 years mean annual temperatures in Antarctica will continue to be well below 0 °C, while in the Arctic they are relatively close to 0 °C over most of the Greenland Ice Sheet. Given the relatively shallow surface slopes of the Greenland Ice Sheet, relatively small increases in atmospheric temperature will have a large impact on net surface mass balance. Assuming an adiabatic lapse rate of 6.8 °C/km and an ice surface slope of 0.4 °, every 1 °C increase in mean annual air temperature will result in an additional 73,000 km^2 of the Greenland Ice Sheet experiencing melt (*Abdalati and Steffen*, 1997).

A substantial sea level rise contribution from either the Greenland Ice Sheet or other glaciers and ice caps over the next century may trigger a dynamic response from the marine-based West Antarctic Ice Sheet (*Alley and others*, 2007). The marine ice sheet instability hypothesis suggests that ice sheets that are grounded on reverse-sloping bedrock below sea level are susceptible to rapid collapse. This rapid collapse occurs via a positive feedback between flotation fraction and grounding line retreat. The West Antarctic Ice Sheet has been portrayed as a candidate for the marine ice sheet instability, as paleoclimatic evidence suggests that it has collapsed over relatively short time-scales in the past (*Overpeck and others*, 2006). Marine cores collected from the Ross Sea embayment suggest that West Antarctic Ice Sheet partially collapsed during the last interglacial warm period (~ 127 KaBP). The proposed trigger mechanism for this partial collapse was increased sea level caused by solar insolation anomalies and terrestrial ice melt in the Arctic (*Overpeck and others*, 2006).

The West Antarctic Ice Sheet is also different from both the Greenland and East Antarctic Ice Sheets in that it has an active subglacial hydrological system (*Wingham and others*,

2006; *Fricker and others*, 2008). In Greenland, there is very limited evidence for subglacial water and no evidence for subglacial lakes (*Oswald and Gogineni*, 2008). In West Antarctica, large volumes of subglacial water (~ 1 km^3) have been observed to drain from one subglacial lake to another, and may be responsible for the onset of fast flow at the heads of the West Antarctic ice streams (*Fricker and others*, 2008). This widespread and dynamic subglacial water system is an important control on ice flow and mass balance that is unique to the West Antarctic Ice Sheet (*Fricker and others*, 2008). Exactly how the subglacial hydrology of the West Antarctic Ice Sheet will influence its mass balance over the next century, however, is highly uncertain.

Unlike Greenland, mass loss via iceberg calving is suppressed in Antarctica by the widespread presence of ice shelves, which cover ~ 40 % of Antarctica's coastline. Antarctic ice shelves have been observed to breakup, removing resistive along-flow stresses that retard the flow of outlet glaciers. Outlet glacier speeds have been recently observed to increase following the breakup of the Larsen Ice Shelf (*Scambos and others*, 2004). Over the next 100 years, it is likely that Antarctica will lose additional ice shelves due to increased surface and submarine ablation and propagation of meltwater-filled crevasses (*Scambos and others*, 2004; *van der Veen*, 2007). This mechanism will likely only influence the West Antarctic Ice Sheet, primarily the Antarctic Peninsula, over the next century. While there are no major ice shelves surrounding the Greenland Ice Sheet, observations suggest that the annual acceleration / deceleration (retreat / advance) cycle of Greenland outlet glaciers is controlled by the absence / presence of sea ice (*Reeh and others*, 2001; *Joughin and others*, 2008a; *Joughin and others*, 2008b).

The mass gain processes of the Greenland and Antarctic Ice Sheets vary slightly. Although Greenland gains the majority of its mass as snowfall, it does gain a small fraction of mass as rainfall. In contrast, Antarctica gains mass almost exclusively through snowfall, with virtually no rainfall. Over the next 100 years, a warming atmosphere is expected to hold increasing amounts of moisture. As a result, the Arctic hydrologic cycle is predicted to accelerate,

with a net increase in precipitation over Greenland (*Finnis and others*, 2007; *Holland and others*, 2007). A similar increase in precipitation can also be expected over the Antarctic Ice Sheets. There is already altimetry evidence for precipitation-driven growth of the interiors of both the Greenland and Antarctic Ice Sheets over the last two decades (*Davis and others*, 2005; *Johannessen and others*, 2005; *Zwally and others*, 2005). Both ice sheets will likely continue to experience increasing accumulation rates, which will partially offset increased marginal ablation and calving rates, over the next century.

1.6 Glaciohydrology and basal sliding

Glaciers and ice sheets influence regional and global climate, and in turn respond to climate change on time-scales from years to millennia. Glaciers and ice sheets presently cover ~ 9.6 % of the Earth's land surface, while at the last glacial maximum (21 KaBP) they covered ~ 22 % (*Marshall*, 2005). The velocity observed at a glacier's surface is the result of three mechanisms of ice flow: (i) internal deformation, (ii) basal slide and (iii) basal sediment deformation. The internal deformation of ice is described as a nonlinear viscosity-dependent relation between stress and strain rate (*Glen*, 1958). This means that small changes in stress result in large changes in strain rate. When ice flows solely due to internal deformation, such as in cold-based glaciers where the basal temperature is < 0 °C, the velocity at the base of the ice column is 0 m/a. Basal slide can only occur when subglacial water is present. Subglacial water, however, is typically only present in warm-based glaciers, where basal temperatures are at the pressure melting point (≈ 0 °C). Basal sediment deformation only occurs when ice flows over a deformable bed, such as a glacial till, and cannot occur when ice is flowing over bedrock. Basal sediment deformation is likely restricted to marginal areas of an ice sheet (*Arnold and Sharp*, 2002). For basal sediment deformation to occur, sediment must fail along a given shear plane. The velocity profile of the deformable sediment is 0 m/a at some depth, where the shear strength

is no longer exceeded, and reaches a maximum at the ice-bed interface (*Tulaczyk and others*, 2000).

Over the past two decades, the Greenland Ice Sheet experienced a widespread acceleration of outlet glaciers (*Rignot and Kanagaratnam*, 2006; *Joughin and others*, 2010), resulting in an increasingly negative mass balance (Section 1.4). Almost all mass balance surveys agree that Greenland's mass loss is concentrated around the low elevation ice sheet periphery, especially around major outlet glaciers, with the high elevation interior exhibiting a slight thickening associated with increased accumulation (*Krabill and others*, 2004; *Luthcke and others*, 2006; *Thomas and others*, 2006; *Velicogna and Wahr*, 2006). At least five distinct mechanisms have been proposed to explain this recent acceleration of outlet glaciers. (i) Observational evidence clearly indicates a link between increased surface meltwater production and enhanced basal sliding velocity on a variety of time-scales (*Zwally and others*, 2002; *Shepherd and others*, 2009; *Bartholomew and others*, 2010). However, in comparison to land-terminating glaciers, enhanced basal sliding appears to explain smaller fractions of enhanced ice displacement in marine-terminating outlet glaciers (*Joughin and others*, 2008a). (ii) It has also been postulated that the recent acceleration of major glaciers, such as Jakobshavn Isbrae, may be a short-term dynamic re-adjustment to a relatively small perturbation of the tidewater terminus (i.e. anomalously high surface or submarine ablation; *Thomas*, 2004). Importantly, this hypothesis suggests that outlet glacier velocities will decrease in a relatively short period of time once the perturbation has been accommodated (i.e. years-scale). (iii) Several studies have recently suggested that observed accelerations stem from a loss of terminus back-stress (*Howat and others*, 2008a; *Joughin and others*, 2008b). This hypothesis suggests a net increase in effective driving stress will result in a long-term enhancement of ice velocities (i.e. centuries-scale). (iv) Alternatively, acceleration may be due to decreased effective basal pressure (ice pressure minus water pressure). The surface ablation-induced thinning of outlet glaciers can

result in an appreciable decrease in basal ice pressure. In marine-terminating glaciers, with no corresponding change in subglacial water pressure (i.e. assuming good hydrologic connectively with the ocean), this results in a net decrease in effective basal pressure (*Pfeffer*, 2007). (v) Finally, recent thermo-mechanical modelling has suggested that ice sheets are susceptible to relatively rapid changes in ice temperature due to slight changes in surface meltwater input to the cryo-hydrologic system (*Phillips and others*, 2010). As ice rheology (or "effective viscosity") is highly sensitive to ice temperature, the warming of ice in lateral shear zones can result in an increase in ice velocities and discharge (*Phillips and others*, 2010; *van der Veen and others*, 2011)

In this thesis I aim to investigate the first of these five proposed mechanisms: the influence of increased surface meltwater production on enhanced basal sliding and the ice dynamics of the Greenland Ice Sheet. An improved understanding of the contemporary influence of surface meltwater on enhanced basal sliding of the Greenland Ice Sheet is of interest in forecasting the potential sea level rise contribution of Greenland over the next century. Periods of enhanced basal sliding (or "speedup events") have been identified in portions of the Greenland Ice Sheet (*Zwally and others*, 2002; *Shepherd and others*, 2009; *Bartholomew and others*, 2010). An increase in the frequency, duration or magnitude of these speedup events of a given glacier will result in an increase in annual ice displacement (or discharge) into the sea (*Bartholomaus and others*, 2008). Studies have identified the vertical velocity component of glacier motion to be important in speedup events, as peaks in mean horizontal speed are associated with peaks in vertical displacement (*Iken and others*, 1983; *Anderson and others*, 2004). Changes in subglacial water storage at the bed are likely responsible for observed changes in vertical displacement. Whenever meltwater inputs exceed the transmission ability of the subglacial conduit system, the subglacial system pressurizes and water is forced into an extensive linked cavity system, "lifting" a glacier off its bed as long as the pressure is maintained. Eventually, the transmission ability of

the conduit system will no longer be exceeded, either by increasing conduit size via melt or deformational opening, or as a result of reduced meltwater input (*Iken and others*, 1983; *Fountain and Walder*, 1998; *Bartholomaus and others*, 2008).

The majority of glaciohydrology research has been conducted on alpine glaciers. Recent observations suggest that the glaciohydrology behavior of the Greenland Ice Sheet is analogous to alpine glaciers (*Shepherd and others*, 2009; *Bartholomew and others*, 2010). In alpine glaciers, englacial and subglacial water flow generally increases rapidly in mid-morning, after the onset of surface melt, and reaches a peak in late afternoon, with a slow decrease to a minimum by early morning (*Fountain*, 1992). In the accumulation zone, firn temporarily stores water and homogenizes variations in the supply rate of surface water to the englacial system. Water must first percolate vertically through the snowpack before reaching the ice surface and beginning to travel horizontally. In contrast, in the ablation zone, the flux of water into the glacier depends directly on the rate of surface melt or rainfall and therefore varies greatly in time (*Fountain and Walder*, 1998). The accumulation zone is mainly drained by distributed englacial and subglacial flow, with some quasi-channels, while meltwater in the ablation zone moves primarily through well-defined channels (*Fountain*, 1992; *Fountain and Walder*, 1998). As the melt water flux to the englacial system only varies slowly in time in the accumulation zone, any englacial channels are usually in steady-state and full of water, so flow is pressurized (*Fountain and Walder*, 1998). In the ablation zone however, englacial conduits are only pressurized near times of peak daily flow or during rainstorms. Flow is therefore generally in an open-channel configuration (*Fountain and Walder*, 1998). The ablation zone englacial system develops more quickly, and to a much greater extent, than the accumulation zone englacial system. The presence of moulins in the ablation zone is evidence of this (*Fountain and Walder*, 1998). The sliding speed of the ablation zone is typically greater than that of the accumulation zone during the diurnal melt peak, but less during the diurnal minimum. Therefore, the ablation zone pulls the

accumulation zone during midday, and is pushed by the accumulation zone during the night (*Fountain and Walder*, 1998).

There is abundant surface water near CU/ETH ("Swiss") Camp and Jakobshavn Isbrae, on the western margin of the Greenland Ice Sheet. In this region, individual lakes can reach sizes of ~ 9 km^2 with water volumes of ~ $5 \cdot 10^7$ m^3. The occurrence of rapid lake outburst events has been observed to migrate inland from the margin throughout the melt season. Although not every lake drains each year, there are around ten major lake outburst events in the Jakobshavn region alone each year (*Box and Ski*, 2007). Assuming a subglacial void thickness of 1 m, the water volume from a large outburst could pressurize a basal area of ~ 97 km^2. This basal pressure could be maintained over a period of hours to days, or even longer if the drainage of the subglacial cavities was constrained by bedrock topography (*Box and Ski*, 2007). In addition to supraglacial lakes, moulins are believed to be an important source of surface meltwater for the subglacial environment. Modeling suggests that supraglacial streams with a discharge as low as 0.15 m^3/s can penetrate down through 300 m of warm-based ice to reach bedrock (*Arnold and Sharp*, 2002).

1.7 Thesis impetus

Changes in glaciohydrology may have been a key contributor to the eventual demise of the Scandinavian Ice Sheet (*Arnold and Sharp*, 2002). Southwest Greenland is projected to warm between 3 and 6 °C by the year 2100 (*ACIA*, 2006). As surface meltwater production increases beyond its long term equilibrium, a greater volume of meltwater can be expected to reach the englacial and subglacial systems in marginal areas. Over the next century, basal sliding rates in this region can be expected to increase in magnitude in response to increased surface meltwater production (*Hanna and others*, 2005; *Bartholomew and others*, 2010). The current uncertainty surrounding the potential sea level rise contribution of the Greenland Ice Sheet makes

understanding the influence of increased surface meltwater production on enhanced basal sliding and the ice dynamics of the Greenland Ice Sheet a pressing question (*IPCC*, 2007).

Sea level rise has diverse geophysical, biological and societal impacts. Although the direct societal impacts of sea level rise are varied, they generally stem from changes in extreme sea levels during floods and storms, rather than changes in mean sea level (*IPCC*, 2007). The societal impacts of sea level rise will be greatest in populated low-lying regions and coastal areas that are susceptible to erosion. The cryospheric contribution to sea level rise now dominates all other terms in the sea level budget (i.e. thermal expansion, terrestrial storage, etc.; *Cazenave and Llovel*, 2010). The sea level rise contribution of fast-moving ice streams and outlet glaciers from ice sheets, however, is not well understood. Presently, forecasts of the cyrospheric contribution to sea level rise are based primarily on surface mass balance (snowfall versus melt) and ignore the possible influence of changes in ice dynamics on sea level rise:

> "Dynamics of the slow-moving ice and of ice shelves are reasonably well understood and can be modeled adequately, but this is not so for fast-moving ice streams and outlet glaciers. Until recently (including IPCC [Intergovernmental Panel on Climate Change], 2001), it was assumed that velocities of these outlet glaciers and ice streams cannot change rapidly, and impacts of climate change were estimated primarily as changes in snowfall and surface melting. Recent observations show that outlet glacier and ice stream speeds can change rapidly, for reasons that are still under investigation. Consequently, [the IPCC Fourth Assessment Report issued in 2007] will not adequately quantify such effects." (*IPCC*, 2007)

By improving our understanding of the influence of surface meltwater on enhanced basal sliding and the ice dynamics of West Greenland, this thesis directly addresses the need

identified by the IPCC Fourth Assessment Report. This thesis makes three main contributions to the glaciology community. Firstly, it has reproduced observations of enhanced basal sliding events in West Greenland with an ice flow model coupled to a hydrology model via a novel, physically-based, sliding rule (Chapters 2 and 3). Secondly, it has established a theoretical basis to expect differences in the enhanced basal sliding resulting from moulin-type and crevasse-type drainage of surface meltwater (Chapter 4). Finally, this thesis has added to the small, but highly relevant, pool of literature that examines the influence of meltwater on the ice dynamics of ice sheets.

Chapter 2

HYDROLOGY MODEL OF THE SERMEQ AVANNARLEQ FLOWLINE

2.1 Chapter introduction

In situ and remotely sensed observations (*Zwally and others*, 2002; *Joughin and others*, 2008a; *Shepherd and others*, 2009; *Bartholomew and others*, 2010) have demonstrated that the surface velocity of marginal ice in Western Greenland exhibits an annual cycle, with peak velocities occurring during the summer melt season. Increased summer ice velocities have been interpreted to reflect enhanced basal sliding due to increased delivery of surface meltwater to the bed. Episodic supraglacial lake drainage events, which have been inferred to temporarily increase subglacial water pressure and result in brief high-velocity events, may be overlaid on this annual ice velocity cycle (*Box and Ski*, 2007; *Das and others*, 2008). While the displacement associated with surface meltwater-induced acceleration is a significant fraction of annual displacement in relatively small land-terminating glaciers, such as the Russell Glacier near Kangerlussuaq, it is a much smaller fraction of annual displacement in major marine-terminating outlet glaciers, such as Jakobshavn Isbrae near Ilulissat (*Joughin and others*, 2008a). In marine-terminating glaciers, the primary seasonal driver of ice velocity is believed to be the annual advance and retreat of the tidewater terminus, which modulates glacier flow through a seasonal back-stress cycle (*Meier and others*, 1994; *Vieli and others*, 2000; *Howat and others*, 2005a; *Joughin and others*, 2008a). Projections of increased Greenland Ice Sheet surface meltwater production over the next century (*Hanna and others*, 2005), provide an impetus to understand the physical basis of the annual velocity cycle of the Greenland Ice Sheet. Recent theoretical (*Schoof*, 2011) and observational (*Sundal and others*, 2011) studies of the Greenland Ice Sheet suggest that future increases in surface meltwater production may result in a transition to more efficient subglacial drainage, and a net decrease in basal sliding velocity.

Studies of alpine glaciers suggest that changes in basal sliding velocity are due to a combination of changes in the rate of glacier water storage (i.e. total glacier water input minus output; *Fountain and Walder*, 1998; *Anderson and others*, 2004; *Bartholomaus and others*, 2008) and changes in flotation fraction (the ratio of subglacial water pressure to basal ice pressure; *Iken and others*, 1983; *Kamb and others*, 1994). Thus, both the total amount of water storage, which is related to englacial water table elevation, and its rate of change influence basal sliding velocity. This explains why "bursts" of basal motion are associated with meltwater "pulses", while sustained meltwater input, which eventually leads to the establishment of efficient subglacial conduits and a negative rate of change of glacier water storage, does not lead to sustained basal sliding. Changes in the rate of glacier water storage (dS/dt) are due to changes in both the rate of meltwater production (i.e. glacier "input") and the rate of water loss from a glacier, governed by the efficiency of subglacial transmissivity via cavities and conduits (i.e. glacier "output"). At the onset of the melt season, the initial surface meltwater input exceeds the transmissivity of the nascent subglacial system. This increases pressure in subglacial cavities and conduits, enhancing basal sliding (e.g. *Fountain and Walder*, 1998; *Anderson and others*, 2004; *Bartholomaus and others*, 2008). Following the onset of melt, both meltwater input and subglacial transmissivity generally increase with time, the former a direct response to meteorological forcing and the latter a response to the widening of the ice-walled conduits due to the dissipation of energy created by viscous friction (*Röthlisberger*, 1972; *Nye*, 1976). Enhanced basal sliding is maintained as long as meltwater input exceeds subglacial transmissivity (i.e. $dS/dt > 0$ or increasing hydraulic head), and is terminated once subglacial transmissivity exceeds dwindling meltwater input (i.e. $dS/dt < 0$ or decreasing hydraulic head). A glacier may experience internal meltwater generation due to geothermal, deformational and frictional heating throughout the year. While subglacial cavities and conduits typically close or diminish in size through internal deformation following the melt season (*Hock and Hooke*, 1993), basal sliding may occur throughout the winter as long as

internal meltwater generation exceeds subglacial transmissivity.

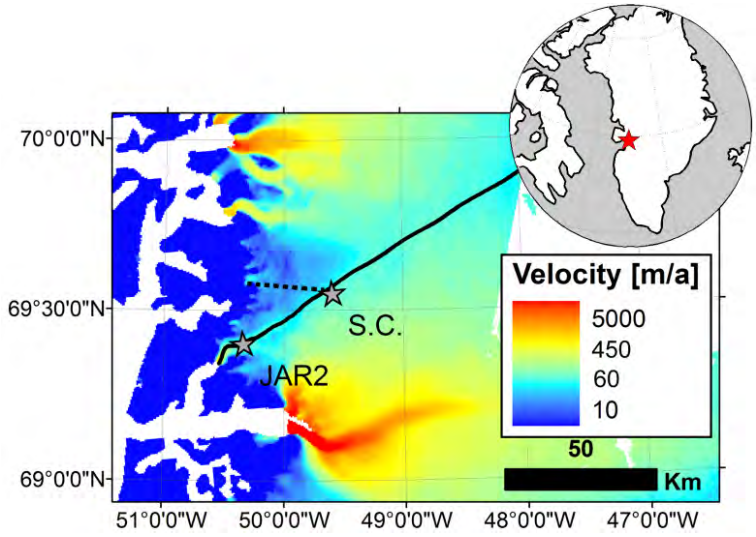

Figure 2.1: *The Sermeq Avannarleq flowline* (*black line*) *overlaid on winter 2005/06 InSAR ice surface velocities* (*Joughin and others, 2010*). *The locations of JAR2 station and Swiss Camp are denoted with stars. The dashed line represents the shortest path to the ice sheet margin from Swiss Camp.*

The desire to quantify the hydrological contribution to enhanced summer basal sliding in the Greenland Ice Sheet provides an impetus to model the magnitude and temporal distribution of changes in the rate of glacier water storage (dS/dt) within the ice sheet. In this chapter, we develop a 1D hydrology model to investigate the annual hydrologic cycle of the Sermeq (Glacier) Avannarleq. Sermeq Avannarleq, a tidewater glacier that calves into a sidearm of Jakobshavn Fiord, is located downstream from CU/ETH ("Swiss") Camp. The ice dynamic flowline for this glacier was determined by following the path of steepest ice surface slope both upstream and downstream from JAR2 automatic weather station (located at 69.42 °N, 50.08°W in 2008) using a digital elevation model of the Greenland Ice Sheet, with 625 m horizontal grid spacing, derived from satellite altimetry and enhanced by photoclinometry (*Scambos and Haran*,

2002). The resultant 530 km flowline runs upglacier from the tidewater terminus of Sermeq Avannarleq (km 0 at 69.37 °N, 50.28 °W), through JAR2 automatic weather station (km 14), within 2 km of Swiss Camp (km 46 at 69.56 °N, 49.34 °W in 2008), to the main ice divide of the Greenland Ice Sheet (km 530 at 71.54 °N, 37.81 °W; Figure 2.1). The tidewater tongue of Sermeq Avannarleq was stable between 1955 and 1985 (*Thomsen and others*, 1988). Field observations suggest that since *c*. 2000 the tidewater tongue, currently ~ 2 km in length, has retreated ~ 2 km and the ice surface of the terminal ~ 5 km of the glacier has become increasingly crevassed

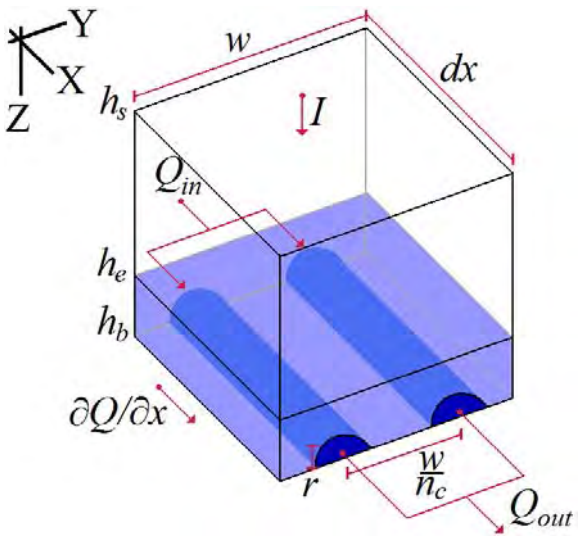

Figure 2.2: *Schematic of the model variables and coordinate system at a given node. Appendix 1 contains a complete list of variable notation.*

2.2 Methods

2.2.1 Hydrology model

We apply a 1D (depth-integrated) hydrology model to the terminal 60 km of the Sermeq Avannarleq flowline to compute subglacial hydraulic head. We conceptualize the glacier hydrologic system as having perfect connectivity between the englacial and subglacial

hydrologic systems (i.e. small hydraulic resistance). The assumption of hydraulic equilibrium between the englacial and subglacial systems is reasonable for capturing the seasonal time-scale behavior of the glacier hydrologic system. In this conceptual model the subglacial hydraulic head is equivalent to the local englacial water table elevation (h_e). We therefore use the terms "subglacial hydraulic head " and "englacial water table elevation" interchangeably. Conduits, which operate at the ice-bed interface, whose geometry evolves through time, control the horizontal water discharge (Q) within the glacier hydrologic system (Figure 2.2). Thus, h_e varies in time and space due to variable conduit inflow and outflow as well as dynamic changes in conduit storage. As this model only has one horizontal layer (or "component") representing both the englacial and subglacial systems, it can be viewed as a simplification of more advanced multi-component models that parameterize the supraglacial, englacial, subglacial and groundwater hydrology components independently (*Flowers and Clarke*, 2002; *Kessler and Anderson*, 2004). As a consequence of not explicitly representing the supraglacial hydrologic system and the hydraulic retention time therein (i.e. firn; *Fountain and Walder*, 1998), surface ablation is routed instantly to the top of the englacial water table. By enforcing water conservation, the rate of change in hydraulic head (or englacial water table elevation) at a given node along the flowline may be calculated from four terms: (i) external meltwater input I (via both surface and basal ablation per unit area) multiplied by the flow band cross width (w), (ii) internal meltwater generation due to viscous melt within the conduits ($\dot{m}/\rho_w$), (iii) horizontal divergence of conduit discharge ($\partial Q/\partial x$), and (iv) changes in conduit storage volume (per unit length along the flowline) through time ($\partial S_c/\partial t$):

$$\varphi w \frac{\partial h_e}{\partial t} = Iw + \frac{\dot{m}}{\rho_w} - \frac{\partial Q}{\partial x} - \frac{\partial S_c}{\partial t} , \qquad \text{Eq. 2.1}$$

where φ is the bulk ice porosity at a given node and w is a cross-flow width. With w = 1,

Equation 2.1 describes the flow per unit width along the flowline. Assuming the ice behaves like a fractured rock-type aquifer rather than a porous medium-type aquifer, this bulk ice porosity (or "macro-porosity") is taken to represent the fractional volume occupied by fully-connected surface-to-bed discrete water storage elements (i.e. the lumped fractional volumes of surface and basal crevasses, conduits, moulins, etc.; *Flowers and Clarke*, 2002). The geometry of these discrete water storage elements remains unspecified (*Kessler and Anderson*, 2004). Observed values of bulk ice porosity generally range between 0.004 and 0.013 in alpine glaciers (*Fountain and Walder*, 1998). Similar to *Kessler and Anderson* (2004), we take bulk ice porosity as 0.01 and assume it is constant in space and time. We also run simulations with φ = 0.005 and 0.015, the water content range constrained by ice temperature modeling of nearby Jakobshavn Isbrae (*Lüthi and others*, 2002).

In the conceptual framework of this model, the total water volume stored per unit length along the flowline at a given node within the glacier hydrologic system (S) is the sum of two terms:

$$S = S_e + S_c \ , \qquad \text{Eq. 2.2}$$

where S_e is the englacial storage volume per unit length and S_c is the subglacial conduit storage volume per unit length. $S_e = \varphi w H_e$, where H_e is englacial water column thickness (h_e - h_b). Assuming a semi-circular conduit geometry, conduit storage volume per unit length (or total cross-sectional area) can be expressed as a function of conduit radius (r):

$$S_c = \frac{\pi r^2}{2}(n_c w) \ , \qquad \text{Eq. 2.3}$$

where n_c is the number of conduits per unit width in the cross-flow (y) direction (defined in

Section 2.2.3).

2.2.2 External meltwater input

At each node along the flowline, external meltwater input (I) occurs as the sum of both surface ablation rate ($\dot{a}_s$) and basal ablation rate ($\dot{a}_b$), according to:

$$I = \dot{a}_s F + \dot{a}_b \ , \qquad \text{Eq. 2.4}$$

where F is the fraction of surface meltwater that reaches the englacial water table. This external meltwater input term does not accommodate episodic supraglacial lake drainage events, which can deliver tremendous amounts of water to a single location

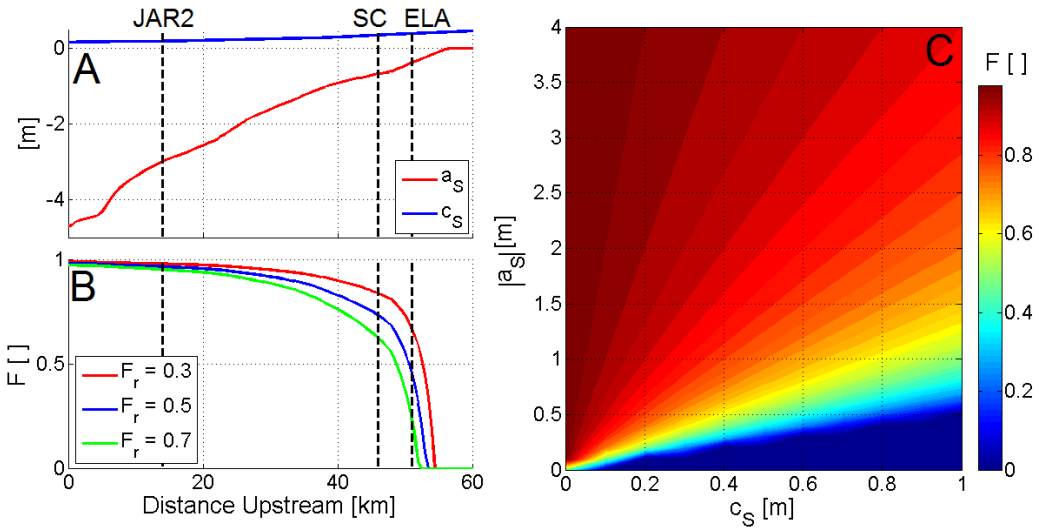

Figure 2.3: A: *Observed annual surface accumulation* (c_s*; Burgess and others, 2010*) *and ablation* (a_s*; Fausto and others, 2009*) *versus distance upstream.* **B:** *Englacial entry fraction* (F) *versus distance upstream with variable values of retention fraction* (F_r). *Vertical dashed lines denote the locations of JAR2, Swiss Camp and the equilibrium line.* **C:** *Englacial entry fraction* (*with* F_r *= 0.5*) *over the observed range of* c_s *and* a_s *values.*

within the glacier hydrologic system (*Das and others*, 2008). Rather, our interest is in the seasonal time-scale response to the annual surface ablation forcing. In the ablation zone, where no firn layer exists, almost all surface meltwater can be expected to reach the glacier hydrologic system. In the accumulation zone, however, meltwater must percolate vertically through the snowpack and firn. As a result of temporary storage or refreezing during this percolation, only a fraction of surface meltwater production reaches the glacier hydrologic system (*Pfeffer and others*, 1991; *Fountain and Walder*, 1998; *Janssens and Huybrechts*, 2000). We approximate the englacial entry fraction based on the ratio of annual surface accumulation (c_s) to annual surface ablation (a_s). This formulation follows *Pfeffer and others* (1991), who suggest that a given fraction of the annual accumulation must melt and saturate before runoff occurs:

$$F = 1 - F_r \left(\frac{c_s}{|a_s|}\right) \text{limit:} \quad F \geq 0 \qquad \text{Eq. 2.5}$$

where F_r is the fraction of surface ablation retained in the firn where annual surface ablation and accumulation are equal. We take F_r as 0.5, which implies that water enters the glacier hydrologic system upstream of the equilibrium line. The along-flowline profile of F varies relatively little when F_r is in the range 0.3 to 0.7 (Figure 2.3).

We interpolate along-flowline annual surface accumulation (c_s) from a previously compiled dataset (*Burgess and others*, 2010). Annual surface ablation (a_s) is taken as a function of elevation, based on previous *in situ* observations (*Fausto and others*, 2009):

$$a_s = \gamma(h_s - h_s^{ela}) - a_s^{ela}\,, \qquad \text{Eq. 2.6}$$

where γ is the present-day ablation gradient ($\Delta a_s/\Delta h_s$; taken as 0.00372; *Fausto and others*, 2009)

and h_s^{ela} is the equilibrium line altitude (taken as 1125 m) and a_s^{ela} is the annual surface ablation at the equilibrium line altitude (taken as 0.4 m). Annual surface ablation is distributed through time to yield a surface ablation rate ($\dot{a}_s$) using a sine function to represent the melt season solar insolation history (c.f. *Pimentel and Flowers*, 2010):

$$\dot{a}_s = \frac{a_s}{2\pi D} \cdot \sin\left(\frac{\pi}{D}(j - j_o)\right), \qquad \text{Eq. 2.7}$$

where j is a given Julian Date, j_o is the Julian Date of melt onset (estimated as $j_o = 0.0183 \cdot h_s + 114$), and D is the duration of the melt season (the Julian Date of melt cessation is similarly estimated as $j_c = -0.0183 \cdot h_s + 248$). While these idealized dates of melt onset and cessation lie within the observed range, this function likely underestimates the date of peak melt, which usually occurs closer to the end of the melt season (Figure 2.4).

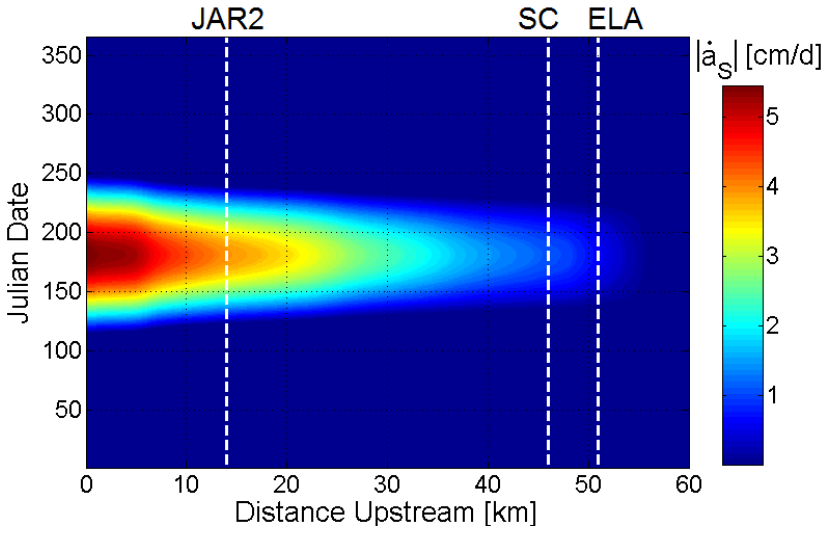

Figure 2.4: *The modeled time-space distribution of absolute surface ablation rate* ($|\dot{a}_s|$). *Vertical dashed lines denote the locations of JAR2, Swiss Camp and the equilibrium line.*

The rate of basal ablation ($\dot{a}_b$) is calculated as:

$$\dot{a_b} = \frac{(Q_d + Q_f + Q_g)}{(\rho_i L)}, \qquad \text{Eq. 2.8}$$

where Q_d and Q_f are the heat input due to deformational (strain) and frictional heating, respectively, Q_g is the geothermal flux, ρ_i is the density of ice (917 kg/m^3), and L is the latent heat of fusion (333,550 J/kg). We assume a geothermal flux of 57 mW/m^2 along the entire flowline (*Sclater and others*, 1980). We also assume that deformational heating is concentrated at the ice-bed interface where it contributes to basal ablation (*Hooke*, 2005). The lack of vertical resolution in the single component hydrology model also necessitates that internally produced meltwater is routed instantaneously to the bed (*Flowers and others*, 2005). Deformational and frictional heating are calculated as

$$Q_d + Q_f = \tau_b\,(\bar{u} + u_b)\ , \qquad \text{Eq. 2. 9}$$

where τ_b is taken as the basal gravitational driving stress, $\bar{u}$ is depth-averaged deformational ice velocity and u_b is basal sliding velocity (*Hooke*, 2005). Both τ_b and $\bar{u}$ are calculated according to the shallow ice approximation using the flow law parameter for ice defined in Section 2.2.5. As this glacier hydrology model is not initially coupled to an ice flow model that incorporates transient basal sliding velocities, we simply parameterize u_b as 15 m/a throughout the ablation zone. Based on observations, this basal sliding velocity can be regarded as characteristic of the Sermeq Avannarleq ablation zone (see Chapter 3). First-order calculations suggest that Q_f and Q_g are small in comparison to Q_d, which makes Q_d the main control on basal ablation.

With a mean value of 3.3 cm (s.d. 1.6 cm) in the ablation zone, annual basal ablation is a very small fraction of annual surface ablation. Beneath the km 7 icefall, however, steep surface

slopes produce a strong deformational heat flux which results in annual basal ablation of 9.3 cm. In comparison, annual surface ablation at the icefall is ~ 3.5 m. These annual basal ablation values are small in comparison to those estimated for nearby Jakobshavn Isbrae, where deformational heating alone is capable of producing > 0.5 m of meltwater annually (*Truffer and Echelmeyer*, 2003). Unlike surface ablation, basal ablation is distributed evenly throughout the year. We neglect submarine basal ablation at the ice-ocean interface, as hydraulic head is prescribed as sea level within the ice tongue.

2.2.3 Conduit discharge

Horizontal divergence of conduit discharge ($\partial Q/\partial x$) is the along-flowline gradient in conduit discharge (Q). For subglacial conduits, where Reynolds numbers are expected to be large, we calculate discharge based on the Darcy-Weisbach equations for turbulent flow in conduits (e.g. *Röthlisberger*, 1972; *Nye*, 1976; *Spring and Hutter*, 1982; *Flowers and others*, 2004; *Pimentel and Flowers*, 2010). As we assume perfect connectivity between the subglacial and englacial systems and that conduits are located at the ice-bed interface, conduit discharge is dependent on the local hydraulic head gradient ($\partial h_e/\partial x$):

$$Q = -\left(\frac{\pi r^2}{2}\right)\sqrt{\frac{8g}{f}D_h\left|\frac{\partial h_e}{\partial x}\right|}\cdot(n_c w)\cdot \text{sign}\left(\frac{\partial h_e}{\partial x}\right), \qquad \text{Eq. 2.10}$$

where g is gravitational acceleration (9.81 m/s^2), f is a friction factor, D_h is the effective hydraulic diameter, r is the conduit radius, n_c is the number of conduits per meter in the cross-flow direction and w is the flow band cross width. We assume a friction factor of 0.05, which is appropriate for turbulent flow in rough walled pipes, where the amplitude of the wall roughness elements is approximately 0.02 times the pipe diameter (*Moody*, 1944). To assess model

sensitivity, we also present a simulation in which *f* is taken as 0.01.

We approximate the observed arborescent nature of subglacial conduit systems (*Fountain and Walder*, 1998) within the framework of our flowline model by making the number of conduits per unit width (n_c) in the cross-flow (y) direction an exponential function of distance upstream from the terminus (x):

$$n_c = n_c^{ter} \cdot \exp\left(\frac{x}{\alpha}\right) , \qquad \text{Eq. 2.11}$$

where n_c^{ter} is the number of conduits per unit width at the terminus (taken as 0.005 or 200 m between conduits) and α is a glacier hydrology length scale controlling the rate of increase in number of conduits per unit width (or the rate of decrease in spacing between conduits) with distance upstream. At any flowline position, the subglacial hydrologic system is represented as a set of non-interacting parallel conduits, with a conduit spacing given by Equation 2.11.

As disequilibrium between the forces promoting conduit opening and closure is permitted in the model (discussed in Section 2.2.5), we must constrain conduit radii between reasonable maximum and minimum dimensions to prevent implausible feedbacks (i.e. permanent closure and unrestricted growth). The need to impose these boundaries may be attributed to the intrinsic limitations of a simplified 1D hydrologic model. The evolving geometry of the subglacial hydrologic system can only be represented accurately with a higher-dimensional model that allows for flow divergence (convergence) away from (towards) highly conductive conduits. A model that incorporates these processes can in principle simulate conduit geometry without prescribed upper and lower bounds for conduit radii. Higher-dimensional modelling would also benefit from a more precise characterization of the bedrock geometry throughout our study area.

Similar to conduit spacing, we also parameterize maximum conduit radius (r_{max}) as an

exponential function of distance upstream from the terminus:

$$r_{max} = r_{max}^{ter} \cdot \exp\left(\frac{-x}{\alpha}\right), \qquad \text{Eq. 2.12}$$

where r_{max}^{ter} is the maximum permissible conduit radius at the terminus (arbitrarily taken as 2 m) and α is the same glacier hydrology length scale as in Equation 2.11, which controls the rate of decrease in maximum conduit radius with distance upstream (r_{min} is taken as 10 % of r_{max}).

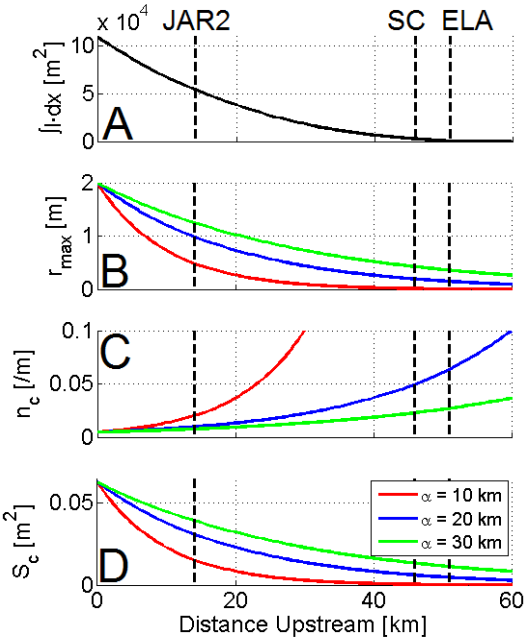

Figure 2.5: A: *Total annual external meltwater input per unit width entering the glacier hydrologic system upstream of a given position* ($\int I \cdot dx$). **B:** *Maximum conduit radius* (r_{max}). **C:** *Conduit spacing in the across flow direction* (n_c). **D:** *Total conduit storage volume per unit length* (S_c). *Line color varies with glacier hydrology length scale* (α). *Vertical dashed lines denote the locations of JAR2, Swiss Camp and the equilibrium line.*

On the assumption that the total conduit storage volume per unit length (S_c) at a given

position along the flowline reflects the integrated annual external meltwater input per unit width that enters the glacier hydrologic system upstream of that position ($\int I \cdot dx$), we can approximate the glacier hydrology length scale (α) as the length scale of the along-flowline $\int I \cdot dx$ profile. A qualitative assessment suggests that α = 20 km renders an along-flowline S_c profile that approximates the $\int I \cdot dx$ profile better than α = 10 or 30 km (Figure 2.5). Thus, we take α = 20 km as the glacier hydrology length scale. Together, Equations 2.11 and 2.12 capture the essence of an arborescent conduit network; namely the decrease in both conduit spacing and conduit radius with distance upstream (Figure 2.6). There are, however, an infinite number of combinations of conduit spacing and radius values that may yield a given discharge, and neither parameter is tightly constrained by field observations. Thus, our maximum and minimum conduit radii may not necessarily reflect actual limits found in nature; they merely reflect limits that, together with the conduit spacing relation we have imposed, lead to reasonable values for the overall transmissivity of the conduit system.

2.2.4 Meltwater generation in conduits

At each node along the flowline, meltwater is generated within the conduits as a consequence of the disspisation of the heat generated by viscous friction in the water; this heat is instanteously conducted to conduit walls (*Nye*, 1976). The rate at which water is produced by internal melt ($\dot{m}$), in units of mass per length per time at a given node, is a function of conduit discharge (Q), local hydraulic head gradient ($\partial h_e/\partial x$) and the latent heat of fusion of ice (L):

$$\dot{m} = \frac{\rho_w g Q}{L} \cdot \left| \frac{\partial h_e}{\partial x} \right| \ . \qquad \text{Eq. 2.13}$$

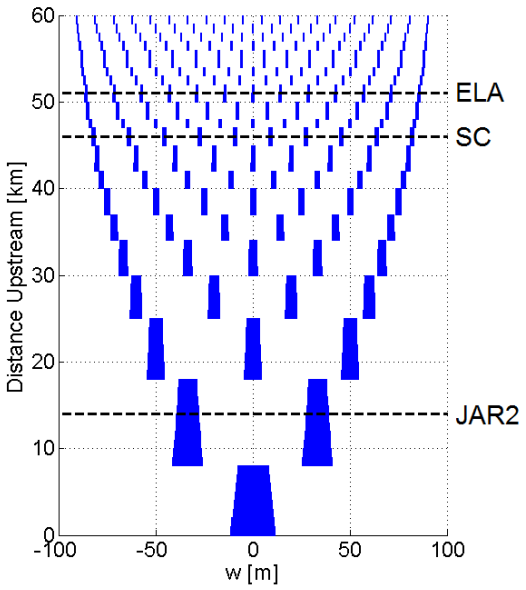

Figure 2.6: *Schematic of the arborescent approximation of the conduit network: number of conduits* (*rounded to nearest integer*) *and maximum conduit diameter* (*5 times exaggerated*) *versus distance upstream when* α *= 20 km. Horizontal dashed lines denote the locations of JAR2, Swiss Camp and the equilibrium line.*

2.2.5 Conduit volume

As the conduits grow and shrink at each node along the flowline, the local conduit storage volume per unit length (S_c; or total cross-sectional area), changes. Conduit storage volume grows through two processes: (i) the volume per unit length created by the ice removed through internal meltwater generation ($\dot{m}/\rho_i$; where $\dot{m}$ is calculated according to Equation 2.13), and deformational opening, which occurs when water pressure (P_w; defined as $\rho_w g H_e$) exceeds ice pressure (P_i; defined as $\rho_i g H_i$). Conversely, conduit storage volume only decreases through deformational closure when $P_i > P_w$. Thus, our model assumes that deformational opening of conduits can occur in response to high subglacial water pressures (*Nye*, 1976; *Ng*, 2000; *Clarke*, 2003). As we are assuming perfect connectivity between the subglacial and englacial systems, the basal water pressure both inside and outside of the conduits may be regarded as equivalent. This

implicitly discounts the possibility of "leakage" of high water pressures from the conduit system to adjacent regions (*Bartholomaus and others*, 2008). As basal ice temperature in the ablation zone is likely at the pressure melting point (*Phillips and others*, 2010), we do not consider conduit closure through refreezing of water within the conduits. The processes that govern the transient rate of change of conduit storage volume per unit length ($\partial S_c/\partial t$) can be expressed as (*Nye*, 1976)

$$\frac{\partial S_c}{\partial t} = \frac{\dot{m}}{\rho_i} - 2A\left(\frac{\pi r^2}{2}\right)\cdot(n_c w)\cdot\left(\frac{|P_i - P_w|}{n}\right)^n \cdot \text{sign}(P_i - P_w)\ , \quad \text{Eq. 2.14}$$

where A is the temperature-dependent flow law parameter (*Huybrechts and others*, 1991) and n is the Glen Law exponent (n = 3). We enhance the temperature-dependent flow law parameter by a factor of three to account for softer Wisconsinan basal ice (*Reeh*, 1985; *Paterson*, 1991), which comprises the bottom ~ 20 % of the ice column along the flowline (*Huybrechts*, 1994).

As recent thermodynamic modeling suggests that basal ice throughout the ablation zone of the Sermeq Avannarleq flowline is at the pressure melting point (*Phillips and others*, 2010), we calculate basal ice temperature (T_i) downstream from the equilibrium line as

$$T_i = 273.15 - \beta H_i\ , \quad \text{Eq. 2.15}$$

where β is the change in melting point with ice thickness (taken as $8.7\cdot10^{-4}$ K/m; *Paterson*, 1994). In the accumulation zone, where downward vertical ice velocities are expected to produce cold basal ice temperatures, we simply prescribe basal ice temperature as 268 K. This is the basal ice temperature predicted just upstream of the equilibrium line by recent thermodynamic modelling (*Phillips and others*, in preparation). We linearly transition from pressure melting point basal ice temperatures in the ablation zone to the cold basal ice temperature of accumulation zone between

the equilibrium line and 5 km upstream of the equilibrium line. The resultant basal ice temperature profile is consistent with the notion that meltwater percolation rapidly warms the ice below the equilibrium line and captures the essence of Sermeq Avannarleq basal ice temperature profiles produced by *Phillips and others* (in preparation; Figure 2.7).

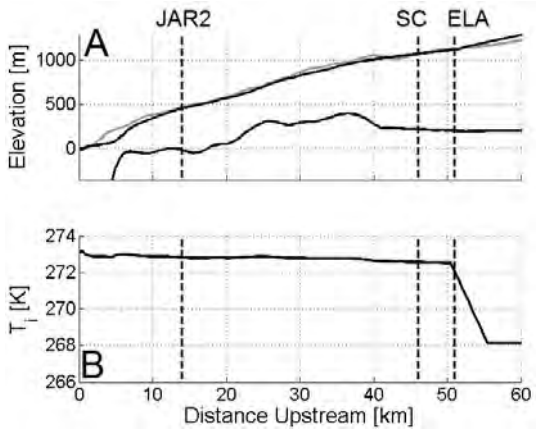

Figure 2.7: A: *Modeled* (*black; Chapter 3*) *and observed* (*grey; Scambos and Haran, 2002*) *ice surface elevation* (h_s) *and observed bedrock topography* (h_b; *Bamber and others, 2001; Plummer and others, 2008*). **B:** *Estimated basal ice temperature* (T_i). *Vertical dashed lines denote the locations of JAR2, Swiss Camp and the equilibrium line.*

2.2.6 Datasets and boundary conditions

This hydrology model employs several observational datasets. Annual surface accumulation and ablation profiles were obtained from previously compiled datasets (*Fausto and others*, 2009; *Burgess and others*, 2010). Both these ice sheet-scale surface climatology datasets use models to interpolate between *in situ* observations, including the four Greenland Climate Network (GC-Net) automatic weather stations along the Sermeq Avannarleq flowline (*Steffen and Box*, 2001). To define ice geometry, we use a modeled ice surface elevation (h_s) profile (see Chapter 3), which compares well with the profile interpolated from a digital elevation model of

the Greenland Ice Sheet derived from satellite altimetry enhanced by photoclinometry (*Scambos and Haran*, 2002; Figure 2.7). A coarse resolution bedrock elevation (h_b) dataset is available along the entire flowline (*Bamber and others*, 2001). While this dataset has nominal 5 km horizontal resolution, actual resolution is dependent on the spacing of airborne flight lines, and thus varies spatially and can exceed 5 km. A finer resolution dataset (nominally 750 m) is available for the terminal 40 km of the flowline (*Plummer and others*, 2008).

Equipotential englacial hydraulic head gradients are theoretically ~ 11 times more sensitive to ice surface slopes than bedrock slopes (*Shreve*, 1972). Thus, first-order ice surface slope (i.e. *regional* or ~ 10 ice thicknesses) may be expected to govern the first-order geometry of subglacial flow direction. For example, the water beneath Swiss Camp can be expected to travel ~ 30 km to the ice sheet margin on an azimuth of ~ 279 ° (i.e. following *regional* ice surface slope; dashed line Figure 2.1). By forcing subglacial water to flow along the ice dynamic flowline to the margin (i.e. following steepest *local* or ~ 1 ice thickness surface slope), subglacial water is being routed ~ 48 km on an azimuth of ~ 225 °. This artificially reduces the hydraulic head gradient ($\partial h_e/\partial x$) by artificially increasing dx. To compensate for this we use simple trigonometry to project the dynamic flowline on the hydrologic coordinates, correcting dx values on a node-by-node basis, and thereby maintain realistic $\partial h_e/\partial x$ values along the length of the flowline.

We apply first-type (specified head) Dirichlet boundary conditions to hydraulic head (h_e). From km 0 to 2, the tidewater terminus, h_e is prescribed as sea level (i.e. h_e = 0 m). We use the cold-to-warm basal ice temperature transition at the equilibrium line (km 51) to approximate the upstream limit of the glacier hydrologic system. We impose a no-flux boundary that extends upwards from the bedrock beneath the equilibrium line to the ice surface at 11 times the local surface slope. This is the steepest theoretical gradient that water travelling through the ice sheet could be expected to take in order to reach the bed at the cold-to-warm basal ice temperature

transition beneath the equilibrium line (*Shreve*, 1972). Thus, upstream of the equilibrium line, there is a portion of the glacier hydrologic system that behaves as a "perched" aquifer (i.e. underlain by cold ice). In this ~ 4 km portion of the flowline, we assume that ice temperature is sufficiently heterogeneous to allow the persistence of englacial conduits (*Catania and Neumann*, 2010). We treat the discharge of these conduits in an identical manner to the conduits downstream of the equilibrium line, except we suspend the processes that govern the transient rate of change of conduit storage volume ($\partial S_c/\partial t$), and prescribe conduit radii as constant (5 cm). We assume that any water entering the ice upstream of the intersection of the perched aquifer and the ice surface refreezes, although we do not perform a full enthalpy solution to incorporate this process as a transient flux. We also assume that basal ablation is zero beneath the cold basal ice in the accumulation zone. The glacier hydrologic system is therefore fully transient over the 49 km between the equilibrium line (km 51) and the tidewater terminus (km 2).

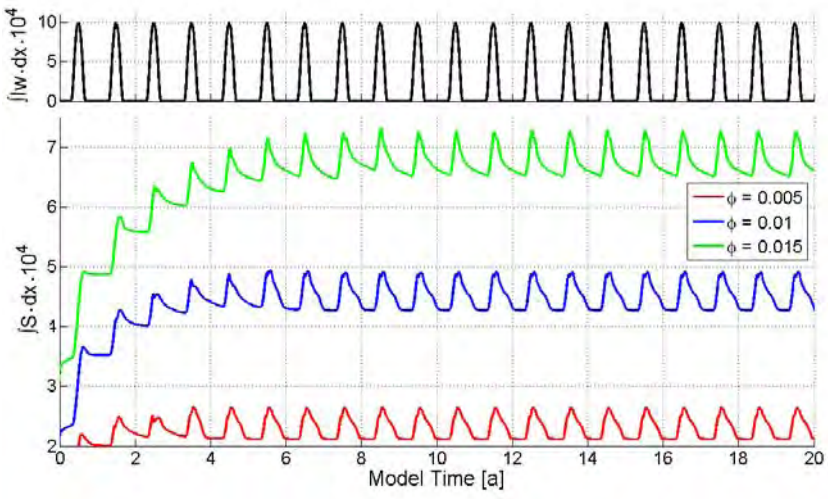

Figure 2.8: *Total flowline prescribed external water input* ($\int Iw \cdot dx$; m^3/a) *and total flowline modeled water storage* ($\int S \cdot dx$; m^3), *for various values of bulk ice porosity* (φ) *during 20-year simulations.*

The differential equations describing transient hydraulic head ($\partial h_e/\partial t$) were discretized in space using first-order finite volume methods (dx = 500 m) with hydraulic head (h_e) at cell centers and fluxes (Q) at cell edges. The semi-discrete set of ordinary differential equations coupled at the computational nodes was then solved using "ode15s", the stiff differential equation solver in MATLAB R2008b, with a 1-day time-step.

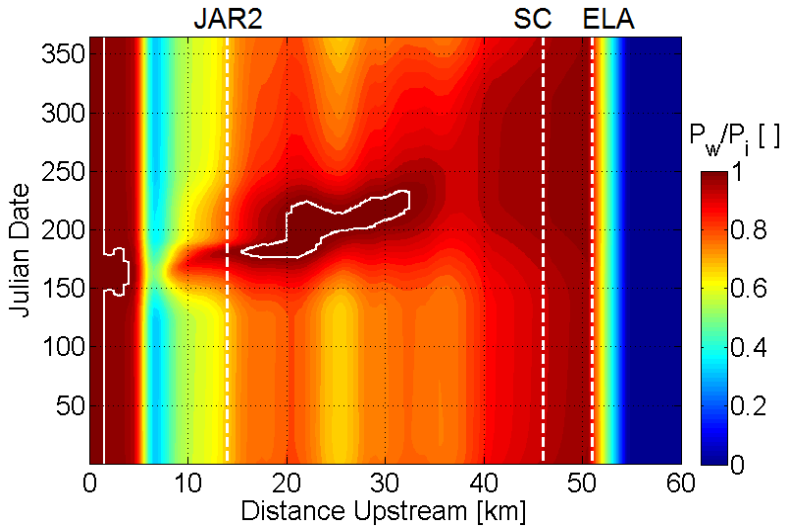

Figure 2.9: *Modeled time-space distribution of flotation fraction* (P_w/P_i). *The white contour line denotes a flotation fraction of 1. Vertical dashed lines denote the locations of JAR2, Swiss Camp and the equilibrium line.*

2.3 Results

The 1D hydrology model achieves a quasi steady-state annual cycle in hydraulic head after ~ 7 years of spin-up (Figure 2.8). Generally, modeled flotation fraction (P_w/P_i) increases with distance upstream to a maximum at the equilibrium line (Figure 2.9). Upstream of the equilibrium line, where basal ice temperatures are assumed to transition from warm-to-cold, the englacial hydrologic system likely behaves as a perched aquifer where it becomes underlain by cold ice. In this region, the high englacial water table elevation should not be interpreted as a

high flotation fraction, because this water pressure is not exerted at the bed. In fact, in this region, we are assuming that no subglacial water is present and hence subglacial water pressure should be zero. The ~ 2 km tidewater tongue remains at flotation year-round (i.e. $P_w/P_i = 1$). In response to meltwater input from surface ablation, flotation fraction exhibits a broad summer peak throughout the ablation zone. This peak occurs progressively later with distance upstream, due to the upstream migration of surface ablation inputs. The modeled hydraulic head fluctuates relatively close to flotation throughout the year; flotation is achieved for a brief period between km 16 and 33.

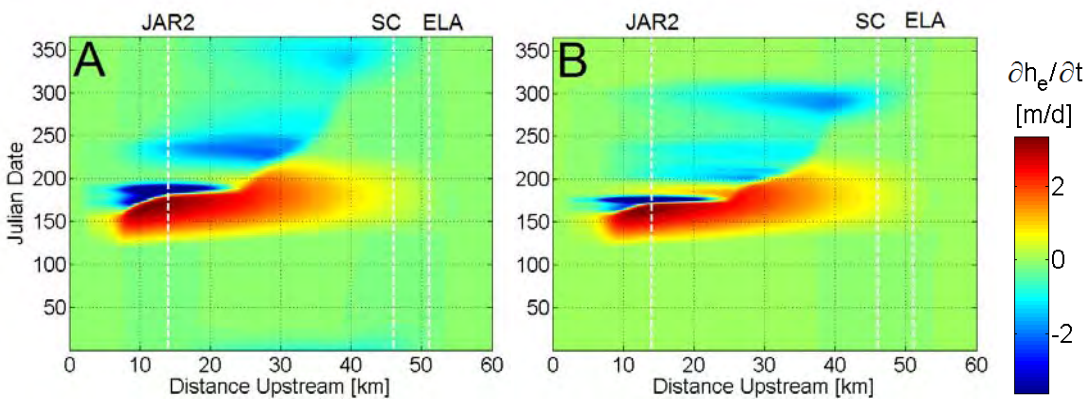

Figure 2.10: *Modeled time-space distribution of the rate of change of hydraulic head (or englacial water table elevation; $\partial h_e/\partial t$) when conduit friction factor (f) equals 0.05* (**A**) *and 0.01* (**B**). *Colorbar saturates below -3.6 m/d. Vertical dashed lines denote the locations of JAR2, Swiss Camp and the equilibrium line.*

The time-space pattern of the rate of change in hydraulic head ($\partial h_e/\partial t$; a proxy for the rate of change in glacier water storage dS/dt) may be conceptualized as the derivative of the time-space pattern of flotation fraction (when the condition $\partial S_c/\partial t << \partial S_e/\partial t$ is satisfied; Figure 2.10). The entire flowline experiences positive rates of glacier water storage (or increasing

hydraulic head) at the beginning of the melt season (as high as 3.6 m/d), and negative rates of glacier water storage (or decreasing hydraulic head) at the end of the melt season (as low as -10.2 m/d). Generally, the total water volume stored along the flowline decreases (or drains) more slowly than it increases (or fills). The magnitude of the modeled annual $\partial h_e/\partial t$ cycle decreases with distance upstream, reaching approximately zero in the vicinity of the equilibrium line (taken as the upstream boundary of temperate basal ice and the englacial hydrologic system). The transition from positive to negative rates of storage also progressively lags with distance upstream. Unlike the positive rates of glacier water storage, which exhibit a smooth time-space distribution, the negative rates of glacier water storage have a more patchy time-space distribution, with certain dates and flowline locations experiencing anomalously fast or slow negative rates of glacier water storage. This is a consequence of the evolution of the subglacial conduit system.

Modeled subglacial conduit storage exhibits sharp along-flowline boundaries between regions of closed and opened conduits (i.e. km 7, 16, 25, 42 and 50; Figure 2.11). This suggests two types of subglacial environments exist: (i) "year-round" (i.e. km 16 to 25 and 42 to 50) and (ii) "seasonally" (i.e. km 7 to 16 and 25 to 42) open subglacial conduit storage. Following the onset of surface ablation, conduits begin to grow upstream from the tidewater terminus (where conduits are open year-round due to a lack of deformational closure pressure in the floating tidewater tongue). When a stretch of seasonally open subglacial conduit storage connects to an upstream stretch of year-round open subglacial conduit storage, there is a temporary anomalously large negative rate of water storage (i.e. decrease in local hydraulic head) as the portion of the flowline underlain by the year-round conduits is drained relatively quickly. Subsequently, the upstream stretch of seasonally open subglacial conduit storage begins to open (due to an increase in local hydraulic head gradient) and the negative rate of water storage returns to a smaller magnitude. The opening of seasonal conduits that serve to connect stretches of year-round

conduit storage are responsible for the patchy time-space distribution of negative rates of glacier water storage.

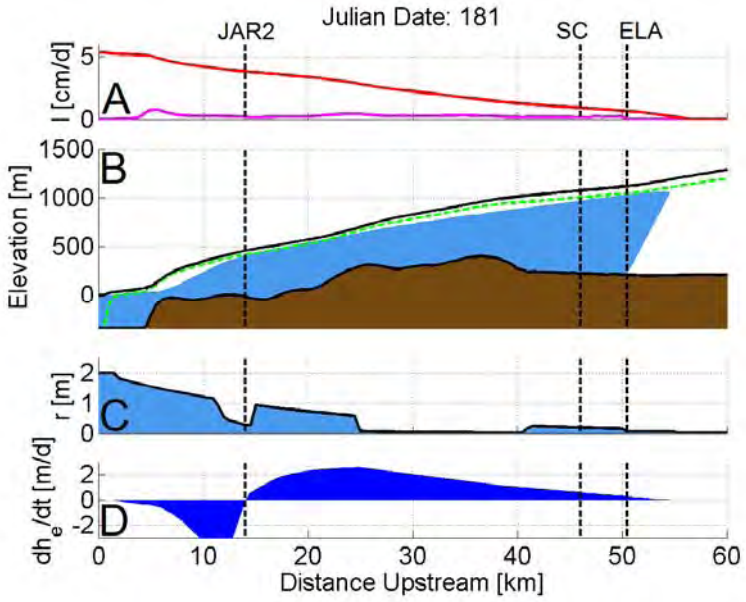

Figure 2.11: *Modeled hydrology along the terminal 60 km of the Sermeq Avannarleq flowline.* **A:** *External meltwater input* (*I*); *both surface* (*red*; a_sF) *and basal* (*magenta*; a_b; *30 times exaggerated*) *ablation.* **B:** *Ice surface elevation* (h_s; *white*), *bedrock elevation* (h_b; *brown*) *and hydraulic head* (*or englacial water table elevation*; h_e; *blue*). *Dashed green line represents the hydraulic head equal to flotation.* **C:** *Conduit radius* (*r*). **D:** *Rate of change in hydraulic head* ($\partial h_e/\partial t$). *Vertical dashed lines identify the positions of JAR2, Swiss Camp and the equilibrium line.*

2.4 Discussion

2.4.1 Hydrology model

Based on the absolute value of flotation fraction, as well as qualitative features in the annual hydraulic head cycle (i.e. a positive phase followed by a negative phase with no significant change during the winter), we conclude that the relatively simple one-component 1D

hydrology model produces a reasonable annual hydrologic cycle along the terminal 60 km of the Sermeq Avannarleq flowline. The modeled hydraulic head oscillates close to flotation throughout the ablation zone of the Sermeq Avannarleq flowline. The suggestion of a relatively high englacial water table is consistent with previous *in situ* observations of flotation fractions between 0.79 and 1.05 in the Pâkitsoq area (69.5 °N, 50.0 °W; *Thomsen and Olesen*, 1991), and between 0.95 and 1.00 in Jakobshavn Isbrae (69.2 °N, 48.7 °W; *Iken and others*, 1993; *Lüthi and others*, 2002). The high modeled flotation fraction along the flowline is due to the dependence of conduit conductivity and discharge on the relative difference between water and ice pressures. Sufficiently high hydraulic head is needed to overcome basal ice pressure and open the conduits. Once open, conduits draw down hydraulic head until reaching a threshold below which hydraulic head is no longer sufficient to counteract basal ice pressure and keep the conduits open. The conduits subsequently close, achieving their minimum prescribed radius (r_{min}), leaving large amounts of residual water stored in the glacier.

Model runs in which bulk ice porosity (φ) is taken as 0.005 and 0.015 return very similar along-flowline profiles of mean annual flotation fraction (Figure 2.12). Thus, a relatively high hydraulic head is likely an inherent feature of a glacier hydrologic system drained solely by conduits. The along-flowline profile of maximum flotation fraction is, however, higher (lower) in the lower (higher) bulk ice porosity simulation. Thus, as currently parameterized, the magnitude of $\partial h_e/\partial t$ is a function of bulk ice porosity. When φ = 0.005, flotation fraction values are unrealistically high in the vicinity of km 25 (~ 1.2 which would be conducive to artesian springs). Bulk ice porosity values as low as 0.0005 have been postulated for alpine glaciers (*Humphrey and others*, 1986). Our sensitivity analysis suggests that increased water storage at the bed must be invoked to produce realistic flotation fraction values when $\varphi << 0.01$. At present, our single component model does not explicitly incorporate the water storage volume created at the ice-bed interface by vertical uplift of the ice sheet (c.f. *Pimentel and Flowers*, 2010). Due to this

limitation a portion of the bulk ice porosity can be assumed to represent the storage volume of discrete voids at the ice-bed interface. In reality, the storage volume at the ice-bed interface is likely a function of hydraulic head, rather than constant in space and time as we have implicitly assumed by using constant porosity.

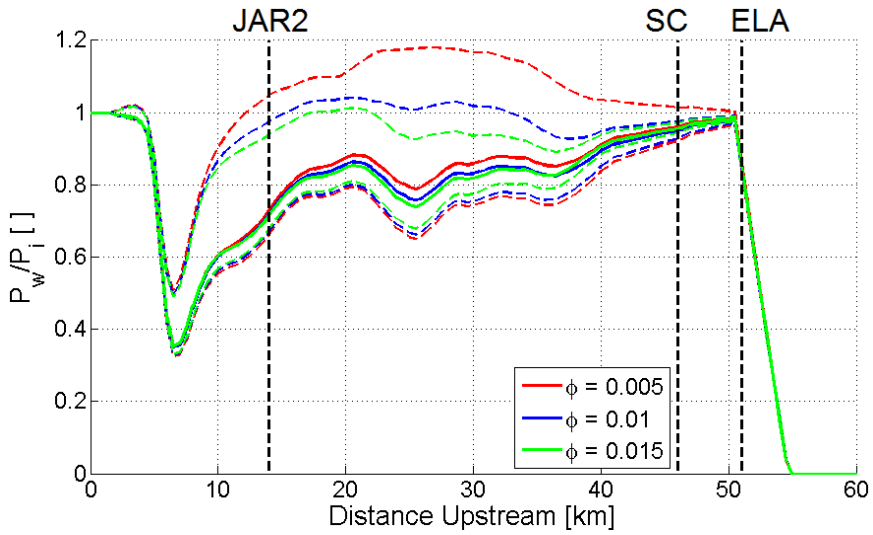

Figure 2.12: *Mean annual flotation fraction* (P_w/P_i) *versus distance upstream for various values of bulk ice porosity* (φ). *Dashed lines represent annual maximum and minimum values. Vertical dashed lines denote the locations of JAR2, Swiss Camp and the equilibrium line.*

The model inference of year-round subglacial conduit storage along certain portions of the flowline (km 16 to 25 and 42 to 50) is supported by limited observations of the persistence of some englacial hydrology features through the winter in the Sermeq Avannarleq ablation zone (*Catania and Neumann*, 2010). The sharp model transitions between year-round and seasonally active conduit storage appear to be due to slight changes in the along-flowline gradient in local hydraulic head ($\partial h_e/\partial x$); subglacial conduit storage volume per unit length (S_c) is proportional to the magnitude of $(\partial h_e/\partial x)^{1.5}$. When a bedrock topography that increases monotonically upstream is imposed, the pockets of year-round subglacial conduit storage form in the same location as

when the observed bedrock topography is imposed (Figure 2.13). As short stretches of year-round subglacial conduit storage appear to form downstream of stretches of relatively steep ice surface topography, we speculate that the along-flowline gradient in ice surface elevation (dh_s/dx) influences the along-flowline gradient in local hydraulic head ($\partial h_e/\partial x$), and hence the location of year-round subglacial conduit storage. When an ice surface topography with sinusoidal undulations (25 m amplitude and 10 km wavelength) is imposed, the pockets of year-round subglacial conduit storage tend to form beneath portions of the flowline with the steepest ice surface slopes (Figure 2.14). Along-flowline gradients in flotation fraction (P_w/P_i) as a result of ice surface topography may also have an influence in the location of year-round subglacial conduit storage. Maintaining year-round subglacial conduit storage through deformational opening, however, could only be expected along portions of the flowline where water pressure exceeds ice pressure year-round. The time-space distribution of modeled flotation fraction suggests that this only occurs in the tidewater tongue (km 0 to 2; Figure 2.9). The model inference that portions of the subglacial conduit storage system may overwinter at the base of the Greenland Ice Sheet to be reactivated the following melt season differs slightly from previous alpine glacier work, which suggests a new channelized subglacial hydrologic system migrates upglacier from the terminus each melt season (*Hubbard and Nienow*, 1997).

During the period of peak decreasing hydraulic head at Swiss Camp (i.e. JD 300 or 325, depending on f parameterization; Figure 2.10) the conduits are drawing down hydraulic head with the efficiency of a semi-circular conduit 40 cm in diameter spaced every 20 m and operating at basal ice and water pressure (i.e. n_c = 0.050 /m and r = 0.20 m). Similarly, during the period of peak decreasing hydraulic head at JAR2 (~ JD 180) the conduit system is parameterized to discharge water with the efficiency of a semi-circular conduit 1.98 m in diameter spaced every 100 m operating at basal ice and water pressure (n_c = 0.010 /m and r = 0.99 m). Although our parameterized conduit system appears to be reasonable, a lack of field observations makes this

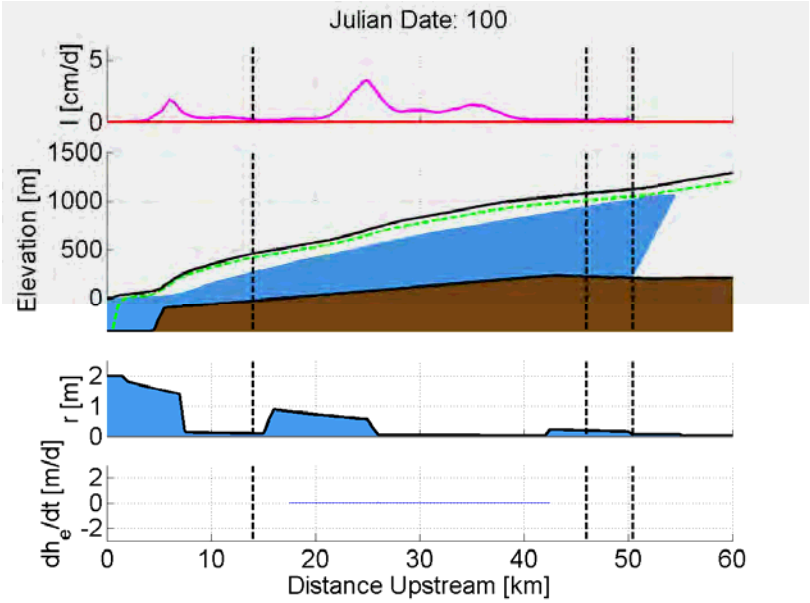

Figure 2.13: *Same as Figure 2.11 except with a modified bedrock topography that increases monotonically upstream*

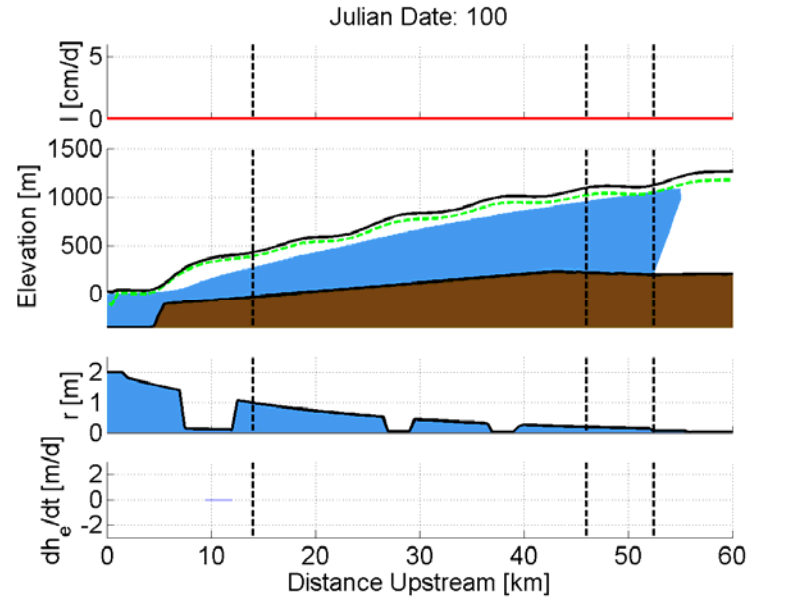

Figure 2.14: *Same as Figure 2.13 except with a sinusoidal pattern (25 m amplitude and 10 km wavelength) imposed on ice surface topography and basal ablation actively disabled.*

configuration speculative. The choice of conduit friction factor (f), which is a measure of resistance (discharge is inversely related to f), appears to influence the timing, but not magnitude, of negative $\partial h_e/\partial t$ values (Figure 2.10). A smaller value of f propagates the perturbation in hydraulic head gradient responsible for conduit opening upstream more quickly than a larger value of f.

Assuming a bulk ice porosity of 0.01, and that the modeled glacier hydrologic cycle is in quasi-steady-state, the mean residence time (t_{res}) of water in the flowline can be calculated as ~ 2.2 years, when w = 1 m, according to

$$t_{res} = \frac{\int S \cdot dx}{\int Iw \cdot dx}, \qquad \text{Eq. 2.16}$$

where $\int S \cdot dx$ is the total flowline modeled water storage (annual mean ≈ 45,000 m^3) and $\int Iw \cdot dx$ is the total flowline prescribed external water input (annual mean ≈ 20,000 m^3/a; Figure 8). The integral notation ($\int \cdot dx$) refers to integration of continuous values over the entire length of flowline (i.e. all x values). Assuming bulk ice porosities of 0.005 and 0.015, the mean residence times are ~ 1.1 and 3.3 years, respectively. This relatively short residence time suggests that the glacier hydrologic system can be expected to respond to external meltwater forcings on a relatively short time-scale (i.e years rather than decades).

2.4.2 Relevance to basal sliding

In the chapter introduction we reviewed the notion that variations in basal sliding velocity can be attributed to variations in the rate of change of glacier water storage (i.e. dS/dt) in alpine glaciers (*Kamb and others*, 1994; *Fountain and Walder*, 1998; *Anderson and others*, 2004; *Bartholomaus and others*, 2008). This conceptual model of basal sliding has recently been extended to the Greenland Ice Sheet (*Bartholomew and others*, 2010). Below, we present both

remotely sensed and *in situ* velocity data from the Sermeq Avannarleq flowline that suggest that observed periods of enhanced basal sliding generally correspond to modeled periods of positive rates of change in glacier water storage (or increasing hydraulic head), while periods of reduced basal sliding conversely correspond to modeled periods of negative rates of change in glacier water storage (or decreasing hydraulic head).

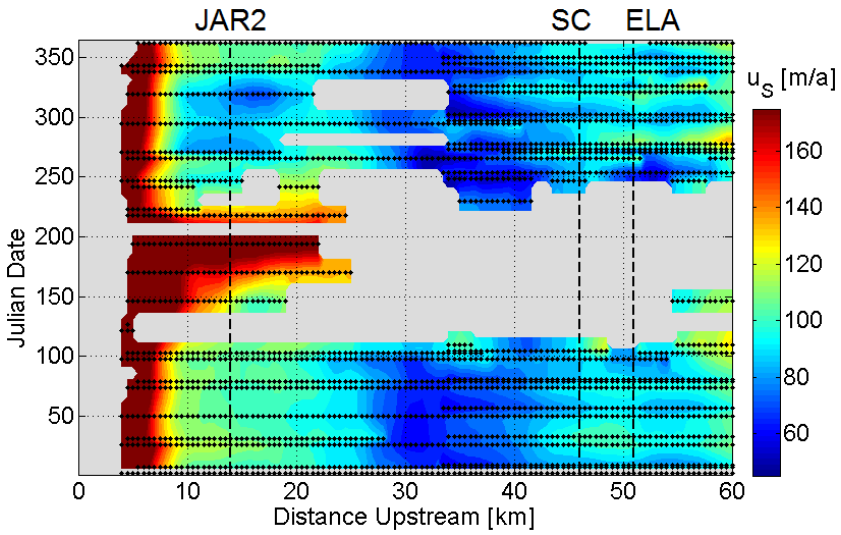

Figure 2.15: *Annual ice surface velocity cycle along the terminal 60 km of the Sermeq Avannarleq flowline* (*colorbar saturates at 175 m/a*). *Dotted black lines indicate individual InSAR velocity profiles. Vertical dashed lines denote the locations of JAR2, Swiss Camp and the equilibrium line.*

Given the proximity of Sermeq Avannarleq to Jakobshavn Isbrae, multiple 2005 and 2006 Interferometric Synthetic Aperture Radar (InSAR)-derived ice surface velocity profiles are available for the terminal 60 km of the Sermeq Avannarleq flowline (*Joughin and others*, 2008b). Linear interpolation between these profiles yields a time-space velocity plot (Figure 2.15). While summer velocities are not available upstream of km 22, the region around JAR2 exhibits a distinct annual velocity cycle. This cycle consists of a summer speedup event, in which velocities

exceed winter velocity, followed by a fall slowdown event, in which velocities fall below winter velocity. These observed velocity anomalies may be interpreted as periods of enhanced and suppressed basal sliding that qualitatively correspond to periods of modeled increasing and decreasing hydraulic head.

High frequency differential global positioning system (GPS) measurements have been acquired at Swiss Camp since June 1996, providing daily resolution of the annual ice surface velocity cycle for the last twelve years (*Larson and others*, 2001; *Zwally and others*, 2002; Figure 2.16). In accordance with the InSAR observations, these *in situ* GPS observations reveal that the ice at Swiss Camp also experiences a summer speedup event, in which ice velocities increase above winter velocities, followed by a fall slowdown event, in which ice velocities decrease below winter velocities. The summer speedup event varies in peak magnitude and timing over the twelve-year record, presumably due to variable surface climatology and meltwater forcing, as well as local supraglacial lake drainage events. While the model is not forced with an observed melt history, the modeled period of increasing hydraulic head (i.e. JD 150 to 200) generally matches the timing of the observed speedup event. The observed slowdown event, however, follows the observed speedup event in relatively quick succession. The modeled peak in decreasing hydraulic head lags the modeled peak in increasing hydraulic head by 125 to 150 days (depending on the value of f; Figure 2.10).

We speculate that this apparent delay in the negative $\partial h_e/\partial t$ phase, which is due to a delay in opening the upstream conduits, is a consequence of 1D hydrological modeling. A 2D (xy) hydrological model would better capture changes in englacial water table gradient at Swiss Camp by allowing conduit discharge both parallel and perpendicular to the ice dynamic flowline. Presently, by forcing water to flow along the entire ice dynamic flowline to the terminus, the 1D model essentially requires the perturbation in local hydraulic head gradient that initiates conduit opening to slowly migrate from the terminus upstream to Swiss Camp. In reality, the glacier

hydrologic system near Swiss Camp is governed by both along-flow and across-flow hydraulic head gradients ($\partial h_e/\partial x$ and $\partial h_e/\partial y$ respectively). A 2D (*xy*) model would better represent the influence of bedrock topography on subglacial discharge, by allowing subglacial discharge to concentrate in topographic low points (*Shreve*, 1972; *Flowers and others*, 2005). Due to this concentration of discharge, 2D models are inherently more capable of developing larger and more efficient conduits than 1D models.

Based on the qualitative agreement between observations of a strong annual ice velocity cycle and the modeled annual glacier hydrologic cycle, we propose that the terminal 50 km of the Greenland Ice Sheet's Sermeq Avannarleq flowline behaves akin to an alpine glacier, whereby the summer speedup event is caused by inefficient subglacial drainage and positive rates of change of glacier water storage (i.e. $dS/dt > 0$; or increasing hydraulic head), while the fall slowdown event reflects the establishment of efficient subglacial drainage and negative rates of change of glacier

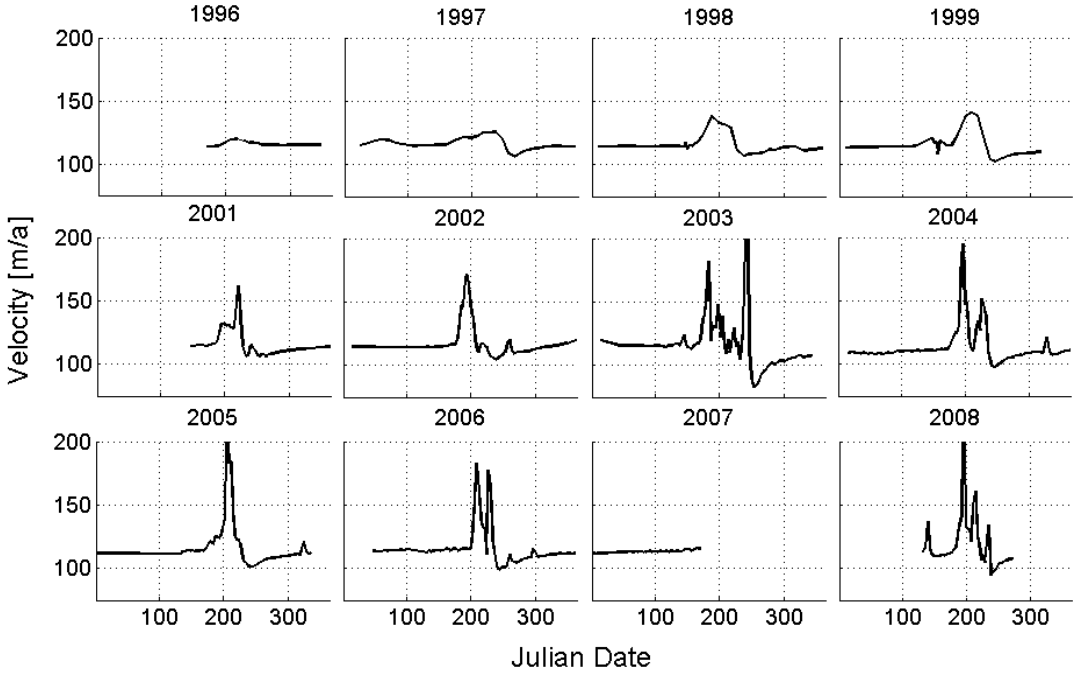

Figure 2.16: *Observed GPS annual velocity cycle at Swiss Camp over the 1996 to 2008 period.*

water storage (i.e. $dS/dt < 0$; or decreasing hydraulic head). A notable departure from the alpine analogy, however, is the model inference that subglacial conduit storage may be capable of overwintering beneath the Greenland Ice Sheet to be re-activated the following melt season, rather than migrating upglacier from the terminus each melt season as observed in alpine glaciers (*Hubbard and Nienow*, 1997). The recovery of both basal sliding velocities and rates of change of hydraulic head ($\partial h_e/\partial t$) to winter values shortly after the fall slowdown, suggests that the glacier hydrologic system is capable of re-pressurizing to maintain winter sliding. Presumably, this occurs by: (i) a reduction in transmissivity due to conduit closure and (ii) continued meltwater input, largely via basal ablation due to geothermal, frictional and deformation (strain) heat fluxes rather than internal meltwater generation ($\dot{m}/\rho_w$).

2.5 Chapter summary remarks

We developed a relatively simple one-component 1D hydrology model to track glacier water storage and discharge through time. In this model, glacier water input is prescribed based on observed ablation rates, while glacier water output occurs through conduit discharge. Conduit discharge varies in response to the dynamic evolution of conduit radius. The hydrology model suggests that subglacial hydraulic head (or, equivalently in this model, englacial water table elevation) annually oscillates relatively close to flotation, even reaching flotation for brief periods along certain stretches of the flowline. This is consistent with the few available borehole observations of englacial water table elevation. Alternatively imposing idealized bedrock and ice surface topographies suggests that along-flowline gradients in ice surface elevation (or ice surface slope), rather than along-flowline gradients in bedrock elevation (or bedrock slope), control the locations of year-round subglacial conduit storage. The sharp transitions between subglacial environments that support year-round and seasonally open subglacial conduit storage

are likely due to slight along-flowline changes in the local englacial hydraulic head gradient. A calculated mean glacier water residence time of ~ 2.2 years infers that large amounts of water are stored in the glacier throughout the year. The glacier hydrologic system can therefore be expected to respond to external meltwater forcings (i.e. reorganize) on a relatively short time-scale. A qualitative comparison between the observed annual ice velocity cycle and the modeled annual cycle of glacier water storage suggests that enhanced (suppressed) basal sliding occurs during periods of positive (negative) rates of glacier water storage. Thus, we speculate that the terminal 50 km of the Sermeq Avannarleq flowline likely experiences a basal sliding regime similar to that of an alpine glacier. Considering the inherent limitations of 1D modeling, the timing of the modeled increasing and decreasing hydraulic head events is also reasonable.

Chapter 3

ICE FLOW MODEL OF THE SERMEQ AVANNARLEQ FLOWLINE

3.1 Chapter introduction

While the majority of the Greenland Ice Sheet terminates on land (*Pfeffer and others*, 2008), its contributions to sea level rise due to ice discharge via marine-terminating outlet glaciers and negative surface mass balance are approximately equal (*van den Broeke and others*, 2009). The ice discharge of marine outlet glaciers is the sum of deformational and basal sliding velocities. Both observations and models have indicated that the ice discharge from Greenland's marine-terminating glaciers is highly sensitive to calving front perturbations, which are subsequently propagated upstream via longitudinal coupling (*Holland and others*, 2008; *Joughin and others*, 2008b; *Nick and others*, 2009). It has been suggested that relatively small increases in surface ablation may result in disproportionately large increases in ice discharge via basal sliding (*Zwally and others*, 2002; *Bartholomew and others*, 2010). More recently, however, some researchers have speculated that projected increases in surface meltwater production will likely result in a net decrease in basal sliding velocity, due to a transition from relatively inefficient to efficient subglacial drainage (*Schoof*, 2011; *Sundal and others*, 2011). This motivates the need to quantitatively address the physical relation between glacier hydrology and basal sliding velocity. We therefore seek a computationally efficient means of reproducing the observed spatial and temporal patterns of basal sliding so that we can ultimately explore the likely response of ice dynamics to climate change scenarios.

Recent interferometric synthetic aperture radar (InSAR) observations have confirmed that an annual velocity cycle is spatially widespread in the marginal ice of Western Greenland (*Joughin and others*, 2008a). This annual velocity cycle is most likely due to seasonal changes in basal sliding velocity. The Sermeq Avannarleq ablation zone, in Western Greenland, exhibits an

annual ice velocity cycle similar to that of an alpine glacier. This cycle is comprised of a summer speedup event followed by a fall slowdown event. A qualitative comparison of this annual ice velocity cycle to a modeled annual glacier water storage cycle suggests that enhanced (suppressed) basal sliding generally occurs during periods of positive (negative) rates of glacier water storage (Chapter 2). This notion is consistent with alpine glacier studies that suggest that changes in basal sliding velocity are due to changes in the rate of glacier water storage (dS/dt or the net of glacier water inputs and outputs; *Kamb and others*, 1994; *Anderson and others*, 2004; *Bartholomaus and others*, 2008; *Bartholomaus and others*, submitted). Thus, three general basal sliding states exist: (i) when meltwater input exceeds the transmission ability of the subglacial hydrologic system (i.e. $dS/dt > 0$ or increasing storage and hydraulic head), (ii) when the transmission ability of the subglacial hydrologic system exceeds the local input of meltwater (i.e. $dS/dt < 0$ or decreasing storage and hydraulic head), and (iii) when meltwater input and subglacial transmission ability are in approximate equilibrium. In alpine settings, peak basal sliding velocity can be expected when dS/dt reaches a maximum (although there is some evidence that peak sliding velocity exhibits a slight phase-lag behind peak dS/dt values; *Bartholomaus and others*, 2008). Following this maximum, both dS/dt and basal sliding velocity decrease, and dS/dt becomes negative during the later part of the melt season.

Our goal is to reproduce the annual ice velocity cycle observed in the Sermeq (Glacier) Avannarleq ablation zone with coupled ice flow and hydrology models. In this chapter, we couple a 2D (vertical cross-sectional) ice flow model to the 1D (depth-integrated) glacier hydrology model presented in Chapter 2 via a novel sliding rule. We do not attempt to reproduce inter-annual variations in the annual ice velocity cycle, but rather achieve a quasi-steady-state mean annual cycle that may serve as a basis for future work investigating the influence of inter-annual variations in surface ablation on annual ice displacement. The 530 km Sermeq Avannarleq flowline runs upglacier from its tidewater terminus (km 0 at 69.37 °N, 50.28 °W) to

the main ice divide of the Greenland Ice Sheet (km 530 at 71.54 °N, 37.81 °W; Figure 3.1). This flowline lies within 2 km of three Greenland Climate Network (GC-Net; *Steffen and Box*, 2001) automatic weather stations: JAR2 (km 14.0 at 69.42 °N, 50.08°W), JAR1 (km 32.5 at 69.50 °N, 49.70 °W) and CU/ETH ("Swiss") Camp (km 46.0 at 69.56 °N, 49.34 °W; all positions reported for 2008). In the previous chapter, we suggest that in the Sermeq Avannarleq ablation zone: (i) hydraulic head (or englacial water table elevation) oscillates around levels that are relatively close to flotation throughout the year, and (ii) observed periods of enhanced (suppressed) basal sliding qualitatively correspond to modeled periods of increasing (decreasing) hydraulic head. In this chapter, we develop a semi-empirical (and thus site-specific) sliding rule to relate variations in the modeled rate of change of glacier water storage (or hydraulic head) to observed variations in basal sliding velocity. The coupled glaciohydrology model accurately reproduces the ice geometry and mean annual velocity observed in the Sermeq Avannarleq ablation zone, and is also capable of reproducing the broad features of the annual velocity cycle through variations in basal sliding velocity.

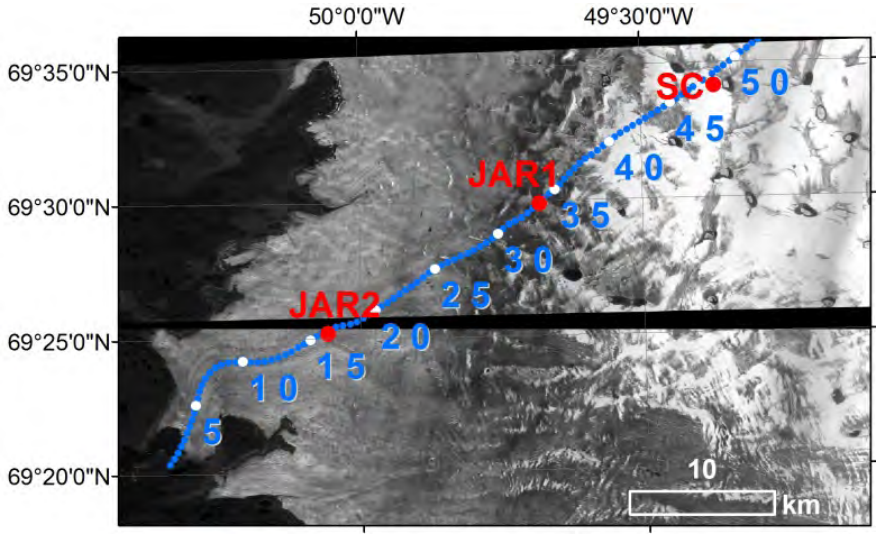

Figure 3.1: *The terminal 55 km of the Sermeq Avannarleq flowline overlaid on a panchromatic WorldView-1 image* (*acquired 15 July 2009*) *with distance from the terminus indicated* (*km*). *GC-Net weather station locations are denoted in red.*

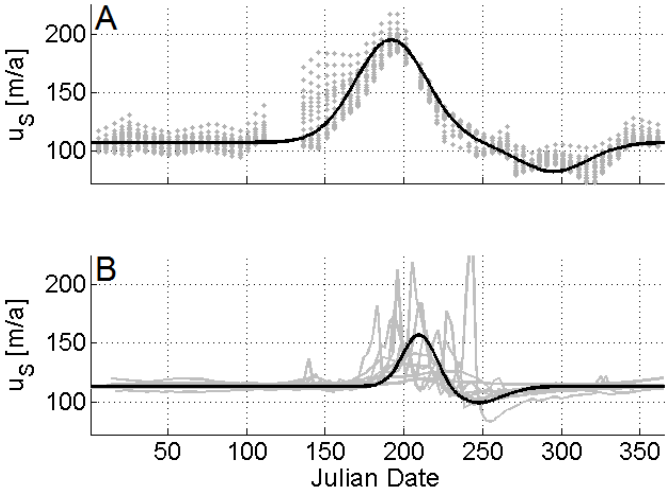

Figure 3.2: A: *Observed InSAR ice surface velocities over the 2005 to 2006 period at JAR2.* **B:** *GPS ice surface velocities over the 1996 to 2008 period at Swiss Camp. Black lines denote the bi-Gaussian characterization of the annual ice surface velocity cycle at each station* (*Equation 3.1*).

3.2 Methods

3.2.1 Observed annual ice surface velocity cycle

We characterize the annual ice surface velocity cycle at two locations along the terminal portion of the Sermeq Avannarleq flowline using both *in situ* and remotely sensed ice surface velocity observations (*Larson and others*, 2001; *Zwally and others*, 2002; *Joughin and others*, 2008a). This characterization provides a representative mean annual ice velocity cycle against which the accuracy of the modeled annual ice velocity cycle can be assessed. Twelve years (1996 to 2008) of *in situ* differential global positioning system (GPS) observations of ice surface velocity are available at ~ 3 day intervals at Swiss Camp, while two years (2005 and 2006) of interferometric synthetic aperture radar (InSAR) ice surface velocity profiles have been complied for the terminal 60 km of the Sermeq Avannarleq flowline (Chapter 2). These InSAR profiles can be used to infer the annual ice velocity cycle at ~ 28 day intervals in the vicinity of JAR2

automatic weather station (km 10 to 18). At both sites, these observations reveal that the ice moves at winter velocity until the beginning of a summer speedup event, which approximately coincides with the onset of summer melt. The summer speedup event is followed by a fall slowdown event, in which ice velocities temporarily fall below winter velocities. The magnitude of the fall slowdown event is both smaller in magnitude and shorter in duration than the summer speedup event. Over the 12-year record at Swiss Camp, both the summer speedup and fall slowdown events vary in peak magnitude and timing (Chapter 2).

We approximate the annual ice surface velocity cycles at JAR2 and Swiss Camp using two Gaussian curves. These Gaussian curves are overlaid on mean winter velocity, with one curve representing the summer speedup event and the other curve representing the fall slowdown event. The use of a bi-Gaussian function allows the amplitude, width and timing of both the summer and fall events to be independently parameterized. Thus, we characterize surface velocity (u_s) as a function of day of year (j) according to:

$$u_s = u_w + (u_{\max} - u_w) \cdot \exp\left(\frac{j - j_{\max}}{d_{\max}}\right)^2 - (u_w - u_{\min}) \cdot \exp\left(\frac{j - j_{\min}}{d_{\min}}\right)^2$$

Eq. 3.1

where u_w is the mean winter velocity, which is taken as the mean observed velocity between day of year 300 (27 Oct) and 100 (10 Apr), and u_{max} and u_{min} represent the summer maximum and fall minimum velocities respectively. The remaining four parameters govern the timing and shape of the speedup and slowdown curves. j_{max} (j_{min}) represents the date of summer maximum (fall minimum) velocity, while d_{max} (d_{min}) represents the duration of the summer (fall) velocity anomaly. These four parameters were manually evaluated by visual inspection for each year of data. For j_{max} and j_{min} we assess an estimated uncertainty equivalent to the temporal resolution of

the velocity data (i.e. ± 3 and ± 28 days for Swiss Camp and JAR2 respectively). No meaningful level of uncertainty can be assessed for d_{max} and d_{min}. For Swiss Camp, this bi-Gaussian characterization was fit to each year of GPS velocity observations between 1996 and 2008 (except for 2007, for which complete data is not available), and the mean value of each parameter was used to approximate the mean annual velocity cycle. For JAR2, this bi-Gaussian characterization was fit to the aggregated 2005 and 2006 velocity data (Figure 3.2; Table 3.1).

Table 3.1: *The mean value of each parameter in the bi-Gaussian characterization of the annual surface ice velocity cycle* (*Equation 3.1*) *for JAR2 and Swiss Camp. The standard deviations of each parameter over the 1996 to 2008 period are shown for Swiss Camp in parentheses*.

	JAR2	Swiss Camp
u_w [m/a]	107	113 (2)
u_{max} [m/a]	195	158 (43)
u_{min} [m/a]	82	99 (8)
j_{max} [d]	192	210 (9)
j_{min} [d]	295	247 (9)
d_{max} [d]	32	15 (8)
d_{min} [d]	32	23 (3)

3.2.2 Ice flow model

We apply a longitudinally coupled 2D (vertical cross-section) ice dynamic model to describe the velocity at 25 vertical levels at each node along the Sermeq Avannarleq flowline. This model solves for the transient rate of change in ice thickness ($\partial H/\partial t$) according to mass conservation:

$$\frac{\partial H}{\partial t} = b - \frac{\partial Q}{\partial x} \qquad \text{Eq. 3.2}$$

where b represents the annual mass balance and $\partial Q/\partial x$ represents the horizontal divergence of ice discharge. To generate quasi-steady-state ice geometry and velocity fields, the ice flow model was subjected to a 1000-year spin-up that was initialized with present-day ice geometry and a "cooler" climate with no hydrology cycle (described more fully in Section 3.2.6). We characterize quasi-steady-state as the transient solution of Equation 3.2 that exhibits no significant changes in ice geometry or velocity during the last 100 years of spin-up. An alternative approach would be to produce a transient present-day snapshot of flowline ice geometry and velocity by spin-up under a prescribed climate. While this transient spin-up would certainly be more desirable for modelling future ice geometry and velocity fields, it is sensitive to uncertainties in the prescribed climate forcing. As our intent is to study the mean annual ice velocity cycle, we employ a steady-state, rather than transient, spin-up. Following the 1000-year spin-up, an annual basal sliding cycle is introduced via the coupled 1D (depth-integrated) hydrology model (Chapter 2). We use a semi-empirical three-phase sliding rule (described in Section 3.2.5) to convert variations in the rate of change of hydraulic head calculated by the hydrology model into variations in basal sliding velocity.

3.2.3 Annual balance

Annual mass balance of a given ice column is the sum of the annual surface accumulation (c_s), surface ablation (a_s), basal accumulation (c_b) and basal ablation (a_b):

$$b = c_s + Fa_s + c_b + a_b \qquad \text{Eq. 3.3}$$

where F is the hydrologic system entry fraction based on the ratio of annual surface accumulation

to annual surface ablation (Chapter 2). As *F* is the fraction of ablation assumed to enter the glacier hydrology system and eventually runoff, the quantity 1-*F* is the fraction of ablation that refreezes and does not leave the ice sheet. Annual surface accumulation is prescribed as the observed mean annual value over the 1991 to 2000 period (*Burgess and others*, 2010). Annual accumulation values increase from ~ 0.25 m at the Sermeq Avannarleq terminus to a maximum (~ 0.5 m) at ~ 100 km upstream, and decrease back down to ~ 0.25 m at the main flow divide (~ 530 km upstream). In the ablation zone, annual surface ablation (a_s) is taken a function of elevation, based on previous *in situ* observations:

$$a_s = \gamma(h_s - h_s^{ela}) - a_s^{ela} \qquad \text{Eq. 3.4}$$

where γ is the present-day ablation gradient ($\Delta a_s/\Delta h_s$; taken as 0.00372; *Fausto and others*, 2009), h_s is the ice surface elevation, h_s^{ela} is the equilibrium line altitude and a_s^{ela} is the annual surface ablation at the equilibrium line altitude (taken as 0.4 m). While the regional equilibrium line altitude was ~ 1250 m over the 1996 to 2006 period (*Fausto and others*, 2009), we impose an equilibrium line altitude of 1125 m, observed over the 1995 to 1999 period, on the annual surface ablation function (*Steffen and Box*, 2001). As our desire is to produce a quasi-steady-state ice geometry, we assume that the historical equilibrium line is more representative of the steady-state surface mass balance forcing. Annual surface abalation is distributed through time to yield surface ablation rate ($\dot{a}_s$) using a sine function to represent the melt season solar insolation history (Chapter 2).

In the ice flow model, we assume that annual basal accumulation is negligible ($c_b \approx 0$ m/a) and that basal ablation is only significant beneath the floating tidewater tongue. We use the relative magnitudes of ice and englacial water pressures (P_i and P_w respectively), to determine which flowline nodes are grounded ($P_i \geq P_w$) or floating ($P_i < P_w$) in a given timestep. During

spin-up and quasi-steady-state we prescribe a constant basal (submarine) ablation rate of a_b = 5 m/a to floating nodes. This prescribed rate is likely a gross underestimate of the contemporary submarine ablation rate at Sermeq Avannarleq, which is estimated to exceed 25 m/a (*Rignot and Jacobs*, 2002; *Rignot and others*, 2010). The ice flow model, however, does not reproduce a floating ice tongue when contemporary submarine ablation rates are imposed for the duration of spin-up. As our intent is to reproduce the contemporary ice geometry as accurately as possible in quasi-steady-state, we depart from the present-day submarine ablation rate as it is most likely not in equilibrium with the present-day tongue geometry.

3.2.4 Ice discharge

We include longitudinal coupling stress ($\bar{\tau}'_{xx}$) as a perturbation (constant through the ice column) to the driving stress from the shallow ice approximation (*van der Veen*, 1987; *Marshall and others*, 2005):

$$\tau(z) = -\rho_i g(h_s - z)\frac{\partial h_s}{\partial x} + 2\frac{\partial}{\partial x}(H\bar{\tau}'_{xx}) \qquad \text{Eq. 3.5}$$

Depth-averaged longitudinal coupling stress ($\bar{\tau}'_{xx}$) is calculated following the approach outlined by *van der Veen* (1987). This formulation derives longitudinal coupling stress by solving a cubic equation describing equilibrium forces independently at each node, based on ice geometry and prescribed basal sliding velocity (u_b):

$$0 = \bar{\tau}'^{\,3}_{xx}\left\{2\frac{\partial h_s}{\partial x}\left(\frac{\partial H}{\partial x} - \frac{\partial h_s}{\partial x}\right) + H\frac{\partial^2 h_s}{\partial x^2} - \frac{1}{2}\right\} + \bar{\tau}'^{\,2}_{xx}\left\{\tau\left(\frac{2}{3}\frac{\partial H}{\partial x} - \frac{3}{2}\frac{\partial h_s}{\partial x}\right)\right\} + \ldots$$
$$\bar{\tau}'_{xx}\left\{\tau^2\left(3\frac{\partial h_s}{\partial x}\frac{\partial H}{\partial x} + \frac{3}{2}H\frac{\partial^2 h_s}{\partial x^2} - 2\left(\frac{\partial h_s}{\partial x}\right)^2 - \frac{1}{6}\right)\right\} + \cdots$$
$$\tau^3\left(\frac{2}{5}\frac{\partial H}{\partial x} - \frac{1}{4}\frac{\partial h_s}{\partial x}\right) + \frac{1}{2A}\frac{\partial u_b}{\partial x} \qquad \text{Eq. 3.6}$$

The longitudinally coupled ice velocity due to deformation (u_d) may be computed at a given depth (z) by numerical integration of the equation for horizontal shear ($\partial u_d/\partial z$; e.g. *van der Veen*, 1987; *Marshall and others*, 2005):

$$\frac{\partial u_d}{\partial z} = 2A\left(\rho_i g(h_s - z)\frac{\partial h_s}{\partial x}\right)^{n-1}\left[-\rho_i g(h_s - z)\frac{\partial h_s}{\partial x} + 2\frac{\partial}{\partial x}\left(H\bar{\tau}'_{xx}\right)\right] \quad \text{Eq. 3.7}$$

where $\partial h_s/\partial x$ represents ice surface slope and n is the Glen Law exponent (n = 3). We enhance the temperature-dependent flow law parameter (A; *Huybrechts and others*, 1991) by a constant factor E across the entire model domain (c.f. *Parizek and Alley*, 2004). This is done to account for softer Wisconsinan basal ice that comprises the bottom ~ 20 % of the ice within the Sermeq Avannarleq flowline (*Huybrechts*, 1994). We evaluate quasi-steady-state ice geometry and velocity fields following spin-up with E ranging between 2 and 4 (*Reeh*, 1985; *Paterson*, 1991), as *in situ* borehole deformation measurements beneath nearby Jakobshavn Isbrae support $E > 1$ (*Lüthi and others*, 2002). At each x node, we use the steady-state ice temperature at 90 % depth derived from independent thermodynamic modeling of the flowline (*Phillips and others*, in preparation) to calculate the flow law parameter. The majority of shear occurs at or below this depth. Thus, along-flowline variations in basal ice temperature result in along-flowline variations in the flow law parameter. Integration of Equation 3.7 yields the vertical distribution of deformational ice velocity (u_d) with depth:

$$u_d(z) = u_b + 2A\left(\rho_i g\frac{\partial h_s}{\partial x}\right)^{n-1}\left[\rho_i g\frac{\partial h_s}{\partial x}\frac{(h_s - z)^{n+1} - H^{n+1}}{n+1} - 2\frac{(h_s - z)^n - H^n}{n}\frac{\partial}{\partial x}\left(H\bar{\tau}'_{xx}\right)\right] \quad \text{Eq. 3.8}$$

We obtain local ice discharge (Q) by numerically integrating the deformational velocity profile (Equation 3.8) from a prescribed basal sliding velocity boundary condition (u_b):

$$Q = u_b H + \int_{h_b}^{h_s} u_d(z) \cdot dz \qquad \text{Eq. 3.9}$$

The numerical integration is performed at each horizontal node along the flowline using 25 evenly-spaced vertical nodes (i.e. $dz = H/25$). Basal sliding velocity is prescribed via a semi-empirical sliding rule that depends on subglacial water pressure (or hydraulic head) calculated by the hydrology model (Section 3.2.5). Thus, basal sliding velocity (u_b) is the main variable that couples the ice flow model to the hydrology model. Following the approach taken in previous ice sheet flowline models (*van der Veen*, 1987; *Parizek and Alley*, 2004), we neglect lateral effects stemming from divergence and convergence (i.e. $\partial Q/\partial y$ and $\bar{\tau}'_{xy}$). While this assumption is likely valid in interior regions of sheet flow, it is less valid near the ice sheet margin, where strong divergence and convergence likely occur. We acknowledge the potential influence of lateral effects on modeled ice velocities in Section 3.3.

3.2.5 Three-phase basal sliding rule

The sliding rules employed in glacier models have improved with advances in the conceptualization of basal sliding. Initial sliding rules prescribed basal sliding velocity as proportional to driving stress, on the assumption that higher driving stress results in greater till deformation (*Weertman*, 1957; *Kamb*, 1970). Observations that subglacial water was capable of enhancing ice velocities by lubricating and pressurizing the subglacial environment led parameterizations in which basal sliding velocity was taken as proportional to subglacial water pressure (*Iken*, 1981; *Iken and others*, 1983), as well as sliding rules that included both effective water pressure (P_i-P_w) and driving stress (*Bindschadler*, 1983; *Iken and Bindschadler*, 1986).

Recent models have utilized basal sliding rules that are Coulomb friction analogues, whereby basal sliding depends on effective water pressure but only occurs above a given effective water pressure, and is bounded not to exceed a given "global limit" when local water pressure achieves flotation (*Schoof*, 2005; *Pimentel and Flowers*, 2010). To have predictive value, a basal sliding rule should ideally be capable of reproducing observed sliding velocities from first principles of hydrology and frictional force balance with a minimum of free parameters. In this section we describe a novel three-phase basal sliding rule that focuses on the hydrologic aspect of basal sliding, by regulating the magnitude and sign of a perturbation to background basal sliding velocities using modeled rates of change in subglacial hydraulic head. While this rule fails the long-term goal of a first principles sliding law, it nonetheless honors simultaneous observations of sliding and the hydrologic system, and has site-specific value.

The Swiss Camp GPS data clearly show that ice velocity is on average ~ 14 % faster during the winter than in the midst of the fall slowdown (113 and 99 m/a respectively; Table 3.1). The fall velocity minimum corresponds closely with the velocity predicted by internal deformation alone. We interpret this as suggesting that Swiss Camp experiences significant background basal sliding velocity during the winter, which is suppressed during the fall velocity minimum. Thus, at Swiss Camp (and similarly at JAR2), the background basal sliding velocity may be approximated as the difference between observed mean winter (u_w) and fall minimum (u_{min}) velocities. We linearly interpolate these basal sliding velocities along the flowline, up to km 70, at which point the ice most likely becomes cold-based (*Phillips and others*, in preparation; Figure 3.3). This background basal sliding velocity profile is used as the basal sliding boundary condition of the ice flow model during spin-up. The year-round persistence of the englacial hydrologic system in Sermeq Avannarleq ablation zone provides a mechanism capable of maintaining year-round basal sliding (*Catania and Neumann*, 2010). Following spin-up, we overlay an annual basal sliding velocity cycle on the background basal sliding

velocity.

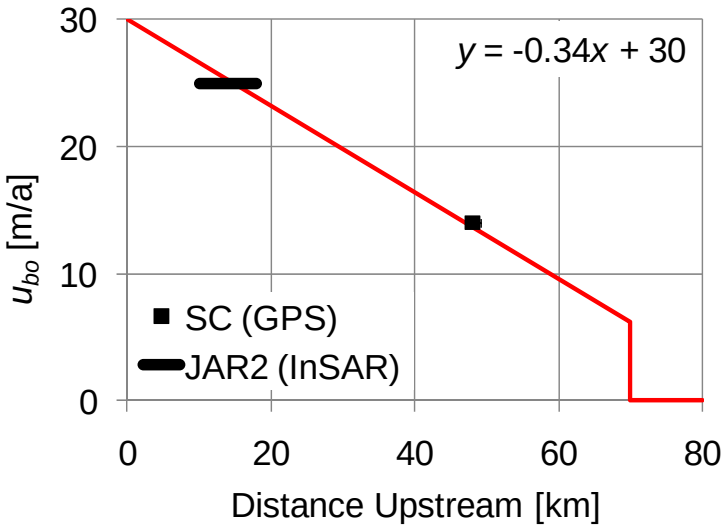

Figure 3.3: *Annual background basal sliding velocity* (u_{bo})*, estimated in the vicinity of JAR2 and at Swiss Camp as the difference between mean winter* (u_w) *and fall minimum* (u_{min}) *velocities, is linearly interpolated along the remainder of the flowline to upstream km 70.*

We relate the observed annual ice velocity cycle with the modeled annual hydraulic head cycle using a semi-empirical, and thus site-specific, sliding rule. Rate of change in hydraulic head can be taken as a surrogate for rate of change in glacier water storage (dS/dt). Following theoretical developments in alpine glaciohydrology (*Kamb and others*, 1994; *Anderson and others*, 2004; *Bartholomaus and others*, 2008), we propose a sliding rule that depends on the sign of the rate of change in hydraulic head ($\partial h_e/\partial t$; Chapter 2) to prescribe "speedup" during periods of increasing hydraulic head and "slowdown" during periods of decreasing hydraulic head. This results in a three-phase basal sliding rule that is capable of imposing: (i) background velocity during the winter when $\partial h_e/\partial t \approx 0$, (ii) enhanced basal sliding during positive rates of change of water storage (or increasing hydraulic head; $\partial h_e/\partial t > 0$), and (iii) the suppression or absence of basal sliding during negative rates of change of glacier water

storage (or decreasing hydraulic head; $\partial h_e/\partial t < 0$). We accomplish this by conceptualizing basal sliding velocity (u_b) as the sum of background basal sliding velocity (u_{bo}) and a perturbation (Δu_b):

$$u_b = u_{bo} + \Delta u_b \qquad \text{limit: } u_b \geq 0 \qquad \text{Eq. 3.10}$$

The alpine glaciohydrology literature suggests that we may expect basal sliding velocity to scale nonlinearly with the rate of change of hydraulic head (i.e. $\Delta u_b \propto (\partial h_e/\partial t)^m$; where $m > 1$; *Anderson and others*, 2004; *Bartholomaus and others*, 2008). We impose $m = 2$ and express the perturbation to the background basal velocity (Δu_b) as:

$$\Delta u_b = \begin{cases} \left(n_c k \left|\frac{\partial h_e}{\partial t}\right|\right)^m \cdot \text{sign}\left(\frac{\partial h_e}{\partial t}\right) & \text{if } \left|\frac{\partial h_e}{\partial t}\right| \geq 0.1 \text{ m/d} \\ 0 & \text{if } \left|\frac{\partial h_e}{\partial t}\right| < 0.1 \text{ m/d} \end{cases} \qquad \text{Eq. 3.11}$$

where n_c is the number of subglacial conduits per meter in the across ice-flow direction (Chapter 2) and k is a tunable site-specific sliding coefficient. The number of conduits per meter in the across ice-flow direction reflects changes in the configuration of the subglacial drainage system with distance upstream, from relatively large widely-spaced conduits near the terminus to relatively small closely-spaced conduits near the equilibrium line. These differences in subglacial hydrologic system configuration can be expected to result in differing sliding responses to a given rate of change in hydraulic head. As the sign of the rate of change in englacial hydraulic head ($\partial h_e/\partial t$) changes between positive and negative, it effectively modulates the sign of Δu_b (i.e. specifying whether the perturbation is acting to enhance or suppress background basal sliding velocity). By parameterizing Δu_b so that it goes to zero when $|\partial h_e/\partial t|$ falls below a critical threshold (taken as 0.1 m/d), Equation 3.11 provides the framework for three phases of basal

sliding: (i) only background basal velocity (i.e. no perturbation) during the winter (when $|\partial h_e/\partial t|$ < 0.1 m/d), (ii) a positive perturbation to background basal sliding velocity during increasing englacial hydraulic head ($\partial h_e/\partial t$ > 0.1 m/d), and (iii) a negative perturbation to background basal sliding velocity during decreasing englacial hydraulic head ($\partial h_e/\partial t$ < -0.1 m/d).

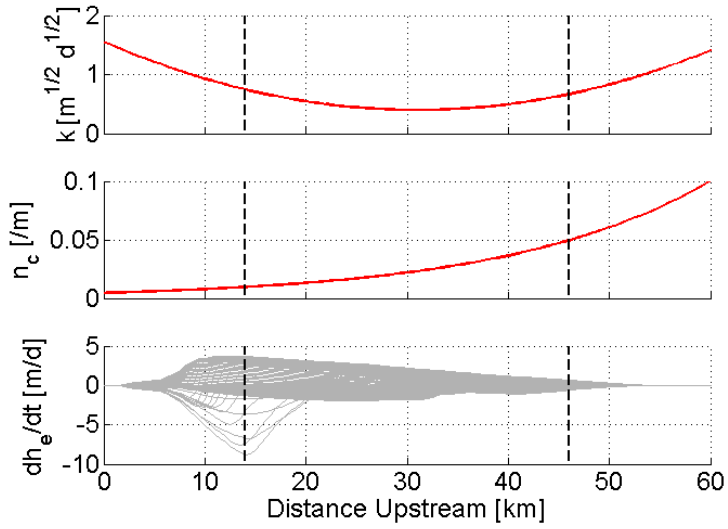

Figure 3.4: *Along flowline distributions of sliding coefficient* (*k*), *subglacial conduits per meter in the across-flow direction* (n_c; *Chapter 2*) *and rate of change in englacial head* ($\partial h_e/\partial t$; *Chapter 2*) *used to calculate basal sliding perturbation* (*Equation 3.11*).

We find the observed velocities at JAR2 and Swiss Camp are reasonably reproduced when *k* varies between 0 and 2 $m^{½}d^{½}$ along the terminal 60 km of the flowline (Figure 3.4). Sliding coefficient values are tuned to reach a minimum at km 30, based on the observation that the annual velocity cycle at JAR1 ($u_w \approx 75$ m/a, $u_{max} \approx 107$ m/a and $u_{min} \approx 63$ m/a; *Colgan and others*, 2009) is damped in comparison to JAR2 and Swiss Camp. We speculate that this is an artifact of the hydrology model, which forces subglacial water to flow over the bedrock high at km 30. In reality, subglacial water likely flows around this bedrock high in the *y* direction, resulting in reduced $\partial h_e/\partial t$ values along the km 25 to 40 portion of the flowline. Upstream of the

equilibrium line (km 51), the englacial hydrologic system likely behaves as a "perched aquifer" and is underlain by cold ice (Chapter 2). We linearly transition basal sliding velocity to 0 m/a over this ~ 4 km zone.

3.2.6 Input datasets and boundary conditions

Following Chapter 2, the ice flow model is initialized with observed ice surface and bedrock topography (*Bamber and others*, 2001; *Scambos and Haran*, 2002; *Plummer and others*, 2008). During spin-up, the observed surface balance was perturbed by decreasing surface ablation in order to reproduce the observed present-day ice geometry. We evaluate quasi-steady-state ice geometry and velocity fields following spin-ups with surface ablation decreased by a factor ranging between 0 and 75 %. Previous Greenland Ice Sheet modeling studies have implemented similar surface mass balance corrections during spin-up (i.e. incorporating "colder glacial climates") in order to achieve equilibrium present-day ice geometries (i.e. *Huybrechts*, 1994; *Ritz and others*, *1997*; *Parizek and Alley*, 2004). This adjustment is typically justified by the notion that the present-day Greenland Ice Sheet geometry reflects colder climatic conditions. Both the observed surface accumulation (*Burgess and others*, 2010) and ablation (*Fausto and others*, 2009) datasets use ice sheet-scale models to interpolate between *in situ* observations, including the GC-Net automatic weather stations along the Sermeq Avannarleq flowline (*Steffen and Box*, 2001; Figure 3.1).

The differential equations describing transient ice thickness ($\partial H/\partial t$) were discretized in space using first-order finite volume methods (dx = 500 m). The semi-discrete set of coupled ordinary differential equations at the computational nodes were then solved using "ode15s", the stiff differential equation solver in MATLAB R2008b. During the 1000-year spin-up the ice flow model is solved with a time-step (dt) of 10 years. Following spin-up, the ice flow model was solved concurrently with the hydrology model (Chapter 2) with a 2 day time-step. Post-spin-up,

basal sliding velocity is calculated according to the three-phase sliding rule described above. We apply a second-type (zero flux) Neumann boundary condition at the main ice flow divide (i.e. we take $Q = 0$ and $\partial h_s/\partial x = 0$ at $x = 530$ km). We treat the floating terminal node ice discharge (or calving flux) as transient, whereby it is computed as the difference between the ice discharge of the adjacent upstream node and the annual balance of the terminal node (rather than prescribing an equilibrium calving flux which is equal to the integral of the upstream surface balance).

The 1D (depth-integrated) hydrology model tracks glacier water storage and discharge through time; glacier water input is prescribed based on observed ablation rates, whereas glacier water output occurs through conduit discharge. Conduit discharge varies in response to the dynamic evolution of conduit radius. When coupled, the ice flow and hydrology models receive the same surface ablation forcing at each time-step. The ice flow model updates the ice thickness vector (and hence equilibrium line position) used by the hydrology model each time-step, while the hydrology model updates the englacial hydraulic head vector used by the basal sliding rule. Specific parameterizations used in the hydrology model are shown in Table 3.2 (c.f. Figure 2.11).

Table 3.2: *Specific parameterization of the 1D* (*depth-integrated*) *hydrology model* (*notation follows Chapter 2*).

Variable	Definition	Value
α	glacier hydrology length scale	20 km
φ	bulk ice porosity	0.01
F_r	firn meltwater rention fraction	0.5
Q_g	geothermal flux	57 mW/m^2
f	conduit friction factor	0.05
n_c^{term}	conduit spacing at terminus	0.005 /m
r_{max}^{term}	maximum conduit radius at terminus	2 m

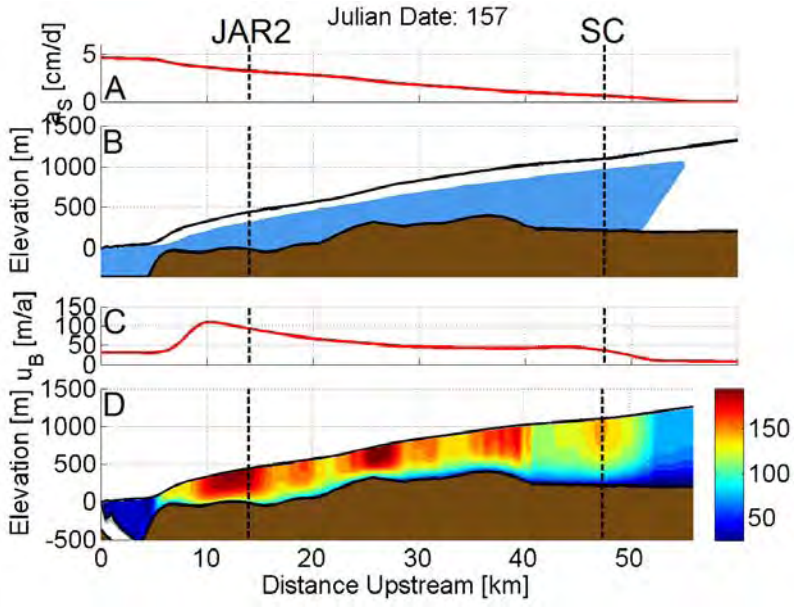

Figure 3.5: *Modeled hydrology and ice flow along the terminal 60 km of the Sermeq Avannarleq flowline.* **A:** *Surface ablation rate* (a_S). **B:** *Ice surface elevation* (h_s; *white*), *bedrock elevation brown* (h_b; *brown*) *and hydraulic head (or englacial water table) elevation* (h_e; *blue; Chapter 2*). **C:** *Semi-empirical basal sliding velocity based on the calculated rate of change in hydraulic head* ($\partial h_e/\partial t$). **D:** *Bedrock elevation brown* (h_b; *brown*) *and horizontal ice velocity* ($u(z)$ *in m/a; color scale saturates at 150 m/a*). *Vertical dashed lines identify the positions of JAR2 and Swiss Camp*

3.3 Results

We assessed quasi-steady-state ice geometry and velocity fields of the ice flow model against observed ice surface elevation (*Scambos and Haran*, 2002) and velocity (*Joughin and others*, 2008b) profiles following a 1000-year spin-up (Figure 3.5). We explored a range of Wisconsinan enhancement factors (2 to 4) and perturbations in surface ablation (decreases of 0 to 75 %). While this range of Wisconsinan enhancement factors all produce ice surface geometries that are similar to the observed profile, a factor of $E = 3$ best reproduces the observed ice surface

velocity field (Figure 3.6). Conversely, while decreases of 0 to 75 % in the contemporary surface ablation rate (a_s) do not greatly influence ice velocities upstream of km 25, they produce significantly different terminus locations and ice surface geometry. We find that the observed ice surface geometry is best reproduced with a 50 % decrease in surface ablation over contemporary observed rates (Figure 3.7). This change in surface ablation may represent either: (i) the increase in surface ablation that has occurred since the termination of the last glaciation, or (ii) error in our ability to correctly delineate the flowline in the accumulation zone. For example, if the flowline length has been underestimated in the accumulation zone, modeled ice discharge across the equilibrium line will be underestimated, and the model would require a decrease in surface ablation rate to maintain the observed ice geometry. Under all E and a_s spin-up scenarios, the ice flow model overestimates ice velocities in the km 25 to 40 portion of the flowline. We speculate that this is an artifact of the 1D (flowline) character of the ice flow model. A 1D (flowline) model would be expected to overestimate ice discharge (and hence ice velocity) in reaches of divergent ice flow. Thus, the overestimation of ice velocities in the vicinity of JAR1 (km 25 to 40) suggests that divergent ice flow may be occurring in this region. Alternatively, this region of overestimated ice velocities may point to the need for along-flowline variations in the Wisconsinan enhancement factor. As basal ice temperature is at the pressure melting point beneath this portion of the flowline, the relatively soft Wisconsinan ice may have been eliminated through basal melt. Generally, however, the ice flow model achieves a quasi-steady-state ice geometry and velocity field that closely matches observations throughout the Sermeq Avannarleq ablation zone (i.e. terminal 60 km of the flowline).

We assess the background basal sliding velocities at JAR2 and Swiss Camp as 25 and 14 m/a, respectively, based on the difference between mean winter and fall minimum velocities (i.e. u_w - u_{min}; Figure 3.3). The observed ice geometry of the Sermeq Avannarleq ablation zone is

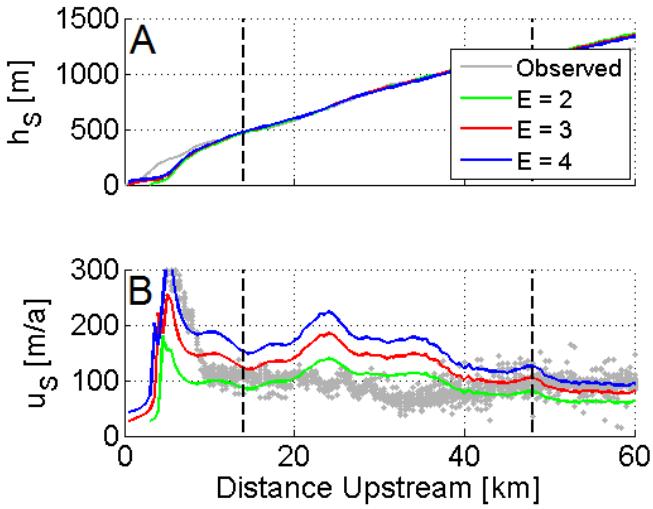

Figure 3.6: **A**: *Modeled ice surface elevation* (h_s) *over a range of Wisconsinan enhancement factors* (*E*) *versus observed* (*Scambos and Haran, 2002*). **B**: *Modeled ice surface velocity* (u_s) *over a range of E values versus observed* (*Joughin and others, 2008b*). *Vertical dashed lines denote the locations of JAR2 and Swiss Camp.*

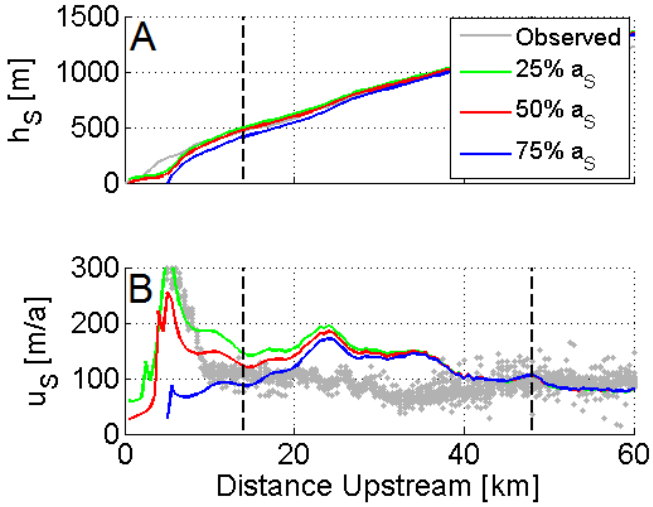

Figure 3.7: **A**: *Modeled ice surface elevation* (h_s) *over a fractional range of contemporary surface ablation* (a_s) *versus observed* (*Scambos and Haran, 2002*). **B**: *Modeled ice surface velocity* (u_s) *over a fractional range of* a_s *versus observed* (*Joughin and others, 2008b*). *Vertical dashed lines denote the locations of JAR2 and Swiss Camp.*

accurately reproduced when these background basal sliding velocities are linearly interpolated along the terminal 70 km of the flowline. When we allow the annual hydrologic cycle to operate, producing seasonal variations in basal sliding around this background basal sliding profile, the three-phase basal sliding rule produces a reasonable annual basal sliding velocity cycle throughout the Sermeq Avannarleq ablation zone (Figure 3.8). The modeled annual basal sliding velocity cycle captures the essence of: (i) background basal sliding velocity during the winter, (ii) a speedup event at the onset of surface ablation, followed by (iii) a slowdown event and return to winter velocity.

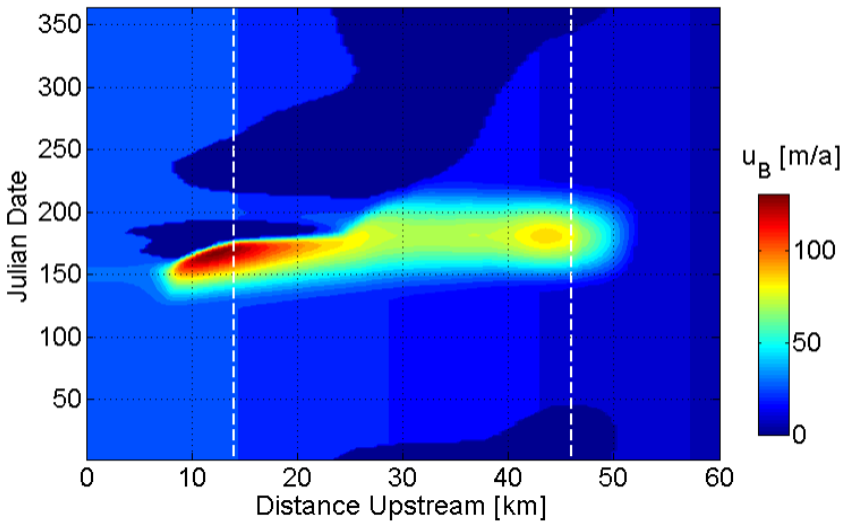

Figure 3.8: *Modeled time-space distribution of basal sliding velocity* (u_B) *along the terminal 60 km of the Sermeq Avannarleq flowline. Dashed lines indicate the positions of Swiss Camp and JAR2 stations.*

The modeled annual displacements of JAR2 and Swiss Camp (i.e. including both the summer speedup and fall slowdown velocity perturbations) agree well with the observed annual displacements approximated by Equation 3.1 (122 versus 117 m and 113 versus 115 m, respectively; Figure 3.9). As the modeled surface ice velocity due to internal deformation is 93

m/a at JAR2 and 95 m/a at Swiss Camp, year-round basal sliding appears to be responsible for 24 and 16 % of the annual net displacement at each station. The observed (modeled) annual velocity cycles suggest that summer speedup events are only responsible for 13 (7) and 3 (7) m of net annual displacement at JAR2 and Swiss Camp respectively (Figure 3.2). These increases in net annual displacement due to summer speedup events are partially offset by decreases in annual displacement due to fall slowdown events. Observed (modeled) fall slowdown events decrease annual displacement by 4 (2) and 2 (3) m at JAR2 and Swiss Camp respectively. While the seasonal timing of modeled maximum and minimum velocities do not precisely match observations, the coupled model reproduces reasonable quasi-steady-state ice geometry and velocity fields with an annual ice basal sliding cycle that captures the essence of the observed speedup and slowdown events.

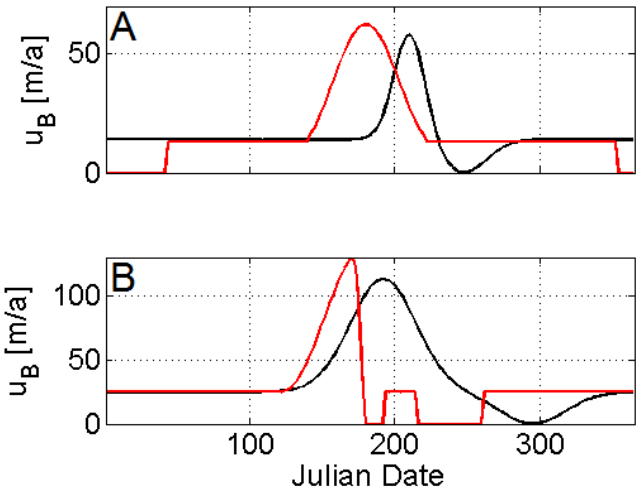

Figure 3.9: *Modeled basal sliding velocity* (*red lines*) *versus observed basal sliding velocity* (*from Equation 3.1:* u_s - u_{min}; *black lines*) *at Swiss Camp* (**A**) *and JAR2* (**B**).

3.4 Discussion

We prescribe basal sliding velocities that depend on the rate of change in subglacial

water pressure to a vertical cross section ice flow model that includes a longitudinal coupling term. This computationally efficient scheme captures the essence of the Sermeq Avannarleq flowline ice geometry and annual velocity cycle, including summer speedup and fall slowdown events. The mean annual glaciohydrology cycle reproduced by this coupled model may serve as a basis for future investigations into the transient response of the Sermeq Avannarleq flowline to predicted increases in surface meltwater production. While we do not drive our basal sliding rule with absolute head values (i.e. subglacial water pressure, h_e), but rather the rate of change in head (i.e. rate of change in subglacial water pressure, $\partial h_e/\partial t$), we achieve a satisfactory annual basal sliding cycle. We interpret this as suggesting that the $\partial h_e/\partial t$ term contains important information that modulates basal sliding. This suggests that sliding rules that are dependent on basal stress and hydraulic head may overlook important extraneous variables that are correlated to $\partial h_e/\partial t$, particularly those related to transient subglacial transmissivity or higher-order features of subglacial hydrologic geometry (i.e. the n_c "conduit spacing" parameter used in this study). Recent observations of hysteresis in the ratio of inferred subglacial water storage (i.e. bed separation) to sliding velocity over the course of a melt season supports this notion (*Howat and others*, 2008b). Thus, we suggest that an improvement towards achieving a physically-based sliding rule would be combining an absolute head/basal stress rule that modulates background (i.e. winter) sliding velocities (which are prescribed in this study) with a $\partial h_e/\partial t$-type parameterization that honors the empirical subtlety that sliding reaches a maximum when $\partial h_e/\partial t$ reaches a maximum (rather than when h_e reaches a maximum).

3.4.1 Modeled speedup and slowdown events

There is a temporal mismatch between modeled and observed velocity maxima and minima at both JAR2 and Swiss Camp (Figure 3.9). Modeled maximum velocity precedes observed maximum velocity by ~ 25 ± 3 days at Swiss Camp. It is more difficult to assess the

temporal difference between modeled and observed maximum velocities at JAR2, where a premature onset of the slowdown event truncates the speedup event, but the discrepancy appears to be less than at Swiss Camp (i.e. < 25 ± 28 days). The early onset of the speedup event can be attributed to the assumption embedded in the hydrology model that meltwater produced at the surface is immediately routed to the top of the englacial water table. This essentially assumes that there is no temporary supraglacial meltwater storage (e.g. within a saturated snowpack or in ponded water), and that supra- and en-glacial travel times are negligible. In reality, temporary supraglacial meltwater storage and travel time can delay the initial meltwater pulse from reaching the englacial water table for several weeks after the onset of melt (*Fountain and Walder*, 1998; *Flowers and Clarke*, 2002; *Jansson and others*, 2003). This lag would be expected to be greater at Swiss Camp, which experiences relatively low surface ablation rates near the equilibrium line, than at JAR2, which experiences relatively high surface ablation rates closer to the margin. The observed delay in peak basal sliding / glacier water storage could also be due to the re-filling of englacial conduits that drained during the winter in the early part of the melt season. A more detailed treatment of supra- and en-glacial meltwater routing in the hydrology model would likely reduce the discrepancies between modeled and observed velocity maxima.

The discrepancy between modeled and observed velocity minima is more variable; the model produces an early onset at JAR2 (~ 70 ± 28 days) and a delay at Swiss Camp (~ 80 ± 3 days). We believe this reflects the difficulty of capturing the behavior of subglacial conduits in an along-flowline 1D hydrology model. The timing of the fall slowdown event depends on the timing of the negative (or decreasing) hydraulic head ($\partial h_e/\partial t$) phase. This phase is initiated by the upstream propagation of a knickpoint in hydraulic head that corresponds to the opening of efficient subglacial conduits that in turn lower hydraulic head (e.g. *Kessler and Anderson*, 2004). A 2D (*xy*) hydrological model, which allows water to flow both parallel and perpendicular to the ice dynamic flowline, would be inherently more realistic in propagating changes in hydraulic

head upstream from various points at the ice margin. Because the timing of the slowdown event is controlled by the evolution of conduit sizes, the fall slowdown event is more dependent on an accurate representation of subglacial conduit dynamics than is the spring speedup event. The spring speedup event initiates as long as conduits have collapsed to their minimum radii (i.e. "closed"), which is a relatively simple geometry to capture given the lengthy winter period over which this geometry can be achieved.

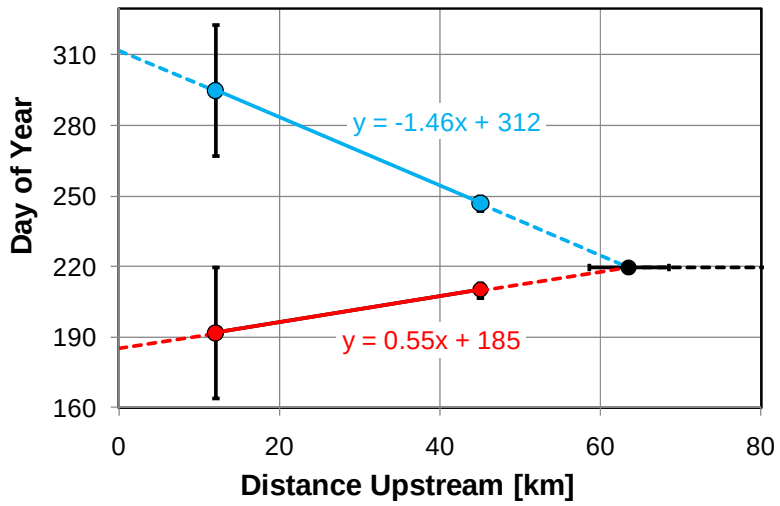

Figure 3.10: *Dates of maximum* (*red*) *and minimum* (*blue*) *velocity at JAR2 and Swiss Camp. The black circle indicates the potential upstream limit of the annual basal sliding velocity cycle* (*64 ± 5 km*). *Vertical whiskers denote uncertainty in* j_{max} *and* j_{min} *at each station.*

The observed dates of summer maximum (j_{max}) and fall minimum (j_{min}) velocity at JAR2 and Swiss Camp suggest that the timing of the summer speedup event is more synchronous than the timing of the fall slowdown event along the flowline (Figure 3.10). The summer speedup event appears to propagate upstream at a rate of ~ 1.8 km/d, while the fall slowdown event propagates more slowly downstream at a rate of ~ 0.69 km/d. We interpret this as suggesting that the timing of the speedup event depends on a meteorological forcing (i.e. the

onset of melt or a critical surface ablation threshold), while the timing of the slowdown event is more dependent on the development of efficient subglacial transmission capacity. This supports the inference from the 1D hydrology model that the flowline fills with water more quickly than it drains (Chapter 2). We speculate that the theoretical upstream limit to which the annual basal sliding velocity cycle can propagate (i.e. the location inland of which the ice sheet does not experience an annual velocity cycle) may be defined by the upstream convergence of the dates of maximum and minimum velocity. The data, poorly constrained by the temporal resolution of the InSAR data at JAR2, suggests that this boundary is ~ 64 ± 5 km upstream from the terminus. This distance upstream corresponds to the 1300 m ice elevation contour. This elevation is approximately coincident with the regional equilibrium line altitude over the 1996 to 2006 period (~ 1250 m; *Fausto and others*, 2009).

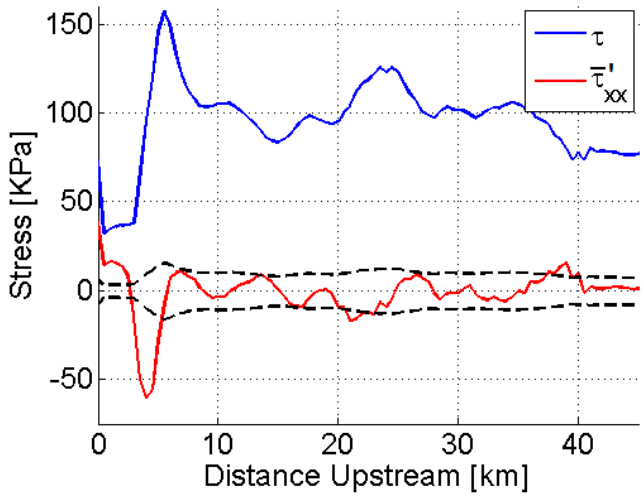

Figure 3.11: *Total driving stress* (τ) *and longitudinal coupling stress* ($\bar{\tau}'_{xx}$) *along the terminal 45 km of the flowline. Dashed lines represent ± 10 % of total driving stress*

3.4.2 Longitudinal coupling

Although *in situ* GPS data indicates that Swiss Camp exhibits an annual velocity cycle,

these data cannot indicate whether this is due to (i) local meltwater production and basal sliding, or (ii) an annual velocity cycle originating downstream from Swiss Camp that is propagated upstream via longitudinal coupling (i.e. lower elevation meltwater lubrication or the annual tidewater calving cycle). A previous study has suggested that 10 to 20 % of the seasonal velocity variations at Swiss Camp could be attributed to a roughly 100 % seasonal velocity increase initiated ~ 12 km downstream from Swiss Camp which is propagated upstream through longitudinal coupling (*Price and others*, 2008). The 2D (vertical cross-section) ice flow model suggests that the absolute longitudinal coupling stress ($|\bar{\tau}'_{xx}|$; Equation 3.7) is only "significant" (defined here as > 10 % of total driving stress) along the terminal ~ 5 km of the flowline (i.e. the floating tongue; Figure 3.11). Upstream of the ice fall at ~ 6 km, where observed ice thickness decreases to < 300 m, the absolute longitudinal coupling stresses seldom exceed 10 % of total driving stress. Additionally, in 3D, any perturbation to the tidewater tongue would also experience rapid radial diffusion (in the *xy* plane) with distance inland. This pattern of minimal inland coupling stresses fits the theoretical observation that coupling stresses are typically only important in the terminal few kilometers of ice sheet flowlines (where surface slope increases) and where the amplitude of bed topography approaches the ice thickness (*van der Veen*, 1987). Where longitudinal coupling stresses are insignificant along the Sermeq Avannarleq flowline, the forces governing ice flow can be assumed to be local in nature. Thus, at Swiss Camp, where absolute longitudinal coupling stress is < 5 % of total driving stress, the annual ice velocity cycle is more likely to be due to local glaciohydrology (i.e. local melt inducing local sliding) than a downstream velocity signal introduced by coupling (i.e. downstream basal sliding or terminus back-stress). This notion is supported by recent observations of a persistent englacial hydrology system in the vicinity of Swiss Camp (*Catania and Neumann*, 2009). Although the current ice geometry renders longitudinal coupling relatively unimportant inland of km 6, this does not imply that the irreversible retreat that has been observed following perturbations to the calving

front of other Greenland tidewater glaciers could not potentially affect this flowline (*Nick and others*, 2009). Other mechanisms are capable of propagating rapid wastage upstream without strong longitudinal coupling stresses, such as "irreversible tidewater retreat" that propagates upstream based on knickpoint migration (*Pfeffer*, 2007).

3.5 Chapter summary remarks

We coupled a 2D (vertical cross-section) ice flow model to a 1D (depth-integrated) hydrology model via a new simple basal sliding rule. Following a 1000-year spin-up, the model produces reasonable quasi-steady-state ice geometry and velocity fields for Sermeq Avannarleq ablation zone in Western Greenland. We present a semi-empirical three-phase basal sliding rule that imposes seasonal perturbations to the background basal sliding velocity. The magnitude of perturbation depends on the rate of change in englacial hydraulic head, geometry of the subglacial network (i.e. mean conduit spacing) and a site-specific coefficient that ranges between 0 and 2 and scales basal sliding velocity. This sliding rule is capable of reproducing the broad features observed in the annual basal sliding cycle in the terminal 60 km of the flowline. These features include (i) background basal sliding during the winter, (ii) a speedup event at the onset of melt, and (iii) a fall slowdown event and return to winter velocities. While the modeled magnitude and spatial distribution of basal sliding compares well with observations, discrepancies exist in the timing of maximum and minimum velocities. These discrepancies likely stem from a simplification of vertical meltwater routing and the flowline nature of the hydrology model, and can potentially be resolved by employing a 2D (*xy*) hydrology model that includes a more realistic vertical meltwater routing. Generally, the three-phase basal sliding rule appears to have potential as a tool for coupling ice flow and hydrology models to examine possible non-linear responses in basal sliding velocity to increased surface meltwater production in a warming climate.

We also examined the relative contribution of longitudinal coupling stress to total driving stress along the flowline. We find that longitudinal coupling stress is insufficient to attribute the annual ice velocity cycle observed at Swiss Camp (46 km upstream from the terminus of Sermeq Avannarleq) to seasonal variations in tidewater calving. Instead, we suggest the annual ice velocity cycle along the majority of the flowline should be attributed to local variations in basal sliding. Local basal sliding is governed by variations in the rate of change in subglacial hydraulic head due to local mismatches between surface meltwater inputs and the ability of the subglacial hydrologic system to transmit water. Future modeling efforts should therefore focus on the proper characterization of all components of the hydrologic system of these glaciers, from the spatio-temporal pattern of melt generation, to supraglacial transport and storage evolution, and the complex evolution of a subglacial system that includes both conduits and cavity components. While we have put forth a plausible sliding rule that connects sliding velocity to the state of the glacier hydrologic system, there remains a significant challenge to develop a rule that is more firmly based upon first principles and focused on effective basal pressure.

Chapter 4

SUPRAGLACIAL HYDROLOGY IN THE SERMEQ AVANNARLEQ ABLATION ZONE

4.1 Chapter introduction

Studies indicate that the Greenland Ice Sheet is currently experiencing a highly negative mass balance (*Alley and others*, 2007) that is accompanied by widespread changes in ice sheet geometry and velocity. Changes in ice sheet geometry are typically characterized as low elevation thinning, due to increased surface ablation and dynamic thinning, and high elevation thickening, due to increased surface accumulation (*Krabill and others*, 2004; *Luthcke and others*, 2006). Changes in ice velocity magnitude and direction are most prevalent around marine-terminating outlet glaciers (*Rignot and Kanagaratnam*, 2006; *Joughin and others*, 2010). Preliminary modeling of the Greenland Ice Sheet's response to a warming climate suggests that this ongoing change in ice geometry will result in a retreat of the ice sheet margin and an increase in ice discharge across the equilibrium line due to the steepening of ice surface slopes (*Parizek and Alley*, 2004). Several studies (*Shepherd and others*, 2009; *Bartholomew and others*, 2010) have suggested that the Greenland Ice Sheet possesses a basal sliding mechanism similar to that of alpine glaciers, whereby enhanced basal sliding occurs when surface meltwater input exceeds subglacial transmission capacity and pressurizes the subglacial hydrology system (*Anderson and others*, 2004; *Bartholomaus and others*, 2008). Basal sliding constitutes a relatively larger fraction of annual displacement in land-terminating glaciers than in marine-terminating glaciers (*Joughin and others*, 2008a). While many studies suggest that relatively small increases in future surface meltwater production may result in disproportionately large increases in basal sliding velocity (*Zwally and others*, 2002; *Shepherd and others*, 2009; *Bartholomew and others*, 2010), other studies suggest this will result in a transition to more efficient subglacial drainage and a net decrease in basal sliding velocity (*van de Wal and others*,

2008; *Schoof*, 2011; *Sundal and others*, 2011).

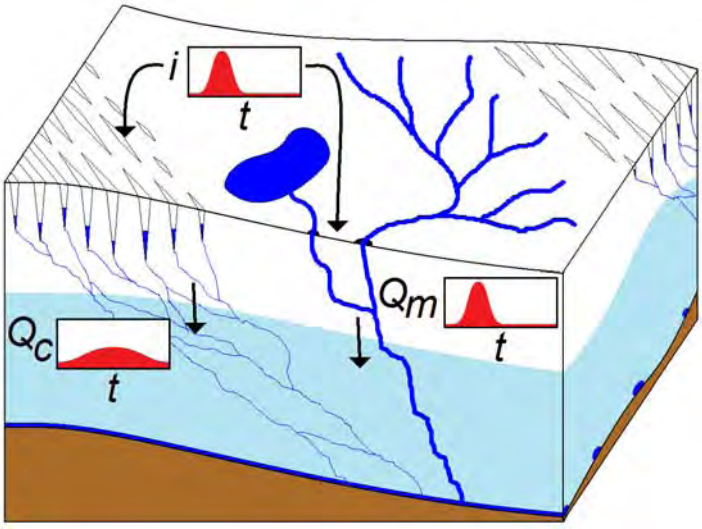

Figure 4.1: *Schematic of two differing supraglacial meltwater drainage pathways. Idealized hydrographs illustrate the increased attenuation of a given surface meltwater input* (i) *by crevasse drainage* (Q_c) *in comparison to moulin drainage* (Q_m).

Surface meltwater is transferred from the supraglacial system to the subglacial system via either moulins or crevasses (Figure 4.1). In heavily crevassed areas, surface meltwater cannot collect into supraglacial rivers and lakes, but rather drains from the ice surface in a more distributed fashion (c.f. *Thomsen and others*, 1988). Moulins are near-vertical conduits through the ice that have been demonstrated to rapidly transmit fluctuations in surface meltwater production to the subglacial system (*Zwally and others*, 2002; *Shepherd and others*, 2009). Unlike moulins, which concentrate surface meltwater production from a relatively large area for "point" delivery to the subglacial system, crevasses drain surface meltwater from comparatively small areas for "distributed" delivery to the subglacial system. Crevasse propagation can precondition ice for moulin formation at crevasse field boundaries (*Holmlund*, 1988; *Phillips and others*, 2011). While crevasses and moulins occur throughout a common elevation band

referred to as the "runoff zone", substantial supraglacial river/moulin systems and lakes typically do not occur within crevassed areas in West Greenland (c.f. *Thomsen and others*, 1988; *Phillips and others*, 2011).

We find that low elevation ice sheet thinning and steepening, due to a combination of enhanced surface ablation and the acceleration of nearby Jakobshavn Isbrae, have increased the ratio of crevasse-type to moulin-type drainage areas. We provide a first-order demonstration that the characteristic transfer time for supraglacial meltwater to reach the subglacial system is approximately two orders of magnitude faster for moulin-type than for crevasse-type drainage. Consequently, we suggest that moulin-type drainage is more efficient in propagating surface meltwater fluctuations (diurnal and otherwise) to the subglacial system than crevasse-type drainage (which attenuates meltwater fluctuations). As basal sliding is associated with meltwater "pulses" rather than sustained meltwater input (*Anderson and others*, 2004; *Bartholomaus and others*, 2008; *Bartholomew and others*, 2010), moulin-type drainage can therefore be expected to be a more efficient mechanism than crevasse-type drainage for overwhelming the subglacial system and enhancing basal sliding. Thus, a net transition from moulin-type to crevasse-type drainage may ultimately modify the basal sliding response of land-terminating portions of the ice sheet that are not presently crevassed to surface meltwater input.

The Sermeq (Glacier) Avannarleq ablation zone, in West Greenland, provides an ideal study site to examine recent changes in supraglacial hydrology. The Sermeq Avannarleq ablation zone is comprised of predominately land-terminating ice, with a relatively small tidewater glacier (Sermeq Avannarleq) that calves into a sidearm of Jakobshavn Fiord. Of the 106 km of ice sheet margin located within our study area, only the ~ 3 km wide Sermeq Avannarleq is marine-terminating. In 1985 the Grønlands Geologiske Undersøgelse (GGU) conducted an intensive survey of the Sermeq Avannarleq ablation zone that included the acquisition of two sets of high-quality panchromatic aerial photographs (July 10 and 24) from which a 1:25,000

supraglacial topography map was produced (*Thomsen*, 1986; *Thomsen and others*, 1988; Figure 4.2). A portion of the 24 July 1985 photographs were recently digitized and amalgamated into an orthomosaic with the intent to study changes in the ice geometry of nearby Jakobshavn Isbrae (~ 30 km southeast of Sermeq Avannarleq; *Motyka and others*, 2010). We compare this digitized historical dataset with a commercially-acquired panchromatic 2009 WorldView-1 image of the Sermeq Avannarleq ablation zone to assess changes in the character of the supraglacial hydrology system over a 24-year period.

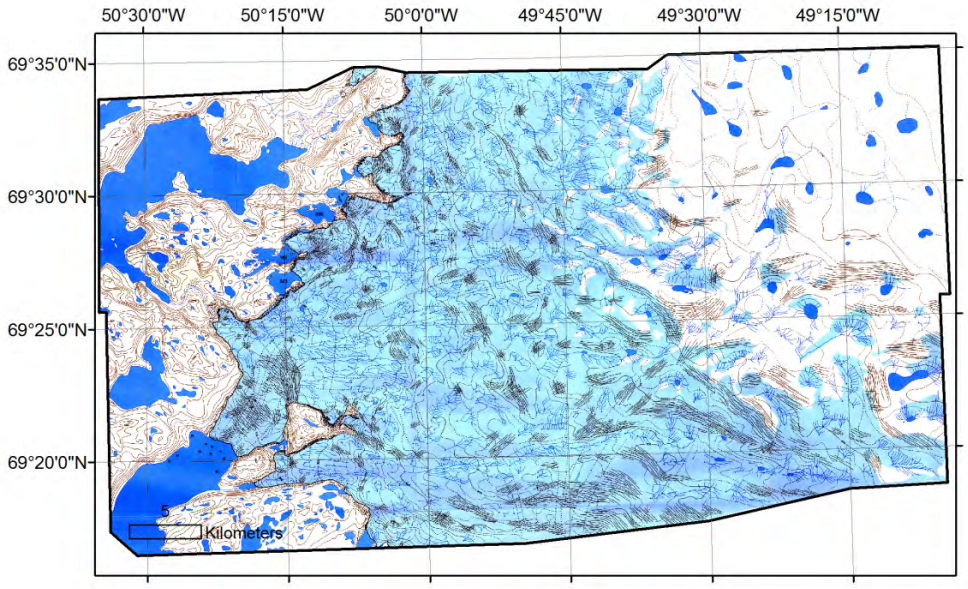

Figure 4.2: *Grønlands Geologiske Undersøgelse* (*GGU*) *supraglacial topography map of the Sermeq Avannarleq ablation zone in 1985* (*Thomsen and others, 1988*).

4.2 Methods

4.2.1 Assessing changes in crevassed area extent

We compared the crevassed area extent in both the 1985 orthomosaic and 2009 WorldView-1 imagery. The WorldView-1 image was resampled to 2.2 m resolution to make its resolution comparable to that of the orthomosaic (~ 2 m; *Motyka and others*, 2010). Crevasse extent was delineated from both images using a Roberts Cross edge detector in ENVI. This

method involves convolving a gradient operator that enhances areas of the image that have sharp changes in pixel value in a given direction (as is characteristic of a crevasse field). After manually digitizing the crevassed area boundaries identified by the Roberts operator results, we performed a manual inspection using the original imagery to verify the accuracy of polygons in representing crevassed regions. We delineated two sets of crevassed area extent polygons: (i) crevasses > 2 m wide (given the pixel size this includes "all" crevassed areas), (ii) and crevasses > 10 m wide (this crevasse subset includes only the most "severely" crevassed areas). We assess our uncertainty in crevassed area extent as the total area occupied by 10 and 100 m buffers around each respective set of crevassed area polygons.

Inter-annual variations in surface mass balance conditions can be expected to influence the ability to identify both crevasses and supraglacial hydrology features. Cumulative melt intensity in both 1985 and 2009 can be compared using positive degree days (PDDs) observed at the nearby Danish Meteorological Institute (DMI) Ilulissat weather station (WMO 04216 / 04221; ~ 35 km east of the ice sheet margin). This comparison suggests that the 1985 melt season was ~ 12 % more intense than the 2009 melt season at the time of image acquisition (416 versus 370 PDD, respectively). Complete winter accumulation records are not available for both 1985 and 2009 at the six DMI weather stations within an ~ 350 km radius of the study site (WMO 04216, 04217, 04218, 04220, 04221, 04224). In order to minimize the potential differences in crevasse extent between 1985 and 2009 attributable to differences in snow cover and detection, we use the 1985 snowline position (*Thomsen and others*, 1988) as the upglacier limit of the crevassed area comparison extent. We note that the 2009 snowline also shares a similar position. We use the 2009 margin as the downglacier limit of the comparison area.

4.2.2 Assessing changes in ice geometry

We also assess changes in the Sermeq Avannarleq ablation zone ice geometry between

1985 and 2009. The GGU map is based on the panchromatic aerial photographs acquired 10 July 1985 (*Thomsen and others*, 1988). Manually digitizing the contour lines of the GGU map allowed for construction of a detailed 1985 ice surface digital elevation model (DEM). Digitized point-elevation values (n = 8852) were interpolated across the study area to a 100 by 100 m grid using a regularized spline function. Given the relatively simple topography of the ice surface, the elevation error introduced through this interpolation is assumed to be minimal in comparison to the absolute vertical accuracy of the contours themselves. Neither the GGU map nor supporting documentation, however, provides an estimate of vertical accuracy (*Thomsen*, 1986; *Thomsen and others*, 1988; *Thomsen*, 1988b). Thus we assume a vertical accuracy equal to the half-contour interval of the GGU map (± 10 m). This 1985 ice surface DEM was differenced from a 2009 ice surface DEM extracted from the ASTER global digital elevation model (GDEM; http://asterweb. jpl.nasa.gov/gdem.asp). The ASTER GDEM has a horizontal grid spacing of 19 m at the latitude of the study site, and a stated absolute vertical accuracy of ± 20 m (*Fujisada and others*, 2005). We calculate the long-term rate of ice thickness change ($\partial H/\partial t$) across the study region by dividing the difference between the 2009 and 1985 ice surface elevations by the 24-year time interval between datasets. As errors in both ice surface elevation datasets may be expected to increase with distance away from bedrock control points, these errors cannot be assumed to be randomly distributed across the study area. We therefore take the uncertainty in the total change in ice thickness as the sum of the vertical uncertainties of both DEMs (± 30 m). The corresponding uncertainty in the long-term rate of ice thickness change is therefore ± 1.25 m/a.

4.2.3 Assessing changes in supraglacial hydrology

We also qualitatively compare the distribution of supraglacial hydrology features (i.e. rivers and lakes) that were manually delineated from both the 1985 orthomosaic and the 2009

WorldView-1 imagery. Additionally, as the GGU map covers a greater area than the orthomosaic, we manually delineated supraglacial lakes (n = 24) with an area greater than 0.2 km^2 from the 1985 GGU map (using feature trace) to compare with those delineated from 2009 WorldView-1 imagery (using reflectance). Lake center coordinates were estimated for each lake in both 1985 and 2009, and used as a proxy to assess positional stability of the supraglacial hydrology system. In the situation where a single large lake drained to form two smaller lakes, the mean center coordinates of the two smaller lakes were compared to the center coordinates of the original lake.

4.2.4 Ice margin comparison

The ice sheet margin was manually delineated from both the 1985 GGU map and the 2009 WorldView-1 image. A mean rate of marginal recession was calculated by dividing the area of bedrock exposed between 1985 and 2009 (23.9 km^2) by the width of ice margin across the study area (106 km) and the time interval between images (Δt = 24 a). While the horizontal accuracy of the WorldView-1 image is estimated to be ± 5 m, the GGU map and supporting documentation do not contain an estimate of horizontal accuracy (*Thomsen*, 1986; *Thomsen and others*, 1988; *Thomsen*, 1988b). We conservatively estimate the horizontal accuracy of the GGU map as ± 10 m, which is twice the stated horizontal accuracy of previous photogrammetric studies that used similar methods in the same region of ice sheet margin (*Andersen*, 1969). The total positional uncertainty when comparing a given location in the 1985 and 2009 images can therefore be taken as the sum of both these positional uncertainties (± 15 m). Thus, we take the uncertainty in the rate of marginal recession to be ± 0.63 m/a.

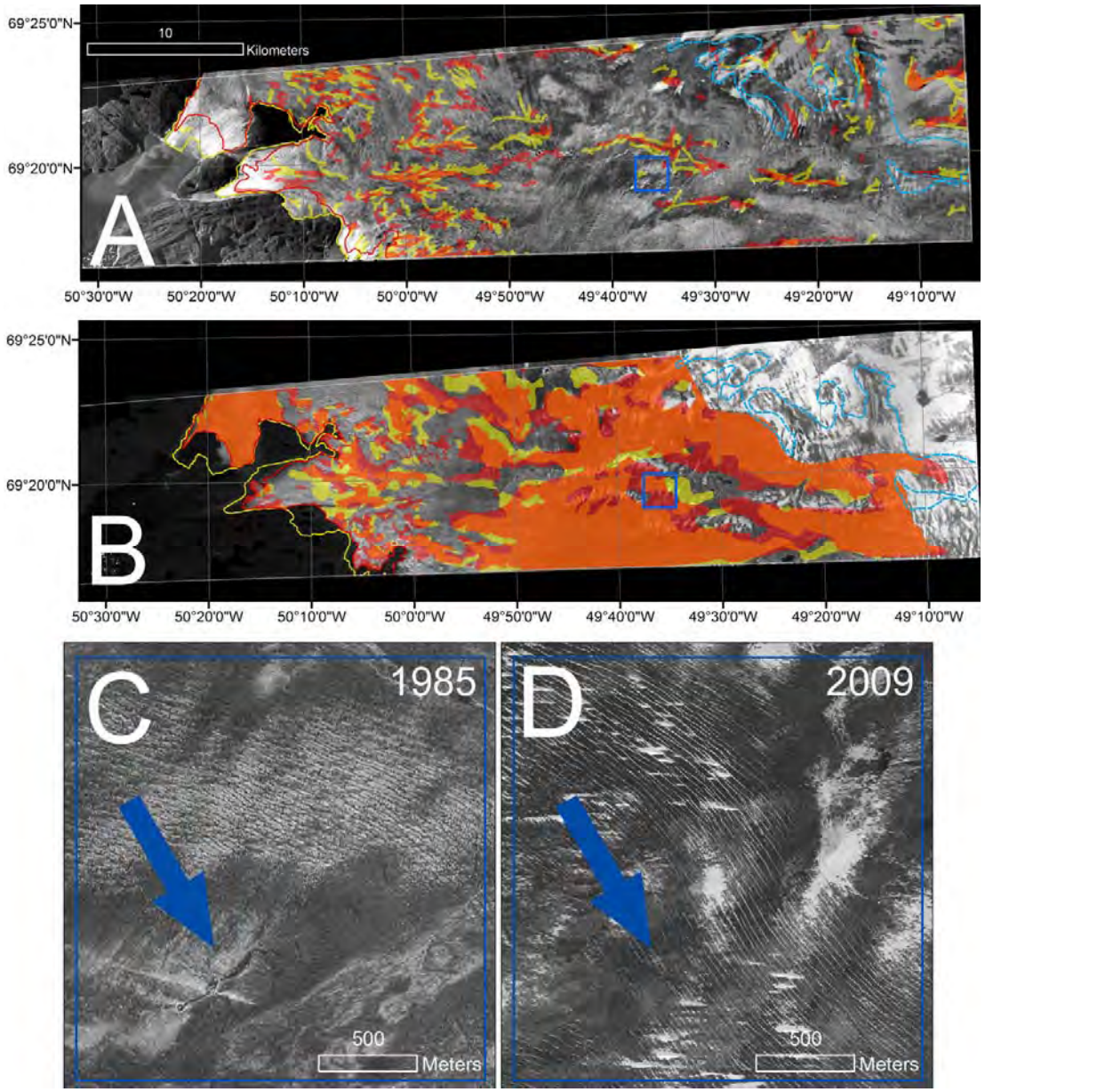

Figure 4.3: A: *Supraglacial rivers and lakes overlaid on a panchromatic 24 July 1985 orthomosaic.* **B:** *Crevassed areas (width > 2 m) overlaid on a panchromatic 15 July 2009 WorldView-1 image. In both images, the locations of features in 2009 and 1985 are denoted in red and yellow, respectively, with overlapping areas in orange. The 1985 snowline is denoted in cyan. The blue detail box illustrates the transition of a supraglacial catchment from moulin-type drainage in 1985* (**C**) *to crevasse-type drainage in 2009* (**D**).

4.3 Results

The total crevassed area extent (i.e. crevasses > 2 m wide) within the 608 km^2 comparison area increased 13 ± 4 % over the 24-year study period (from 258 ± 5 km^2 in 1985 to 291 ± 5 km^2 in 2009; Figure 4.3). Similarly, the severely crevassed area extent (i.e. crevasses > 10 m wide) increased 20 ± 60 % (17 ± 55 km^2) over the same period (83 ± 26 km^2 to 99 ± 28 km^2). The increase in total crevasse extent, as well as severely crevassed extent, may be generalized as an expansion of existing crevasse fields. While a qualitative assessment suggests a corresponding decrease in the area occupied by supraglacial rivers, we do not assess this decrease in a quantitative fashion here. We simply note that crevasses and prominent supraglacial hydrologic features (e.g. several km lake and river systems) are typically mutually exclusive (c.f. *Thomsen and others*, 1988). Therefore, the net increase in ice sheet area drained by crevasse systems between 1985 and 2009 implies a net decrease in ice sheet area drained by river/moulin systems (c.f. Figures 4.3C and 4.3D).

The 24 supraglacial lakes demonstrated a remarkable positional stability over the study period, with a mean center point displacement of 125 ± 15 m (s.d. 86 m) between 1985 and 2009 (Figure 4.4). The lakes examined had a mean area change (ΔA) of 12 %; nine increased in area (ΔA > 25 %), eight decreased in area (ΔA < -25 %) and seven showed no appreciable change in area ($|\Delta A|$ < 25 %). A two-tailed paired *t*-test of the 1985 and 2009 lake area populations found no significant difference (p = 0.41 and n = 24). Supraglacial rivers and crevassed regions also exhibited a high positional stability between 1985 and 2009.

While the mean long term thinning rate ($\partial H/\partial t$) is comparable to uncertainty across the entire ablation zone (1.19 ± 1.25 m/a), there are large portions of the ablation zone where local thinning rates exceed uncertainty (Figure 4.5). Generally, thinning rates increase towards the south and west, exceeding 3 ± 1.25 m/a near the margin in the southwest corner of the study area. These thinning rates are consistent

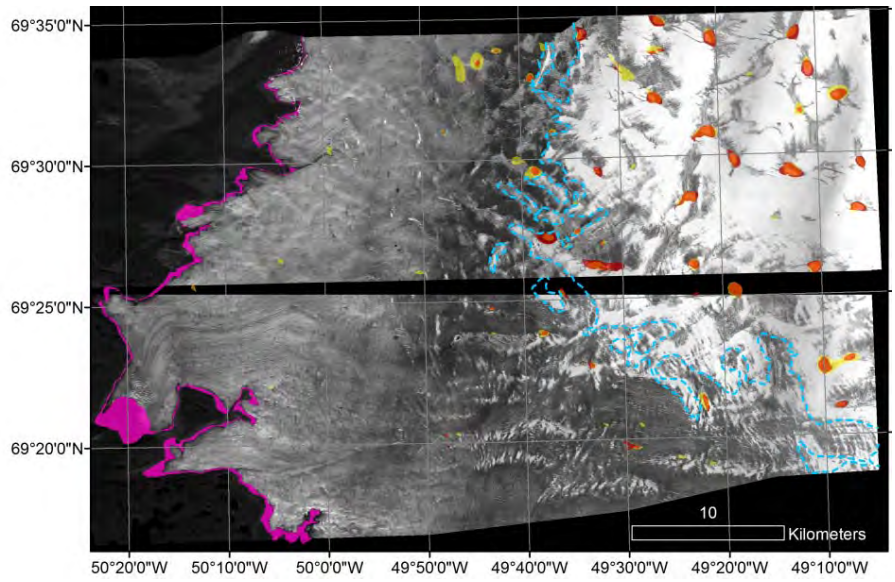

Figure 4.4: *WorldView-1 panchromatic image, acquired 15 July 2009, of the Sermeq Avannarleq ablation zone. Magenta shading denotes margin retreat since 1985. Lake areas in 2009 and 1985 are shown in red and yellow respectively. Overlapping lake areas are orange. Blue dashed line denotes the 1985 snowline.*

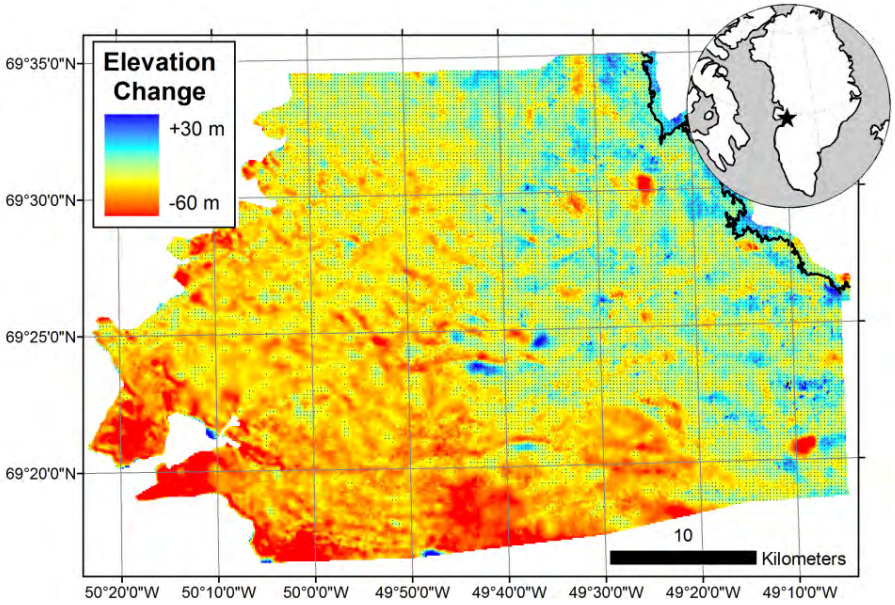

Figure 4.5: *Elevation change across the Sermeq Avannarleq ablation zone between 1985 and 2009 (Colorbar saturates at +30 and -60 m). Black line denotes the equilibrium line altitude over the period. Stippling identifies $|\Delta H| < 30$ m.*

(i.e. within error) of previously published estimates (*Motyka and others*, 2010). This spatial pattern of thinning was accompanied by a mean rate of glacier margin retreat of 9.39 ± 0.63 m/a averaged over the 106 km of ice sheet margin within the study area (Figure 4.4). Analysis of secondary attributes of the 1985 and 2009 DEMs suggests that the mean surface slope of the ablation zone increased by 0.10 ° (≈ 7 %) over the 24-year period. A two-tailed paired *t*-test indicates that this increase in mean ice slope from 1.45° (s.d. 0.98 °) in 1985 to 1.55 ° (s.d. 0.91 °) in 2009 is significant at the $p < 0.001$ level. The spatial pattern of slope change is complex (Figure 4.6).

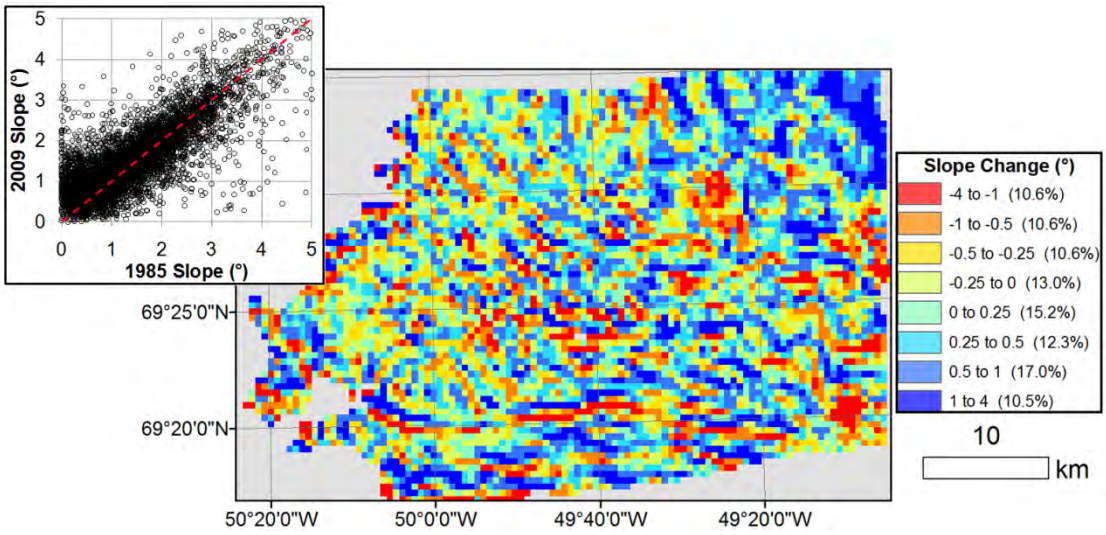

Figure 4.6: *Change in ice surface slope derived from a comparison of 1985 (Thomsen and others, 1988) and 2009 (ASTER GDEM) digital elevation models at 500 m grid spacing. Values in parentheses indicate the percent area in each class.* **Inset:** *Scatter plot of 1985 and 2009 ice surface slopes at each grid point with line y = x shown for reference.*

4.4 Discussion

4.4.1 Cause of increased crevasse extent

In this section we discuss how a combination of low elevation ice thinning and

steepening are likely responsible for the observed increase in crevasse extent. The general 2D continuity equation for ice suggests that there are two possible causes of ice sheet thinning ($\partial H/\partial t < 0$) at a given location: a decrease in local mass balance ($\dot{b}$) and an increase in divergence of ice flux ($\underline{\nabla} \cdot \underline{Q_i}$; *Hooke*, 2005):

$$\frac{\partial H}{\partial t} = \dot{b} - \underline{\nabla} \cdot \underline{Q_i} \qquad \text{Eq. 4.1}$$

A previous investigation suggests that land-terminating marginal ice within the study area has thinned by up to 104 ± 8 m between 1985 and 2007 (*Motyka and others*, 2010). *In situ* surface mass balance observations suggest that this thinning exceeds that attributable to surface mass balance alone (i.e. it is unreasonable to invoke $\dot{b} \approx$ -4.7 m/a over the 1985 to 2007 interval; *Fausto and others*, 2009). While the strong relation between $\partial H/\partial t$ and elevation suggests that a large portion of the observed thinning stems from surface mass balance forcing (Figure 4.7), an increase in the divergence of ice flux must be invoked to explain excessive thinning. The most likely cause for an increase in the divergence of ice flux within the study area is an increase in ice flux towards Jakobshavn Isbrae. This would essentially increase "southbound" ice flux at the expense of "westbound" ice flux within the study area, leading to an overall positive divergence of ice flux, and thus ice thinning.

A comparison of 1985 velocity vectors derived from photogrammetry (*Fastook and others*, 1995) with 2005/06 velocity vectors derived from InSAR observations (*Joughin and others*, 2010) suggests that the recent acceleration of Jakobshavn Isbrae has indeed increased southbound ice flow at the expense of westbound ice flow in the Sermeq Avannarleq zone (Figure 4.8). Surface crevasses, which typically form perpendicular to a glacier's longitudinal stress field (i.e. across-flow under extensional flow), can be used to infer ice flow direction. Since 1985, crevasse orientations throughout the study area have rotated, by up to 45° in some

locations, in directions consistent with an increase in ice flux towards Jakobshavn Isbrae (Figure 4.8). We expect that the majority of this reorganization likely occurred after 1998, rather than in a monotonic fashion (*Motyka and others*, 2010).

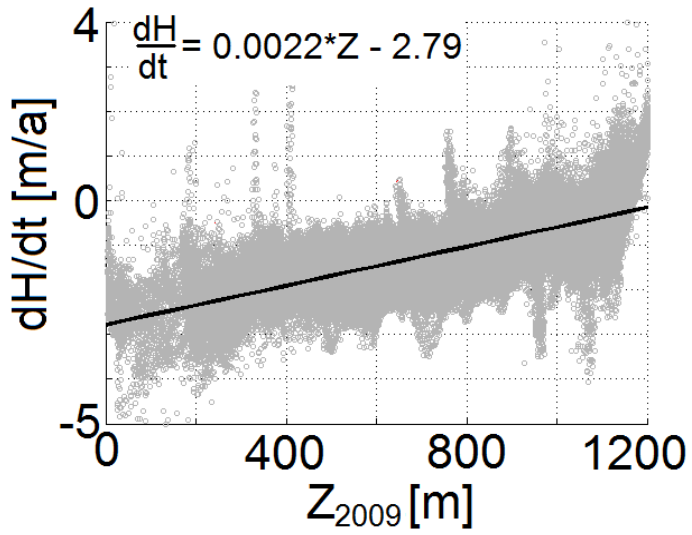

Figure 4.7: *Rate of elevation change over the 1985 to 2009 period* (*dH*/*dt*) *versus 2009 ice surface elevation* (Z_{2009}) *across the study area*.

As the lithostatic stress opposing crevasse propagation is proportional to ice thickness and the tensile stress promoting crevasse propagation is proportional to local surface slope (*Van der Veen*, 1998), changes in ice thickness and local surface slope influence crevasse propagation. Ice thinning and steepening both act to enhance crevasse propagation. Application of the crevasse model proposed by *Van der Veen* (1998) suggests that for an initial ice thicknesses of 500 m and an crevasse depth of 20 m (values representative of the Sermeq Avannarleq ablation zone), the combination of a 65 m decrease in ice thickness and a 0.12 ° increase in surface slope increases crevasse depth by ~ 30 %. Given that crevasse propagation is greatly enhanced by hydrofracture when crevasses are water-filled (*Van der Veen*, 1998), a substantial increase in surface meltwater production since 1985 is also expected to facilitate crevasse propagation. As a

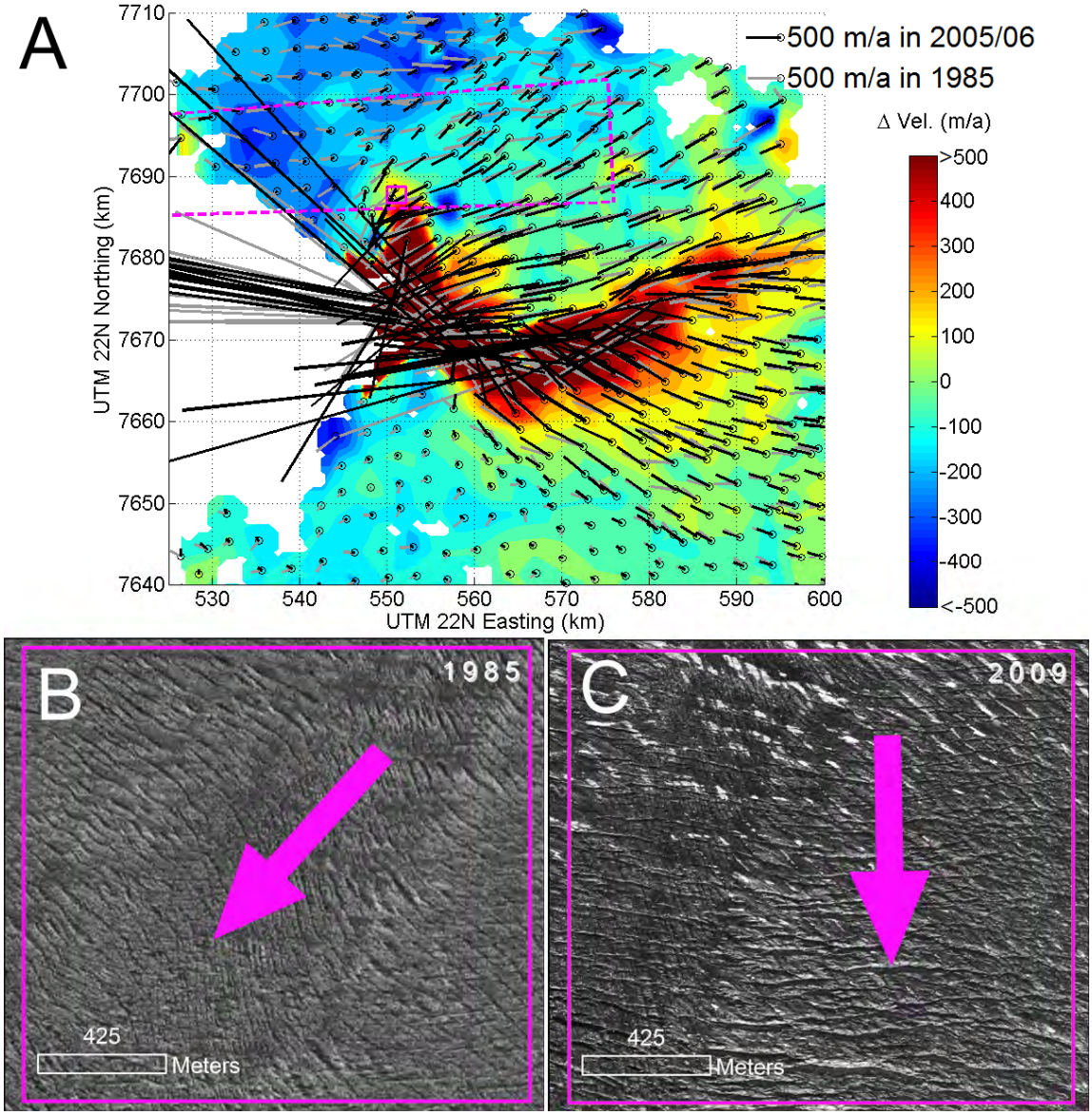

Figure 4.8: A: *Comparison between 1985* (*Fastook and others,* 1995) *and 2005/06* (*Joughin and others,* 2010) *velocity vectors in the Jakobshavn Isbrae region. Colored contours denote change in absolute velocity. The dashed magenta box denotes the extent of Figures 4.3A and 4.3B. The magenta detail box is a highlighted region in which crevasse rotation between 1985* (**B**) *and 2009* (**C**) *is shown. Arrows denote the approximate local crevasse orientation in each year.*

crevasse field delineates the local extent of a critical ratio between tensile and lithostatic stresses, widespread thinning and steepening is expected to cause an existing crevasse field to expand outwards.

Previous studies indicate that recent changes at Jakobshavn Isbrae are part of a widespread change in the low elevation velocity structure and geometry of the Greenland Ice Sheet (*Luthcke and others*, 2006; *Rignot and Kanagaratnam*, 2006; *Thomas and others*, 2006; *Joughin and others*, 2010). Around the Greenland Ice Sheet, the "runoff zone" elevation band, which is characterized by meltwater runoff via crevasses and moulins (*Phillips and others*, 2011), resides below the higher elevation "dark zone", the elevation band of maximum meltwater accumulation in supraglacial lakes (*Greuell*, 2000). Thus, we expect our observations in the SA runoff zone are part of an ice sheet wide response in crevasse extent throughout the extensive low elevation runoff zone.

4.4.2 Supraglacial lake drainage frequency

Both supraglacial lakes and rivers demonstrate high positional stability over the 24-year period. Thus, these features may be regarded as "perennial" features of the supraglacial hydrology landscape (rather than transient "annual" features). Previous investigations have suggested that the primary control on supraglacial lake position is the expression of bedrock anomalies at the ice surface (*Thomsen and others*, 1988). Given the antipodal relation between areas occupied by crevasses and supraglacial hydrology features, we suggest, however, that the primary control for supraglacial hydrology features (both rivers and lakes) is the absence of surface crevassing.

Supraglacial lakes have been observed to increase in size throughout one or several melt seasons, until a critical water pressure threshold is achieved, at which time they drain rapidly, presumably through hydrofracture (*Box and Ski*, 2007; *van der Veen*, 2007; *Das and others*,

2008). Across the 24 supraglacial lakes, relative changes in lake area are neither related to initial lake area nor elevation ($p > 0.05$, $|r| < 0.35$ and $n = 24$; Table 4.1). This means that over the study period higher elevation (or larger) lakes were not more prone to either increases or decreases in their area than lower elevation (or smaller) lakes. This random spatial distribution of relative lake area changes is likely a consequence the random temporal distribution of lakes throughout the filling and draining lifecycle. As lake area is a good proxy for lake volume (*Box and Ski*, 2007), the absence of a significant change in lake area over the last 24-years may be interpreted as evidence of no significant change in lake volume over the study period. Thus, we speculate that lakes have compensated for increasing surface meltwater production since 1985 with an acceleration of the filling and draining lifecycle (i.e. increasing the frequency of drainage events), rather than with an increase in lake storage.

4.4.3 Crevasse versus moulin drainage

Meltwater is transferred from the supraglacial system to the subglacial system via either moulins or crevasses. We focus this discussion on moulins which drain supraglacial rivers rather than those responsible for episodic lake drainage events.

Table 4.1: *Summary of observed changes of the 24 supraglacial lakes: arbitrary lake ID, latitude, longitude, elevation, area in 1985* (A_{1985}), *area in 2009* (A_{2009}), *change in area* (ΔA), *and center point displacement* (ΔCP), *over the period.*

Lake	Latitude [°N]	Longitude [°E]	Elev [m]	A_{1985} [10^5 m^2]	A_{2009} [10^5 m^2]	ΔA [10^5 m^2]	ΔA [%]	ΔCP [m]
L11	69.375	-49.143	1156	11.44	6.25	-5.19	-45	161
L2	69.535	-49.130	1155	3.24	6.00	2.76	85	124
L7	69.514	-49.356	1153	4.07	6.88	2.81	69	123

L19	69.553	-49.494	1144	2.17	3.57	1.40	65	255
L13	69.490	-49.210	1140	4.19	1.05	-3.14	-75	81
L25	69.420	-49.313	1137	3.90	4.99	1.09	28	55
L3	69.475	-49.390	1120	4.85	7.62	2.76	57	78
L21	69.536	-49.441	1116	7.91	10.50	2.58	33	171
L5	69.570	-49.344	1095	4.03	1.72	-2.30	-57	155
L14	69.432	-49.176	1080	8.83	8.85	0.02	0	47
L8	69.436	-49.540	1080	8.79	0.64	-8.15	-93	350
L12	69.526	-49.196	1080	6.16	6.08	-0.08	-1	66
L17	69.436	-49.380	1080	3.43	6.63	3.20	93	16
L23	69.552	-49.180	1042	6.46	7.10	0.65	10	245
L34	69.563	-49.438	1041	4.73	5.35	0.61	13	186
L42	69.467	-49.104	1002	20.00	9.41	-10.59	-53	84
L32	69.500	-49.670	985	4.10	3.43	-0.67	-16	0
L37	69.497	-49.309	982	7.86	6.36	-1.50	-19	27
L10	69.572	-49.207	979	2.41	1.83	-0.59	-24	151
L18	69.455	-49.624	941	3.37	0.00	-3.37	-100	125
L33	69.548	-49.649	940	4.45	13.74	9.29	209	35
L6	69.397	-49.635	936	2.00	0.40	-1.61	-80	72
L28	69.493	-49.095	922	2.75	9.31	6.56	238	23
L41	69.565	-49.704	832	2.36	1.01	-1.35	-57	44
MEAN (s.d.)	n/a	n/a	1062 (91)	5.56 (3.94)	5.36 (3.62)	0.20 (4.23)	-3.6 (86)	125 (86)

Assuming that the changes in englacial water volume due to internal meltwater generation and

deformational closure are negligible, the rate of change of water volume (dV/dt) in either type of englacial transfer system may be conceptualized as the difference between the rate of surface meltwater input ($a_s A$) and the rate of englacial output (or "discharge"; which we represent as V/τ):

$$\frac{dV}{dt} = a_s A - \frac{V}{\tau} \qquad \text{Eq. 4.2}$$

where a_s is the surface ablation rate, A is the ice surface drainage area (i.e. supraglacial water catchment), and τ is a characteristic englacial transfer time (*Flowers and Clarke*, 2002). This characteristic transfer time represents the mean time required for supraglacial meltwater input to travel from the ice surface to the subglacial system. Rather than determining englacial discharge based on conduit geometry, the above formulation assumes that the englacial system behaves as a linear reservoir (*Flowers and Clarke*, 2002). The total englacial conduit volume (V) may be estimated as:

$$V \approx H \cdot S_c \qquad \text{Eq. 4.3}$$

where H is ice thickness and S_c is the cross-sectional area of the englacial conduit draining either a crevasse or a moulin.

Assuming that englacial conduit volume evolves to achieve a quasi-steady-state diurnal cycle (i.e. $\int(dV/dt)\cdot dt \approx 0$ over the diurnal cycle), the characteristic englacial transfer time may be approximated as:

$$\tau \approx \left(\frac{H \cdot S_c}{A \cdot a_s}\right) \qquad \text{Eq. 4.4}$$

We find this assumption reasonable, given that empirical observations on alpine glaciers

demonstrate that the 1/*e* timescale for conduit closure beneath ~ 500 m of ice is expected to be ~ 5 hours when water pressures are low (*Bartholomaus and others*, 2008). Thus, the primary mode of variability in conduit geometry can be expected to reflect the primary mode of variability in meltwater input (i.e. the diurnal cycle). Furthermore, high temporal resolution GPS observations indicate that the "summer speedup event" in West Greenland is comprised of a series of diurnal events (*Shepherd and others*, 2009). In addition, at Sermeq Avannarleq, there is observational evidence of the persistence of englacial hydrologic features throughout the year (*Catania and Neumann*, 2010).

This formulation implicitly takes ice thickness as a proxy for englacial travel distance, and neglects the reality that the englacial conduits draining moulins and crevasses may travel through the ice column at varying angles off-vertical. While moulins draining supraglacial lakes are likely capable of near-vertical hydrofracture through the ice sheet (e.g. *Das and others*, 2008), the englacial conduits draining crevasses typically do not have "infinite" water input, and are theoretically expected to descend through the ice sheet at 11 times the regional ice surface slope (*Shreve*, 1972). Thus, water routed through crevasses can be expected to travel a greater distance through the ice sheet to reach the bed than water routed through moulins. Accounting for this difference in englacial travel distance would further increase the discrepancy between the typical moulin and crevasse englacial transfer times we present below.

To provide a first-order demonstration of the fundamental difference in englacial transfer time between crevasse-type and moulin-type drainage systems, we evaluate Equation 4.4 for both systems. For moulins, we assume that englacial conduits are generally circular in shape, with cross-sectional area approximated as $\pi\bar{r}^2$ (where $\bar{r}$ is depth-averaged englacial conduit radius). For crevasses, we do not impose a circular cross-sectional conduit geometry, but rather approximate S_c as $l\bar{w}$ (where l is crevasse length and $\bar{w}$ is depth-averaged englacial crevasse width). In both scenarios we take mean daily ablation rate as 4 cm/d and ice thickness as 500 m.

In the moulin scenario we assume that 1 km^2 of ice sheet area drains into a single moulin with $\bar{r}$ = 1 m. In the crevasse scenario we assume that the same ice sheet area is drained by multiple crevasses, with each crevasse draining an area of $A = dl$ (where d is a mean crevasse spacing of 100 m) and assume $\bar{w}$ = 0.1 m. Using these specified values, the mean englacial transfer times for moulin-type and crevasse-type drainage are ~ 1 hour and ~ 12 days, respectively. As H/a_s may be regarded as constant in a given region, S_c/A controls this ~ 200-fold difference in τ. This suggests that drainage systems with relatively large S_c/A (i.e. crevasse-type) can be expected to attenuate surface meltwater fluctuations in comparison to those with relatively small S_c/A drainage (i.e. moulin-type).

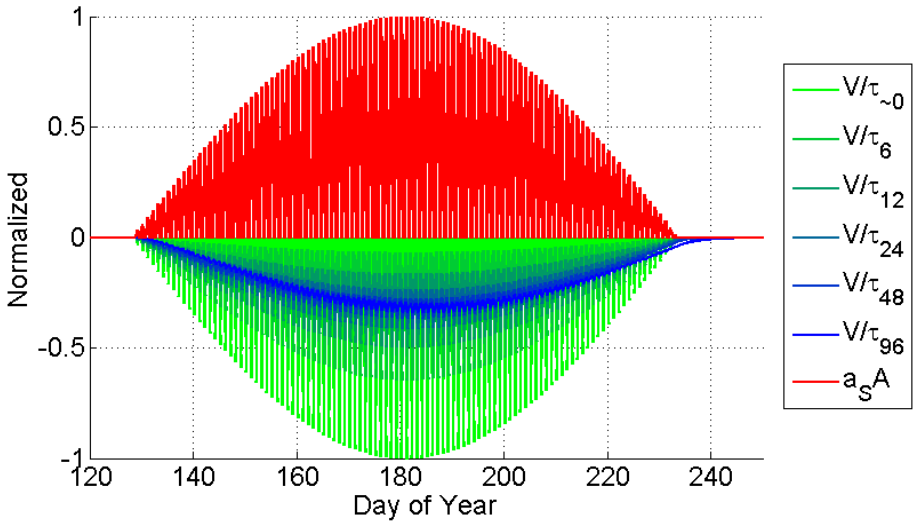

Figure 4.9: *Normalized surface meltwater input rate* (a_sA) *and englacial discharge rate* (V/τ) *over a range of englacial transfer times* (τ = ~ 0, 6, 12, 24, 48 *and* 96 *hours*).

The dampening or attenuating of meltwater fluctuations can be demonstrated by numerically solving Equation 4.2 over a range of τ values. Using the surface ablation function described below, this illustrates that englacial discharge variability is nonlinearly dependent on englacial transfer time (Figure 4.9). This suggests that crevasse-type drainage (i.e. relatively large

S_c/A) can be expected to significantly dampen or attenuate surface meltwater fluctuations in comparison to moulin-type drainage (i.e. relatively small S_c/A).

The dampening or attenuating of meltwater fluctuations can also be demonstrated by analytically solving Equation 4.2; this reveals an inverse relation between englacial transfer time and englacial discharge variability. To facilitate an analytical solution, we approximate surface ablation rate (a_s) as a sinusoidal function of the form:

$$a_s(t) = \overline{a_s}\left[\frac{1}{2}\left(1 - \sin\left(\frac{2\pi t}{T}\right)\right)\right] \qquad \text{Eq. 4.5}$$

where t is time and T is period of the surface ablation cycle (24 hours). Using this surface ablation forcing, the analytical solution of Equation 4.2 may be expressed as:

$$V(t) = \frac{\overline{a_s}A\tau}{2}\left[1 + \left(\frac{1}{\sqrt{1+4\pi^2\tau^2/T^2}}\right)\cos\left(\frac{2\pi t}{T} - \varphi\right)\right] \qquad \text{Eq. 4.6}$$

where $V(t)$ is the total englacial water volume after many cycles of forcing and ϕ is a phase angle equal to:

$$\varphi = \tan^{-1}\left(\frac{-T}{2\pi\tau}\right) \qquad \text{Eq. 4.7}$$

After many cycles of forcing (i.e. loss of memory of the initial water volume) conduit discharge ($Q(t)$) is obtained by dividing Equation 4.6 by τ:

$$Q(t) = \frac{\overline{a_s}A}{2}\left[1 + \left(\frac{1}{\sqrt{1+4\pi^2\tau^2/T^2}}\right)\cos\left(\frac{2\pi t}{T} - \varphi\right)\right] \qquad \text{Eq. 4.8}$$

Thus, it becomes evident that the amplitude of conduit discharge is inversely proportional to characteristic englacial transfer time. For small τ (i.e. $\leq T/2\pi$), as expected in moulin-type drainage, variations in conduit discharge precisely follow those of surface ablation forcing and there is little attenuation of the diurnal signal. For large τ (i.e. $>T/2\pi$), as expected in crevasse-type drainage, englacial discharge exhibits smaller amplitude variations. Generally, moulin-type drainage can be expected to transmit fluctuations in meltwater production from the supraglacial system to the subglacial system more efficiently than crevasse-type drainage, which significantly dampens or attenuates meltwater fluctuations (see idealized hydrographs in Figure 4.1). As basal sliding requires meltwater to overwhelm the transmission capacity of the subglacial system, it is therefore reasonable to expect regions experiencing efficient moulin-type drainage (i.e. meltwater "pulses") to exhibit enhanced basal sliding sensitivity to surface meltwater inputs in comparison to regions experiencing inefficient crevasse-type drainage (i.e. sustained meltwater input). In addition to "englacial hydraulic adjustment" (*van de Wal and others*, 2008), this mechanism could provide a complementary explanation for observations of decreasing mean annual velocities of land-terminating ice in West Greenland.

We note that the potential change from moulin to crevasse-type drainage is a one-time transition limited to areas of the low elevation ice sheet runoff zone that are not presently crevassed; ice sheet areas that are already crevassed would not be expected to be sensitive to this mechanism. Additionally, enhanced basal sliding due to meltwater lubrication contributes to a larger fraction of annual displacement in land-terminating glaciers than marine-terminating glaciers (*Joughin and others*, 2008a). Therefore changes in basal sliding can be expected to have a greater affect on land-terminating glaciers than marine-terminating glaciers. Land-terminating glaciers are currently delivering only a fraction of the mass loss of Greenland's marine-terminating glaciers (*Rignot and Kanagaratnam*, 2006).

4.4.4 Possibility to enhance mass loss

While we postulate that a net increase in crevasse extent may result in a net decrease in basal sliding sensitivity, and hence a decrease in ice discharge and a more positive overall mass balance, a net increase in crevasse extent may enhance mass loss through other mechanisms. Firstly, cyro-hydrologic warming is highly sensitive to the mean spacing of englacial hydrologic pathways (*Phillips and others*, 2010). A net increase in crevasse extent can be expected to expose an increased area of the ice sheet to closely-spaced hydrologic pathways that facilitate cryo-hydrologic warming. These pathways would be capable of warming ice temperatures and enhancing deformational ice velocities in newly crevassed regions of the ice sheet (c.f. *van der Veen and others*, 2011). A positive feedback could be possible if the subsequent change in the ice velocity field further expands crevassed areas. Secondly, the presence of crevasses has been shown to more than double the absorption of solar radiation (and hence enhance surface ablation) in comparison to ice sheet areas without crevasses (*Pfeffer and Bretherton*, 1987). Thus, a widespread increase in crevasse extent can be expected to result in a widespread decrease in annual surface balance.

4.5 Chapter summary remarks

Comparison of the ice geometry of the Sermeq Avannarleq ablation zone between 1985 and 2009 confirms preliminary model inferences of the Greenland Ice Sheet's response to a warming climate, namely a retreat of the ice sheet margin and steepening of the ablation zone (*Parizek and Alley*, 2004). We suggest that the recent acceleration of Jakobshavn Isbrae has resulted in an increase in crevasse extent in the Sermeq Avannarleq ablation zone, due to a combination of ice thinning and changing flow direction. We argue that the resultant transition from moulin-type to crevasse-type drainage can be expected to result in a net dampening of basal

sliding sensitivity to surface meltwater input. This dampening would be most significant in portions of the ice sheet that are land-terminating and not presently crevassed. Due to the absence of an ice sheet wide time series of crevasse extent, the potential prevalence of this transition outside our study area is not precisely known at present. We expect, however, that our observations at Sermeq Avannarleq are part of a widespread response in crevasse extent throughout the low elevation runoff zone of the Greenland Ice Sheet. While an increase in crevasse extent is expected to reduce basal sliding sensitivity, we acknowledge that any mass balance gain stemming from decreased basal sliding may be offset by counteracting processes. In particular, increased crevasse extent may enhance surface ablation through increased absorption of solar radiation, as well as enhance deformational ice velocities by exposing an increased ice sheet area to closely-spaced hydrologic pathways that facilitate cryo-hydrologic warming (c.f. *Phillips and others*, 2010).

Chapter 5

SUMMARY AND FUTURE DIRECTIONS

5.1 Summary

The notion that changes in glaciohydrology may have been a key factor in the eventual demise of the Scandinavian Ice Sheet (*Arnold and Sharp*, 2002) provides an impetus to study the influence of surface meltwater on the contemporary ice dynamics of the Greenland Ice Sheet. The Greenland Ice Sheet was likely in near balance in the colder climate of the 1970s and 1980s (*Rignot and others*, 2008). Over the past two decades, however, the Greenland Ice Sheet has experienced widespread changes in both ice geometry and velocity in response to recent increases in surface ablation (*Luthcke and others*, 2006; *Rignot and Kanagaratnam*, 2006; *Thomas and others*, 2006; *Joughin and others*, 2010). These changes may be summarized as low elevation thinning and high elevation thickening with a widespread acceleration of marine-terminating outlet glaciers. These changes have resulted in an increasingly negative ice sheet mass balance. The Greenland Ice Sheet is presently estimated to be losing up to 286 km^3 of ice per year (*Velicogna*, 2009). This is equivalent to a sea level rise contribution of ~ 0.4 mm/a (*Cazenave and Llovel*, 2010). This mass loss appears to be equally split between surface mass balance (i.e. melt and runoff) and ice dynamics (i.e. ice discharge; *van den Broeke and others*, 2009). While predicting the relative contributions of these two terms to future sea level rise is complicated by potential non-linear feedbacks, the ice dynamic contribution is generally regarded as more difficult to forecast than its surface mass balance counterpart. Societal interest in sea level rise over the next century makes understanding the physical basis of the ongoing mass loss of the Greenland Ice Sheet a pressing question (*IPCC*, 2007).

The widespread recent acceleration of Greenland outlet glaciers has been attributed to at least five different mechanisms: (i) enhanced basal sliding velocity due to increased meltwater

input (*Zwally and others*, 2002; *Shepherd and others*, 2009; *Bartholomew and others*, 2010), (ii) a relatively short-term dynamic re-adjustment to anomalous surface or submarine ablation (*Thomas*, 2004), (iii) increased effective driving stress due to the loss of terminus back-stress (*Howat and others*, 2008a; *Joughin and others*, 2008b), (iv) decreased effective basal pressure (ice pressure minus water pressure) due to ice thinning (*Pfeffer*, 2007) and (v) increased effective ice viscosity due to increased ice temperature from increased surface meltwater input (*Phillips and others*, 2010, *van der Veen and others*, 2011). This thesis sought to investigate the influence of recent increases in surface meltwater production on the ice dynamics of the Greenland Ice Sheet. By improving our understanding of the role of surface meltwater in enhanced basal sliding, this thesis directly addresses the need identified by the IPCC Fourth Assessment Report to better constrain the potential sea level rise contribution of outlet glaciers (*IPCC*, 2007).

Chapter 2 developed a relatively simple one-component (1D) hydrology model to track glacier water storage and discharge through time. An important element of this model was that conduit radius (and hence transmissivity) was allowed to evolve through time, within a prescribed range, in response to melt opening and deformational closure. This model suggests that mean annual subglacial hydraulic head remains relatively close to flotation throughout the Sermeq Avannarleq ablation zone, reaching a maximum in the vicinity of the equilibrium line. This is consistent with the few available observations. Additionally, a modeled mean englacial water residence time of ~ 2.2 ± 1.1 years implies that large quantities of water are stored in the ice throughout the year. Together, these model inferences suggest that conditions suitable for basal sliding are widespread in the Sermeq Avannarleq ablation zone, and that the hydrologic system can be expected to reorganize in response to external meltwater forcings on relatively short time-scales. Chapter 2 also presents a qualitative comparison between the observed annual ice velocity cycle and the modeled annual glacier hydrology cycle. This comparison suggests that the ablation zone of the Sermeq Avannarleq flowline experiences a basal sliding regime

similar to that of an alpine glacier, whereby enhanced (suppressed) basal sliding occurs during periods of positive (negative) rates of glacier water storage.

Chapter 3 coupled the 1D hydrology model to a 2D (vertical cross-section) ice flow model via a novel basal sliding rule. This allowed the relation between rate of change in hydraulic head and basal sliding velocity to be expressed in a quantitative fashion. The semi-empirical sliding rule imposes seasonal perturbations to a background basal sliding velocity whose sign and magnitude depend on the rate of change in hydraulic head. The coupled model is capable of reproducing the broad features observed in the annual basal sliding cycle in the Sermeq Avannarleq ablation zone. These features include (i) background basal sliding during the winter, (ii) a speedup event at the onset of melt, and (iii) a fall slowdown event and return to winter velocities. The coupled ice flow model presented in Chapter 3 was also used to examine the relative contribution of longitudinal coupling stress to total driving stress along the Sermeq Avannarleq flowline. The longitudinal coupling stress appears to be insufficient to attribute the annual ice velocity cycle observed at Swiss Camp (46 km upstream from the terminus) to seasonal variations in tidewater calving. Together, these results suggest that local meltwater-induced acceleration is more important than the loss of terminus back-stress in controlling seasonal variations in inland ice speed, and offer a framework for relating sliding velocity to the state of the glacier hydrologic system.

Chapter 4 provides a basis for future 2D hydrology modeling by investigating the spatial heterogeneity of surface meltwater entry points into the englacial system in the Sermeq Avannarleq ablation zone. This chapter provides a first-order demonstration that moulin-type drainage is more efficient in enhancing basal sliding than crevasse-type drainage. A comparison of 1985 and 2009 high resolution imagery suggests that the Sermeq Avannarleq ablation zone is experiencing a net increase in crevasse extent (and hence a decrease in moulin-type drainage). The mechanism of this increase in crevasse extent is postulated to be a combination of ice

thinning, which decreases the lithostatic stress opposing crevasse propagation, and changing flow direction, which reorganizes the longitudinal stress field. As the recent acceleration of Jakobshavn Isbrae is part of a widespread change in the low elevation ice geometry and velocity of the Greenland Ice Sheet, these observations at Sermeq Avannarleq are likely part of an equally widespread response in crevasse extent throughout the runoff zone of the ice sheet. In addition to potentially dampening basal sliding response, an increase in crevasse extent may enhance mass loss through increased surface ablation and accelerated cryo-hydrologic warming. Together, these observations suggest that future 2D coupled glaciohydrology models must incorporate transient crevasse fields as well as a number of crevasse-ice dynamic feedback processes that are not included in contemporary models.

5.2 Future Directions

Arctic mean air temperatures have increased at almost twice the mean global rate over the past century (*Johannessen and others*, 2004). Over the next century, surface warming is expected to be greater in the Arctic than anywhere else on Earth. By 2100 southwest Greenland is projected to warm between 3 and 6 °C (*Johannessen and others*, 2004; *ACIA*, 2006). A warmer Arctic atmosphere is expected to result in: (i) a decrease in sea ice thickness and extent (*Serreze and others*, 2007b), (ii) an increase in upward heat flux from the ocean to the atmosphere (*Lawrence and others*, 2008; *Serreze and others*, 2009), (iii) an increase in downwelling longwave radiation (*Lawrence and others*, 2008; *Serreze and others*, 2009), (iv) an acceleration of the hydrologic cycle with an increase in net precipitation (*Holland and others*, 2007), and (v) an increase in cyclone frequency (*Finnis and others*, 2007). The cumulative consequence of these changes will be a decrease in the surface mass balance of the Greenland Ice Sheet, and hence a decrease in terrestrial ice storage. Estimates of the sea level rise contribution of the Greenland Ice Sheet until 2100 vary from 0.18 m to a theoretical upper limit (based on kinematic

constraints) of 2.01 m (*IPCC*, 2007; *Pfeffer and others*, 2008). Complex physically-based models, which include non-linear feedbacks, are required to better constrain this range. While this thesis contributes to the parameterization of well-known processes (i.e. quantifying basal sliding velocity as a function of rate of change in glacier water storage), and also presents processes that are not currently incorporated in ice sheet models (i.e. changes in the ratio of crevasse-type to moulin-type meltwater drainage), there remain multiple avenues for future research to further improve the predictive power of ice sheet models.

The 1D hydrological model developed in this thesis has inherent limitations, namely the assumption of negligible lateral (*y*-direction) water flow. A 2D hydrology model would remove the need for prescribing conduit geometry and allow a more refined characterization of the annual hydrologic cycle in the Sermeq Avannarleq region and other portions of the Greenland Ice Sheet. While the magnitude of the annual variability in englacial water storage may be sufficiently large to influence the inter-annual comparison of ice sheet-wide GRACE mass conservation solutions, the annual cycle in englacial water storage has not yet been modeled for the entire ice sheet. This is attributable to the computational expense associated with solving the transient englacial water volume for the entire Greenland Ice Sheet at spatial and temporal resolutions similar to those used in this thesis. Traditionally, decreased spatial resolution can be exchanged for increased temporal resolution (and vice versa). When modeling ice sheet hydrology, however, Chapter 2 suggests that relatively high spatial resolution (i.e. $dx \leq 500$ m) is required to accurately represent the routing of subglacial water by bedrock topography. Additionally, recent studies indicate that the "seasonal" speedup event of the Greenland Ice Sheet may actually be comprised of a series of diurnal speedup events (*Shepherd and others*, 2009). In this case, accurately capturing the influence of englacial water on basal sliding velocity would require a relatively high temporal resolution (i.e. $dt < 12$ hr). Thus, to meaningfully investigate the ice sheet-wide englacial hydrology cycle, a computationally expensive 2D hydrology model

of relatively high spatial and temporal resolution would be required.

A 2D hydrology model would also benefit from the incorporation of spatially variable englacial transfer times (i.e. the time scale required for surface meltwater to reach the subglacial system). While Chapter 4 suggests that these transfer times can be parameterized as a function of surface morphology, the implementation of a transient solution for crevasse extent presently eludes virtually all ice sheet models. Given the typical length scales of a model grid cell and a crevasse, a transient solution for crevasse extent requires crevasses to be parameterized as sub-grid cell features. An additional difficulty in incorporating crevasses into ice sheet models is that crevasse propagation models often require more input variables than are readily available or observable (i.e. site-specific ice fracture toughness), and thus default to using complex parameterizations (*van der Veen*, 1998). While Chapter 4 demonstrates that the ratio of crevasse-type to moulin-type drainage areas has not been constant in the Sermeq Avannarleq ablation zone over the past 24 years, a natural starting point for the incorporation of crevasses and their associated processes into an ice sheet model would be to specify an ice sheet-wide crevasse density dataset based on observations. At present, however, neither a time series, nor even a single snapshot, of ice sheet-wide crevasse extent has been published. The analysis of ICESat waveforms, the shape of which differs between flat and crevassed ice surfaces due to differing ratios of surface and pseudo-volume scattering, may allow existing data to be reanalyzed to produce ice sheet-wide crevasse datasets (*McLamb and others*, 2010).

The three-phase basal sliding rule presented in Chapter 3 appears to have potential as a tool for coupling ice flow and hydrology models to examine possible non-linear responses in basal sliding velocity to increased surface meltwater production in a warming climate. To have true predictive value, however, a basal sliding rule must be capable of reproducing observed sliding velocities from first principles of hydrology and frictional force balance with a minimum of free parameters. Over the past half-century, sliding rules have improved from prescribing

basal sliding velocity as proportional to driving stress (*Weertman*, 1957) to employing Coulomb friction analogues developed in other disciplines (*Schoof*, 2005). Thus, while the three-phase sliding rule presented in Chapter 3 fails the absolute goal of providing a first principles sliding law, it improves upon previous sliding rules by connecting basal sliding velocity to the state of the glacier hydrologic system. A significant challenge remains in developing a sliding rule that is more firmly based upon first principles (i.e. focused on effective basal pressure) that can be universally incorporated into ice sheet models in a computationally efficient manner. As local basal sliding appears to governed by local mismatches between surface meltwater inputs and the ability of the subglacial hydrologic system to transmit water, a proper characterization of all components of the glacier hydrologic system may be a pre-requisite to a universal sliding rule. This characterization would include everything from the spatio-temporal pattern of melt generation, to supraglacial transport and storage evolution, and the complex evolution of a subglacial system that includes both conduits and cavity components.

In 1787 Bernhard Friedrich Kuhn (1762-1825) summarized the annual glaciohydrology cycle of the Upper and Lower Grindelwald Glaciers in the Swiss Alps with the following:

> "At the onset of the cold season it becomes slowly more quiet; the vaults close themselves and the ice sinks back to the ground. Also the thundering and banging, which is so striking for the visitors, becomes more seldom, and is no longer heard in the middle of the winter." (*Blatter and others*, 2010)

While the scientific community's understanding of the physical basis of glacier motion has greatly improved over the two and half centuries since Kuhn's observations, the major advances of the past half century have been largely focused on specific processes (i.e. thermo-mechanics of ice deformation, subglacial water flow, etc.; *Blatter and others*, 2010). Although fundamental

questions remain regarding lesser studied processes (i.e. calving rate, basal sliding, etc), today's most pressing questions regard the interactions between processes. As a consequence of interest generated by the 2007 IPCC Fourth Assessment Report and the 2007-2009 International Polar Year, glaciology has never been more socially relevant than at present. As a discipline, glaciology is well-positioned to enjoy its most illuminating century yet.

References

Abdalati, W. and K. Steffen. 1997. Snowmelt on the Greenland Ice Sheet as Derived from Passive Microwave Satellite Data. *J. Climate.* 10: 165-175.

Abdalati. W. and K. Steffen. 2001. Greenland ice sheet melt extent: 1979–1999. *J. Geophys. Res.* 106: 33,983–33,988.

Arctic Climate Impact Assessment (ACIA). 2006. Chapter 4: Future Climate Change. *Cambridge University Press*. ISBN: 13978-0521-86509-8.

Alley, R., M. Spencer and S. Anandakrishnan. 2007. Ice-sheet mass balance: assessment, attribution and prognosis. *Ann. Glaciol.* 46: 1-7.

Andersen, E. 1969. Report of the geodetic, geophysic, and photogrammetric work at the west coast region of Greenland. *Expedition Glaciologique Internationale au Groenland*. 2(2): 1-14.

Anderson, R., S. Anderson, K. MacGregor, E. Waddington, S. O'Neel, C. Riihimaki and M. Loso. 2004. Strong feedbacks between hydrology and sliding of a small alpine glacier. *J. Geophys. Res.* 109 (F03005): doi:10.1029/2004JF000120.

Arnold, N. and M. Sharp. 2002. Flow variability in the Scandinavian ice sheet: modelling the coupling between ice sheet flow and hydrology. *Quat. Sci. Rev.* 21: 485-502.

Bamber, J., R. Layberry, P. Gogineni. 2001. A new ice thickness and bed data set for the Greenland ice sheet 1: Measurement, data reduction, and errors. *J. Geophys. Res.* 106 (D24): 33,773-33,780.

Bartholomaus, T., R. Anderson and S. Anderson. 2008. Response of glacier basal motion to transient water storage. *Nat. Geosci*. 1: 33-37.

Bartholomaus, T., R. Anderson and S. Anderson. *Submitted*. Growth and collapse of the subglacial distributed hydrologic system on Kennicott Glacier, Alaska, and its effects on basal sliding. *J. Glaciol*.

Bartholomew, I., P. Nienow, D. Mair, A. Hubbard, M. King and A. Sole. 2010. Seasonal evolution of subglacial drainage and acceleration in a Greenland outlet glacier. *Nat. Geosci.* 3: doi:10.1038/ngeo863.

Bindschadler, R. 1983. The importance of pressurized subglacial water in separation and sliding at the glacier bed. *J. Glaciol.* 29: 3-19.

Bengtsson, L., V. Semenov and O. Johannessen. 2004. The Early Twentieth Century Warming in the Arctic - A Possible Mechanism. *J. Climate.* 17: 4045-4057.

Blatter, H., R. Greve and A. Abe-Ouchi. 2010. A short history of the thermomechanical theory and modelling of glaciers and ice sheets. *J. Glaciol.* 56: 1087-1094.

Box, J. and K. Steffen. 2001. Sublimation on the Greenland ice sheet from automated weather station observations. *J. Geophys. Res.* 106: 33965-33981.

Box, J. and K. Ski. 2007. Remote Sensing of Greenland supraglacial melt lakes: implications for subglacial hydraulics. *J. Glaciol.* 53: 257-265.

Braithwaite, R. 1995. Positive degree-day factors for ablation on Greenland ice sheet studies by energy-balance modelling. *J. Glaciol.* 41: 153-160.

Burgess, E., R. Forster, J. Box, E. Mosley-Thompson, D. Bromwich, R. Bales and L. Smith. 2010. A spatially calibrated model of annual accumulation rate on the Greenland Ice Sheet (1958–2007). *J. Geophys. Res.* 115 (F02004): doi:10.1029/2009JF001293.

Catania, G., and T. Neumann. 2010. Persistent englacial drainage features in the Greenland Ice Sheet. *Geophys. Res. Lett.* 37 (L02501): doi:10.1029/2009GL041108.

Cazenave, A. and W. Llovel. 2010. Contemporary Sea Level Rise. *Annu. Rev. Mar. Sci*. 2: 145-173. doi:10.1146/annurev-marine-120308-081105.

Clarke, G. 2003. Hydraulics of subglacial outburst floods: new insights from the Spring-Hutter formulation. *J. Glaciol.* 48: 299-313.

Colgan, W., T. Phillips, R. Anderson, H. Zwally, W. Abdalati, H. Rajaram and K. Steffen. 2009. Similarities in basal sliding between Greenland and alpine glaciers. Abstract C23B-0499 presented at 2009 Fall Meeting, AGU, San Francisco, USA.

Das, S., I. Joughin, M. Behn, I. Howat, M. King, D. Lizarralde and M. Bhatia. 2008. Fracture propagation to the base of the Greenland Ice Sheet during supraglacial lake drainage. *Science*. 320: 778-781.

Ditlevsen, R., H. Svensmark and S. Johnsen. 1996. Contrasting atmospheric and climate dynamics of the last-glacial and Holocene periods. *Nature*. 379: 810-812.

Fastook, J., H. Brecher and T. Hughes. 1995. Derived bedrock elevations, strain rates and stresses from measured surface elevations and velocities: Jakobshavns Isbrae, Greenland. *J. Glaciol.* 41: 161-173.

Fausto, R., A. Ahlstrøm, D. van As, C. Bøggild and S. Johnse. 2009. A new present-day temperature parameterization for Greenland. *J. Glaciol.* 55: 95-105.

Finnis, J., M. Holland, M. Serreze and J. Cassano. 2007. Response of Northern Hemisphere extratropical cyclone activity and associated precipitation to climate change, as represented by the Community Climate System Model. *J. Geophys. Res.* 112 (G04S42), doi:10.1029/2006JG000286.

Flowers, G. and G. Clarke. 2002. A multicomponent coupled model of glacier hydrology 1. Theory and synthetic examples. *J. Geophys. Res.* 107 (2287): doi:10.1029/2001JB001122.

Flowers, G., H. Björnsson, F. Pálsson and G. Clarke. 2004. A coupled sheet-conduit mechanism for jökulhlaup propagation. *Geophys. Res. Lett*. 31 (L05401): doi:10.1029/2003GL019088.

Flowers, G., S. Marshall, H. Björnsson and G. Clarke. 2005. Sensitivity of Vatnajökull ice cap hydrology and dynamics to climate warming over the next 2 centuries. *J. Geophys. Res.* 110 (F02011): doi:10.1029/2004JF000200.

Fountain, A. 1992. Subglacial water flow inferred from stream measurements at South Cascade Glacier, Washington, USA. *J. Glaciol.* 38: 51-64.

Fountain, A. and J. Walder. 1998. Water Flow through Temperate Glaciers. *Rev. Geophys.* 36: 299-328.

Fujisada, H., G. Bailey, G. Kelly, S. Hara and M. Abrams. 2005. ASTER DEM Performance. *IEEE Trans. Geosci. Rem. Sens.* 43: 2707-2714.

Glen, J. 1958. The flow law of ice: a discussion of the assumptions made in glacier theory, their experimental foundations and consequences. *Int. Assoc. Hydro. Sci. Pub.* 47: 171-183.

Greuell, W. 2000. Melt-water accumulation on the surface of the Greenland Ice Sheet: effect on albedo and mass balance. *Geograf. Ann.* 82A: 489-498.

Hanna, E., R. Huybrechts, I. Janssens, J. Cappelen, K. Steffen and A. Stephens. 2005. Runoff and mass balance of the Greenland ice sheet: 1958-2003. *J. Geophys. Res.* 110 (B13108): doi:10.1029/2004JD005641.

Hock, R. and R. Hooke. 1993. Evolution of the internal drainage system in the lower part of the ablation area of Storglaciären, Sweden. *Geo. Soc. Am. Bull.* 105: 537-546.

Hock, R. 2005. Glacier melt: a review of processes and their modeling. *Prog. in Phys. Geog.* 29: 369-391.

Holland, M., J. Finnis, A. Barrett and M. Serreze. 2007. Projected changes in Arctic Ocean freshwater budgets. *J. Geophys. Res.* 112 (G04S55): doi:10.1029/2006JG000354.

Holland, D., R. Thomas, B. de Young, M. Ribergaard and B. Lyberth. 2008. Acceleration of Jakobshavn Isbrae triggered by warm subsurface ocean waters. *Nat. Geosci.*1: doi:10.1038/ngeo316.

Holmlund, P. 1988. Internal geometry and evolution of moulins, Storglaciären, Sweden. *J. Glaciol*. 34: 242-248.

Hooke, R. 2005. Principles of Glacier Mechanics. Cambridge University Press.

Howat, I., I. Joughin, S. Tulaczyk and S. Gogineni. 2005. Rapid retreat and acceleration of Helheim Glacier, east Greenland. *Geophys. Res. Lett.* 32 (L22502): doi:10.1029/2005GL024737.

Howat, I., B. Smith, I. Joughin and T. Scambos. 2008a. Rates of southeast Greenland ice volume loss from combined ICESat and ASTER observations. *J. Geophys. Res.* 35 (L17505), doi:10.1029/2008GL034496.

Howat, I., S. Tulaczyk, E. Waddington and H. Björnsson. 2008b. Dynamic controls on glacier basal motion inferred from surface ice motion. *J. Geophys. Res.* 113: doi:10.1029/2007JF000925.

Hubbard, B. and P. Nienow. 1997. Alpine Subglacial Hydrology. *Quat. Sci. Rev.* 16: 939-955.

Humphrey, N., C. Raymond and W. Harrison. 1986. Discharges of turbid water during mini-surges of Variegated Glacier, Alaska, U.S.A. *J. Glaciol.* 32: 195-207.

Huybrechts, P., A. Letréguilly and N. Reeh. 1991. The Greenland ice sheet and greenhouse warming. *Glob. Plan. Chg.* 3: 399-412.

Huybrechts, P. 1994. The present evolution of the Greenland ice sheet: an assessment by modelling. *Glob. Pln. Chg.* 9: 39-51.

Iken, A. 1981. The effect of the subglacial water pressure on the sliding velocity of a glacier in an idealized numerical model. *J. Glaciol.* 27: 407-421.

Iken, A., H. Rothlisberger, A. Flotron and W. Haeberli. 1983. The uplift of Unteraargletscher at the beginning of the melt season, a consequence of water storage at the bed? *J. Glaciol.* 29: 28-47.

Iken, A. and R. Bindschadler. 1986. Combined measurements of subglacial water pressure and surface velocity of Findelengletscher, Switzerland: conclusions about drainage system and sliding mechanism. *J. Glaciol. 3*2: 101-119.

Iken, A., K. Echelmeyer, W. Harrison and M. Funk. 1993. Mechanisms of fast flow in Jakobshavn Isbrae, West Greenland: Part I. Measurements of temperature and water level in deep boreholes. *J. Glaciol.* 39: 15-25.

Intergovernmental Panel on Climate Change (IPCC). 2007. Summary for Policymakers. In: Climate Change 2007: The Physical Science Basis. Contribution of Working Group I to the Fourth Assessment Report of the Intergovernmental Panel on Climate Change. Ed. S. Solomon, D. Qin, M. Manning, Z. Chen, M. Marquis, K. Avery, M. Tignor and H. Miller. Cambridge University Press.

Janssens, I. and P. Huybrechts. 2000. The treatment of meltwater retention in mass-balance parameterizations of the Greenland ice sheet. *Ann. Glaciol.* 31: 133-140.

Jansson, P., R. Hock and T. Schneider. 2003. The concept of glacier storage: a review. *J. Hydro.* 282: 116-129.

Johannessen, O., L. Bengtsson, M. Miles, S. Kuzmina, V. Semenov, G. Alekseev, A. Nagurnyi, V. Zakarhov, L. Bobylev, L. Pettersson, K. Hasselmann and H. Cattle. 2004. Arctic climate change: observed and modelled temperature and sea-ice variability. *Tellus.* 56A: 328-341

Joughin, I., S. Das, M. King, B. Smith, I. Howat and T. Moon. 2008a. Seasonal speedup along the western flank of the Greenland Ice Sheet. *Science*. 320: 781-783.

Joughin, I., I. Howat, M. Fahnestock, B. Smith, W. Krabill, R. Alley, H. Stern and M. Truffer. 2008b. Continued evolution of Jakobshavn Isbrae following its rapid speedup. *J. Geophys. Res.* 113(F04006), doi:10.1029/2008JF001023.

Joughin, I., B. Smith, I. Howat, T. Scambos and T. Moon. 2010. Greenland flow variability from ice-sheet-wide velocity mapping. *J. Glaciol.* 56: 415-430.

Kamb, B. 1970. Sliding motion of glaciers: Theory and observation. *Rev. Geophys.* 8: 673-728.

Kamb, B., H. Engelhardt, M. Fahnestock and N. Humphrey. 1994. Mechanical and hydrologic basis for the rapid motion of a large tidewater glacier 2. Interpretation. *J. Geophys. Res.* 99: 15,231-15,244.

Kessler, M. and R. Anderson. 2004. Testing a numerical glacial hydrological model using spring speed-up events and outburst floods. *Geophys. Res. Lett.* 31 (L18503): doi:10.1029/2004GL020622.

Krabill, W., E. Hanna, P. Huybrechts, W. Abdalati, J. Cappelen, B. Csatho, E. Frederick, S. Manizade, C. Martin, J. Sonntag, R. Swift, R. Thomas and J. Yungel. 2004. Greenland Ice Sheet: Increased coastal thinning. *Geophys. Res. Lett*. 31 (L24402), doi:10.1029/2004GL021533.

Larson, C., J. Plumb, J. Zwally and W. Abdalati. 2001. Analysis of GPS data collected on the Greenland Ice Sheet. *Polar Geography.* 25: 22-40.

Lawrence, D., A. Slater and R. Thomas and M. Holland. 2008. Accelerated Arctic land warming and permafrost degradation during rapid sea ice loss. *J. Geophys. Res.* 35 (L11506), doi:10.1029/2008GL033985.

Luthcke, S., H. Zwally, W. Abdalati, D. Rowlands, R. Ray, R. Nerem, F. Lemoine, J. McCarthy and D. Chinn. 2006. Recent Greenland Ice Mass Loss by Drainage System from Satellite Gravity Observations. *Science.* 314: 1286-1289.

Lüthi, M., M. Funk, A. Iken, S. Gogineni, M. Truffer. 2002. Mechanisms of fast flow in Jakobshavn Isbrae, West Greenland: Part III. Measurements of ice deformation, temperature and cross-borehole conductivity in boreholes to the bedrock. *J. Glaciol.* 48: 369-385.

Marshall, S. 2005. Recent advances in understanding ice sheet dynamics. *Earth Plan. Sci. Lett.* 204: 191-204.

Marshall, S., H. Björnsson, G. Flowers and G. Clarke. 2005. Simulation of Vatnajökull Ice Cap dynamics. *J. Geophys. Res.* 110 (F03009): doi:10.1029/2004JF000262.

McCabe, G. and D. Wolock. 2010. Long-term variability in Northern Hemisphere snow cover and associations with warmer winters. *Clim. Change.* 99: doi:10.1007/s10584-009-9675-2.

McLamb, W., W. Colgan, T. Phillips, W. Abdalati, K. Steffen, R. Motyka and H. Rajaram. 2010. Changes in ice geometry and supraglacial hydrology, Sermeq Avannarleq ablation zone, West Greenland. Abstract C23B-0625 present at 2010 Fall Meeting, AGU, San Francisco, USA

Meier, M., S. Lundstrom, D. Stone, B. Kamb, H. Engelhardt, N. Humphrey, W. Dunlap, M. Fahnestock, R. Krimmel and R. Walters. 1994. Mechanical and hydrologic basis for the rapid motion of a large tidewater glacier: 1. Observations. *J. Geophys. Res.* 99: 15,219–15,229.

Moody, L. 1944. Friction factors for pipe flow. *Trans. Amer. Soc. Mech. Eng.* 66: 671–684.

Motyka, R., M. Fahnestock and M. Truffer. 2010. Volume change of Jakobshavn Isbrae, West Greenland: 1985–1997–2007. *J. Glaciol.* 56: 635-646.

Ng, F. 2000. Canals under sediment-based ice sheets. *Ann. Glaciol.* 30: 146-152.

Nick, F., A. Vieli, I. Howat and I. Joughin. 2009. Large-scale changes in Greenland outlet glacier dynamics triggered at the terminus. *Nat. Geosci.* 2: doi:10.1038/ngeo394.

Nye, J. 1976. Water flow in glaciers: jökulhlaups, tunnels and veins. *J. Glaciol.* 17: 181– 207.

Oerlemans, J. 2000. Analysis of a 3 year meteorological record from the ablation zone of Morteratschgletscher, Switzerland, energy and mass balance. *J. Glaciol.* 46: 571-579.

Ohmura, A. 2001. Physical basis for the temperature-based melt-index method. *J. App. Meteor.* 40: 753-761.

Oswald, G. and S. Gogineni. 2008. Recovery of subglacial water extent from Greenland radar survey data. *J. Glaciol.* 54: 94-102.

Overpeck, J., K. Hughen, D. Hardy, R. Bradley, R. Case, M. Douglas, B. Finney, K. Gajewski, G. Jacoby, A. Jennings, S. Lamoureux, A. Lasca, G. MacDonald, J. Moore, M. Retelle, S. Smith, A. Wolfe and G. Zielinski. 1997. Arctic Environmental Change of the Last Four Centuries. *Science.* 278: 1251-1256.

Overpeck, J., B. Otto-Bliesner, G. Miller, D. Muhs, R. Alley and J. Kiehl. 2006. Paleoclimatic evident for future ice-sheet instability and rapid sea-level rise. *Science.* 311: 1747-1750.

Parizek, B. and R. Alley. 2004. Implications of increased Greenland surface melt under global-warming scenarios: ice-sheet simulations. *Quat. Sci. Rev.* 23: 1013-1027.

Parry, V., P. Nienow, D. Mair, J. Scott, B. Hubbard, K. Steffen and D. Wingham. 2007. Investigations of meltwater refreezing and density variations in the snowpack and firn within the percolation zone of the Greenland ice sheet. *Ann. Glaciol.* 46: 61-68.

Paterson, W. 1991. Why ice-age ice is sometimes "soft". *Cold Reg. Sci. Tech.* 20: 75-98.

Paterson, W. 1994. The Physics of Glaciers. Oxford, England: Butterworth- Heinemann.

Pfeffer, T. and C. Bretherton. 1987. The effect of crevasses on the solar heating of a glacier surface. *IAHS Pub. 170*: 191-205.

Pfeffer, W., M. Meier and T. Illangasekare. 1991. Retention of Greenland Runoff by Refreezing: Implication for Projected Future Sea Level Change. *J. Geophys. Res.* 96: 117-122.

Pfeffer, W. and N. Humphrey. 1996. Determination of timing and location of water movement and ice layer formation by temperature measurements in subfreezing snow. *J. Glaciol.* 42: 292-304.

Pfeffer, W. and N. Humphrey. 1998. Formation of ice layers by infiltration and refreezing of meltwater. *Ann. Glaciol.* 26: 83-91.

Pfeffer, T. 2007. A simple mechanism for irreversible tidewater glacier retreat. *J. Geophys. Res.* 112 (F03S25): doi:10.1029/2006JF000590.

Pfeffer, W., J. Harper and S. O'Neel. 2008. Kinematic constraints on glacier contributions to 21st-century sea-level rise. *Science.* 321: 1340-1343.

Phillips, T., H. Rajaram and K. Steffen. 2010. Cryo-hydrologic warming: A potential mechanism for rapid thermal response of ice sheets. *Geophys. Res. Lett.* 37 (L20503): doi:10.1029/2010GL044397.

Phillips, T., S. Leyk, H. Rajaram, W. Colgan, W. Abdalati, D. McGrath and K. Steffen. 2011. Modeling Moulin Distribution on Sermeq Avannarleq Glacier using ASTER and WorldView Imagery and Fuzzy Set Theory. *Rem. Sens. Environ.* 115: 2292-2301.

Pimentel, S., and G. Flowers. 2010. A numerical study of hydrologically driven glacier dynamics and subglacial flooding. *Proc. R. Soc. A.* doi:10.1098/rspa.2010.0211.

Plummer, J., S. Gogineni, C. van der Veen, C. Leuschen and J. Li. 2008. Ice Thickness and bed map for Jakobshavn Isbrae, CReSIS Tech Report #2008-1.

Price, S., A. Payne, G. Catania and T. Neumann. 2008. Seasonal acceleration of inland ice via longitudinal coupling to marginal ice. *J. Glaciol.* 54: 213-219.

Reeh, N. 1985. Was the Greenland ice sheet thinner in the late Wisconsinan than now? *Nature.* 317: 797-799.

Reeh, N., H. Thomsen, A. Higgins and A. Weidick. 2001. Sea ice and the stability of north and northeast Greenland floating glaciers. *Ann. Glaciol.* 33: 474-480.

Reeh, N. 2008. A nonsteady-state firn-densification model for the percolation zone of a glacier. *J. Geophys. Res.* 113 (F03023), doi:10.1029/2007JF000746.

Rignot, E. and S. Jacobs. 2002. Rapid Bottom Melting Widespread near Antarctic Ice Sheet Grounding Lines. *Science.* 296: 2020-2023.

Rignot, E. and P. Kanagaratnam. 2006. Changes in the Velocity Structure of the Greenland Ice Sheet. *Science.* 311: 986-990.

Rignot, E., J. Box, E. Burgess and E. Hanna. 2008. Mass balance of the Greenland ice sheet from 1958 to 2007. *Geophys. Res. Lett.* 35 (L20502): doi:10.1029/2008GL035417.

Rignot, E., M. Koppes and I. Velicogna. 2010. Rapid submarine melting of the calving faces of West Greenland glaciers. *Nature Geosci*. 3: 187-191. doi:10.1038/ngeo765.

Ritz, C., A. Fabre and A. Letréguilly. 1997. Sensitivity of a Greenland ice sheet model to ice flow and ablation parameters: consequences for the evolution through the last climatic cycle. *Clim. Dynam.* 13: 11-24.

Röthlisberger, H. 1972. Water pressure in intra- and subglacial channels. *J. Glaciol.* 11: 177–203.

Scambos, T. and T. Haran. 2002. An image-enhanced DEM of the Greenland ice sheet. *Ann. Glaciol.* 34: 291-298.

Schoof, C. 2005. The effect of cavitation on glacier sliding. *Proc. R. Soc. A.* 461: 10.1098/rspa.2004.1350

Schoof, C. 2011. Ice-sheet acceleration driven by melt supply variability. *Nature.* 468: doi:10.1038/nature09618.

Sclater, J., C. Jaupart and D. Galson. 1980. The heat flow through oceanic and continental crust and the heat loss of the Earth. *Rev. Geophys. Space Phys.* 18: 269– 311.

Serreze, M., J. Walsh, F. Chapin, T. Osterkamp, M. Dyurgerov, V. Romanovsky, W. Oechel, J. Morison, T. Zhang and R. Barry. 2000. Observational evidence of recent changes in the northern high latitude environment. *Climatic Change.* 46: 159-207.

Serreze, M., A. Barrett, A. Slater, R. Woodgate, K. Aagaard, R. Lammers, M. Steele, R. Moritz, M. Meredith and C. Lee. 2006. The large-scale freshwater cycle of the Arctic. *J. Geophys. Res.* 110 (C11010), doi:10.1029/2005JC003424.

Serreze, M. A. Barrett, A. Slater, M. Steele, J. Zhang and K. Trenberth. 2007a. The large-scale energy budget of the Arctic. *J. Geophys. Res.* 112 (D11122), doi:10.1029/2006JD008230.

Serreze, M., M. Holland and J. Stroeve. 2007b. Perspectives on the Arctic's Shrinking Sea-Ice Cover. *Science.* 315: 1533-1536.

Serreze, M., A. Barrett, J. Stroeve, D. Kindig and M. Holland. 2009. The emergence of surface-based Arctic amplification. *The Cryosphere*. 3: 11-19.

Shepherd, A., A. Hubbard, P. Nienow, M. King, M. McMillan and I. Joughin. 2009. Greenland ice sheet motion coupled with daily melting in late summer. *Geophys. Res. Lett.* 36 (L01501): doi:10.1029/2008GL035758

Shreve, R. 1972. Movement of Water in Glaciers. *J. Glaciol.* 11: 205-214.

Spring, U. and K. Hutter. 1982. Conduit flow of a fluid through its solid phase and its application to intraglacial channel flow. *Int. J. Eng. Sci.* 20: 327– 363.

Steffen, K. and J. Box. 2001. Surface climatology of the Greenland ice sheet: Greenland Climate Network 1995-1999. *J. Geophys. Res.* 106: 33,951-33,964.

Stroeve, J., M. Serreze, M. Holland, J. Kay, J. Maslanik and A. Barrett. 2011. The Arctic's rapidly shrinking sea ice cover: a research synthesis. *Clim. Change.* 106: doi:10.1007/s10584-011-0101-1.

Sundal, A., A. Shepherd, P. Nienow, E. Hanna, S. Palmer and P. Huybrechts. 2011. Melt-induced speed-up of Greenland ice sheet offset by efficient subglacial drainage. *Nature.* 469: doi:10.1038/nature09740.

Tedesco, M. 2007. Snowmelt detection over the Greenland ice sheet from SSM/I brightness temperature daily variations. *Geophys. Res. Lett.* 34: doi:10.1029/2006GL028466.

Thomas, R., W. Abdalati, E. Frederick, W. Krabill, S. Manizade and K. Steffen. 2003. Investigation of surface melting and dynamic thinning on Jakobshavn Isbrae, Greenland. *J. Glaciol.* 49: 231-239.

Thomsen, H. 1986. Photogrammetric and Satellite Mapping of the Margin of the Inland Ice, West Greenland. *Ann. Glaciol.* 8: 164-167.

Thomsen, H., L. Thorning and R. Braithwaite. 1988. Glacier-hydrological conditions on the Inland Ice north-east of Jakobshavn/Ilulissat, West Greenland. *Grönl. Geol. Undersögelse, Rapp.* 138.

Thomsen, H. and O. Olesen. 1991. Hydraulics and hydrology on the Inland Ice. *Grönl. Geol. Undersögelse, Rapp.* 152: 36-38.

Truffer, M. and K. Echelmeyer. 2003. Of Isbrae and ice streams. *Ann. Glaciol*. 36: 66–72.

Tsukernik, M., D. Kindig and M. Serreze. 2007. Characteristics of winter cyclone activity in the northern North Atlantic: Insights from observations and regional climate modeling. *J. Geophys. Res.* 113: doi:10.1029/2006JD007184.

Tulaczyk, S., W. Kamb and H. Engelhardt. 2000. Basal mechanics of Ice Stream B, West Antarctica 1. Till mechanics. *J. Geophys. Res.* 105: 463-482. doi:10.1029/1999JB900329.

van de Wal, R., M. van den Broeke, C. Smeets, C. Reijmer, J. Donker and J. Oerlemans. 2008. Large and Rapid Melt-Induced Velocity Changes in the Ablation Zone of the Greenland Ice Sheet. *Science.* 321: doi:10.1126/science.1158540.

van den Broeke, M., J. Bamber, J. Ettema, E. Rignot, E. Schrama, W. van de Berg, E. van Meijgaard, I. Velicogna and B. Wouters. 2009. Partitioning Recent Greenland Mass Loss. *Science.* 326: doi:10.1126/science.1178176.

van der Veen, C. 1987. Longitudinal stresses and basal sliding: A comparative study. In: Dynamics of the West Antarctic Ice Sheet. Ed. C. van der Veen and J. Oerlemans. D. Reidel Publishing Company.

van der Veen, C. 1998. Fracture mechanics approach to penetration of surface crevasses on glaciers. *Cold Reg. Sci. Tech.* 27: 31-47.

van der Veen, C., J. Plummer and L. Stearns. 2011. Controls on the recent speed up of Jakobshavn Isbrae, West Greenland. *J. Glaciol.* 57: 770-782.

Velicogna, I. and J. Wahr. 2005. Greenland mass balance GRACE. *Geophys. Res. Lett.* 32 (L18505): doi:10.1029/2005GL023955.

Velicogna, I. and J. Wahr. 2006. Acceleration of Greenland ice mass loss in spring 2004. *Nature.* 443: 329-331.

Velicogna, I. 2009. Increasing rates of ice mass loss from the Greenland and Antarctic ice sheets revealed by GRACE. *Geophys. Res. Lett.* 36 (L19503): doi:10.1029/2009GL040222.

Vinther, B., S. Johnsen, K. Andersen, H. Clausen and A. Hansen. 2003. NAO signal recorded in the stable isotopes of Greenland ice cores. *Geophys. Res. Lett.* 30: doi:10.1029/2002GL016193.

Vieli, A., M. Funk and H. Blatter. 2000. Tidewater glaciers: Frontal flow acceleration and basal sliding. *Ann. Glaciol.* 31: 217– 221.

Weertman, J. 1957. On the sliding of glaciers. *J. Glaciol.* 3: 33-38.

Zwally, H., W. Abdalati, T. Herring, K. Larson, J. Saba and K. Steffen. 2002. Surface melt-induced acceleration of Greenland Ice Sheet flow. *Science.* 297: 218-222.

Appendix 1

CHAPTER 2 VARIABLE NOTATION

Variable	Definition [units]
α	glacier hydrology length scale [m]
β	change in melting point with ice thickness [K/m]
γ	ablation gradient [ ]
φ	bulk ice porosity [ ]
ρ_i	density of ice [kg/m^3]
ρ_w	density of water [kg/m^3]
τ_b	gravitational driving stress [Pa]
A	flow law parameter [/Pa^3/a]
D	melt season duration [d]
D_h	effective hydraulic diameter [m]
F	entry fraction [ ]
F_r	rention fraction [ ]
H_i	ice thickness [m]
H_e	englacial water thickness [m]
I	rate of external meltwater input [m/a]
L	latent heat of fusion of ice [J/kg]
P_i	ice pressure [Pa]
P_w	water pressure [Pa]
Q	conduit discharge [m^3/a]
Q_d	heating due to deformation (strain) [W/m^2]
Q_f	heating due to friction [W/m^2]

Q_g	geothermal flux [W/m^2]
S	total storage per unit length [m^2]
S_c	subglacial conduit storage volume per unit length [m^2]
S_e	englacial storage volume per unit length [m^2]
T_i	basal ice temperature [K]
$\dot{a}_b$	basal ablation rate [m/a]
a_s	annual surface ablation [m]
$\dot{a}_s$	surface ablation rate [m/a]
c_s	annual surface accumulation [m]
$\dot{c}_s$	surface accumulation rate [m/a]
f	conduit friction factor [ ]
g	gravitational acceleration [m/s^2]
h_b	bedrock elevation [m]
h_e	hydraulic head (or englacial water table elevation) [m]
h_s	ice surface elevation [m]
j	given Julian Date [d]
j_c	Julian Date of melt cessation [d]
j_o	Julian Date of melt onset [d]
$\dot{m}$	conduit meltwater production [kg/m/s]
n	Glen Law exponent [ ]
n_c	conduits per meter in the across flow direction [/m]
r	conduit radius [m]
r_{max}	maximum conduit radius [m]
r_{min}	minimum conduit radius [m]
u_s	ice surface velocity [m/a]

u_b	basal sliding velocity [m/a]
$\bar{u}$	depth-averaged ice velocity [m/a]
w	cross-flow width [m]
x	distance upstream from terminus [m]

Appendix 2

CHAPTER 3 VARIABLE NOTATION

Variable	Definition [units]
γ	ablation gradient [ ]
ρ_i	density of ice [kg/m^3]
τ	total driving stress [Pa]
$\bar{\tau}'_{xx}$	longitudinal stress [Pa]
A	flow law parameter [/Pa^3/a]
E	Wisconsinan enhancement factor [ ]
F	englacial hydrology system entry fraction [ ]
H	ice thickness [m]
P_i	ice pressure [Pa]
P_w	water pressure [Pa]
Q	ice discharge [m^2/a]
a_b	annual basal ablation [m]
a_s	annual surface ablation [m]
$\dot{a}_s$	surface ablation rate [m/a]
b	annual mass balance [m]
c_b	annual basal accumulation [m]
c_s	annual surface accumulation [m]
d_{max}	duration of summer speedup event [d]
d_{min}	duration of fall slowdown event [d]
g	gravitational acceleration [m/s^2]
h_b	bedrock elevation [m]

h_e	hydraulic head [m]
h_s	ice surface elevation [m]
j	given date [D]
j_{max}	date of summer maximum velocity [D]
j_{min}	date of fall minimum velocity [D]
k	sliding coefficient [$m^{½}d^{½}$]
m	sliding rule exponent [ ]
n	Glen Law exponent [ ]
n_c	subglacial conduits per meter [/m]
u_{b0}	background basal sliding velocity [m/a]
u_b	basal sliding velocity [m/a]
u_d	deformational velocity [m/a]
u_{max}	surface summer maximum velocity [m/a]
u_{min}	surface fall minimum velocity [m/a]
u_s	surface velocity [m/a]
u_w	surface winter velocity [m/a]
x	distance upstream [m]
z	given elevation within the ice [m]

Appendix 3

CHAPTER 4 VARIABLE NOTATION

Variable	Name [Units]
ϕ	phase angle [ ]
τ	englacial surface-to-bed water transfer time [s]
A	supraglacial water catchment [m^2]
H	ice thickness [m]
Q_i	horizontal ice discharge [m/a]
Q	englacial conduit discharge [m^3/s]
S_c	cross-sectional conduit area [m^2]
T	period of surface ablation cycle [s]
V	englacial water volume [m^3]
a_s	surface ablation rate [m/a]
b	local mass balance rate [m/a]
l	crevasse length [m]
t	time [a]
$\bar{r}$	depth-averaged moulin radius [m]
$\bar{u}$	depth-averaged englacial water velocity [m/s]
$\bar{w}$	depth-averaged crevasse width [m]

Appendix 4

DISSERTATION "WORD CLOUD"

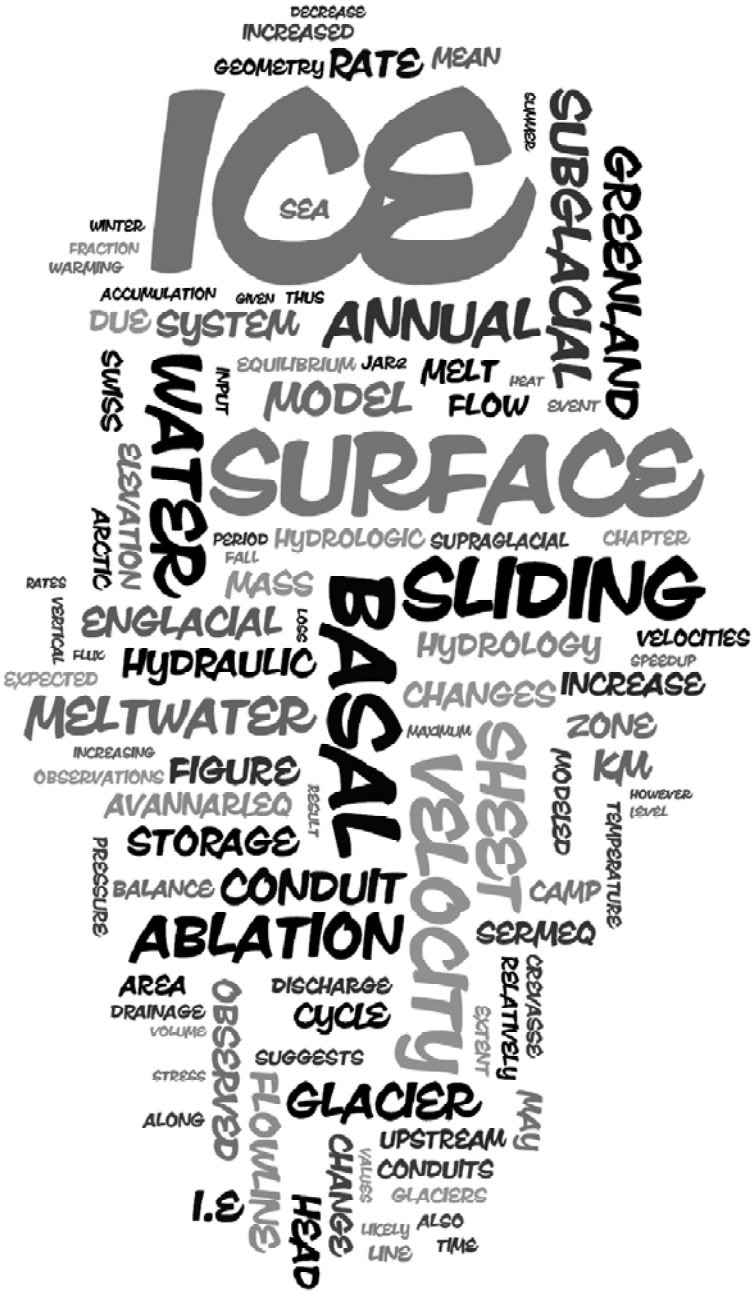

A “word cloud” in the approximate shape of Greenland generated from the text of this dissertation. Word frequency is reflected in graphic prominence (www.wordle.net).